UC Irvine
UC Irvine Electronic Theses and Dissertations

Title

Characterizing antimicrobial synergy between histones and pore-forming antimicrobials in bacterial and fungal pathogens

Permalink

https://escholarship.org/uc/item/91f0c86c

Author

Duong, Leora

Publication Date

2024

Peer reviewed|Thesis/dissertation

UNIVERSITY OF CALIFORNIA,
IRVINE

Characterizing antimicrobial synergy between histones and
pore-forming antimicrobials in bacterial and fungal pathogens

DISSERTATION

submitted in partial satisfaction of the requirements
for the degree of

DOCTOR OF PHILOSOPHY

in Biological Sciences

by

Leora Duong

Dissertation Committee:
Associate Professor Albert Siryaporn, Chair
Professor Steven Gross
Professor Melissa Lodoen
Professor Eric Pearlman
Assistant Professor Travis Wiles

2024

DEDICATION

To all my elementary, middle, and high school teachers

for being the incredible support systems that I never knew I needed

TABLE OF CONTENTS

LIST OF FIGURES

Page

your strength, encouragement, and company the most. Thank you for birthing a cute baby daughter and always brightening my days with her photos and videos. I hope to be the best "Dr. Auntie Leora" as ES grows up and becomes an amazing human being, just like her mom and dad. To all my other family and friends, I hope you know who you are, and know that I very much appreciate having your love and support. Thank you all for being with me during this academic journey.

Next, I would like to thank all my former teachers for playing a more vital role in my life and career journey than they know. Special thanks go to Ms. Tanner, Ms. Jaeger, Dr. Rasori (née Woelbing), Ms. O'Brien, Mrs. Kennedy (née Wiesner), Ms. Weathers, and Ms. JJ. Despite the environment I grew up in, you all relentlessly believed in me and always encouraged me to aim for bigger and better in life. You all will always hold special places in my heart, and I appreciate you all so much.

Notably, I thank my research advisors, Professors Albert Siryaporn and Steven Gross, for guiding me throughout my PhD research project and reminding me how exciting novel science can be. Thank you both for supporting my career endeavors as I explore the relatively unfamiliar avenues of an industrial career. Albert, thank you for teaching me to think more critically, communicate more clearly, be the expert in my own project, and pay close attention to the small, yet critical, details. Thank you for also working with me on my presentation slides over the years, to make sure they are clear and tell a story. Steve, thank you for always being there to listen and support me without judgement, encouraging me when I start to doubt my abilities to push forward, reminding me of the importance of the "big picture," and empowering me to advocate for myself.

Moreover, I express a large sum of gratitude to my incredible and supportive committee members: Professors Melissa Lodoen, Eric Pearlman, and Travis Wiles. Thank you all for your guidance and support throughout my PhD training. Melissa, thank you for being a wonderful

example of what it looks like to be an amazing and multifaceted woman in STEM. You embody grace, strength, kindness, success, intelligence, and so much more. I very much aspire to pay forward the support you have given me to the next generation of women scientists. Eric, thank you for your unwavering faith in my abilities as a scientist and a human being, and always making sure I leave your office feeling capable, intelligent, and supported. I am also grateful that we found a way to collaborate throughout my dissertation project, so that I would still have the honor of working with you, but sans all the mouse handling. Thank you (and your amazing lab!) for providing critical expertise in eye physiology and infection, the innate immune system, and pathogenic fungi. Finally, Travis, I am so grateful that a talented microbiologist, like yourself, has joined UCI and brought a plethora of exciting bacterial research with you. Thank you for inspiring me with unique ways to conduct bacterial research, including the use of clear zebrafish larvae, axolotls, and all sorts of fluorescent bacteria. I am also very thankful for your constant enthusiasm for all things science, for always offering to find ways to help move my project forward, and for making time for me when I need support.

To the wonderful colleagues, and now friends, that I have met at UCI: JLB, KU, LO, CP, VZ, JA, MM – thank you for being with me on this (sometimes wild) academic ride. I appreciate your lunch hours spent with me, your comradery, your talent, your ambition, and your kindness. I wish you all nothing but the greatest success, whatever that may look like to you. To the past and current members of both the Siryaporn and Gross labs, thank you for all the open, honest, and enjoyable conversations. I very much appreciate your company in lab, your support for my career, and most importantly, your shared excitement for all things microscopy or bacteria. To the professors and students that I had the honor of TA-ing for, thank you for the great memories and the rewarding experience. To our collaborators, particularly those in the Pearlman, Patterson,

Plikus, and Siwy labs, thank you for your expertise, conversations, and hard work. To my mentor, ATG, thank you for making time to meet with me, despite your busy schedule, and for encouraging me to branch out and apply to different industry internships. Your guidance as I improve my CV, interview skills, and salary negotiation tactics are incredibly valuable. Of course, I thank all the mental health counselors that provided me the necessary support and skills to navigate stressful situations. I am a better and more self-aware human being now because of our work together.

VITA

Leora Duong

2024	Ph.D. in Biological Sciences, University of California, Irvine
2021-24	National Science Foundation Graduate Research Fellow
2023	Molecular Profiling Intern, Merck & Co., Inc.
2022	M.S. in Biological Sciences, University of California, Irvine
2021-22	Teaching Assistant, Department of Molecular Biology and Biochemistry, University of California, Irvine
2018-19	Clinical Laboratory Technician, Illumina, Inc.
2018	B.S. in Microbiology, Immunology, and Molecular Genetics, University of California, Los Angeles
2016-18	Undergraduate Research Assistant, University of California, Los Angeles

PUBLICATIONS

9. **Duong, L.**, Wu, Y., Hurst, P.J., Abbondante, S., Marshall, M.E., McCarthy, K., Kasallis, S., Reddy, B.J.N., Bru, J.L., Perinbaum, K., Pearlman, E., Patterson, J., Gross, S., Siryaporn, A. Antimicrobial peptides help histones form novel pores by overcoming bacterial lipopolysaccharide protection. *Submitted.*

8. Foik, I.P., Shu, R., Urban, L.A., Huang, A.P., Abbondante, S., Marshall, M.E., **Duong, L.**, Downing, T.L., Siryaporn, A. 2022. Activation of a bacterial flow sensor by hypochlorous acid from stimulated neutrophils. *Manuscript in preparation.*

7. Silva, S., Combs, C., Russell, W.S., **Duong, L.**, McCarthy, K., Siryaporn, A., Siwy, Z.S. 2023. Label-free, fast electronic classification of bacteria. *Biophysical Journal.* 122(3), 455a.

6. Hedde, P.N., Le, B.T., Gomez, E.L., **Duong, L.**, Steele, R.E., Ahrar, S. 2023. SPIM-Flow: An Integrated Light Sheet and Microfluidics Platform for Hydrodynamic Studies of Hydra. *Biology* 12(1), 116.

5. **Duong, L.**, Gross, S., Siryaporn, A. 2021. Developing Antimicrobial Synergy with AMPs. *Frontiers in Medical Technology* 3, 640981.

4. **Duong, L.**, Gross, S., Siryaporn, A. 2020. A novel antibacterial strategy: histone and antimicrobial peptide synergy. *Microbial Cell* 7(11), 309-311.

3. Doolin, T., Amir, H.M., **Duong, L.**, Rosenzweig, R., Urban, L.A., Bosch, M., Pol, A., Gross, S.P., Siryaporn, A. 2020. Mammalian histones facilitate antimicrobial synergy by disrupting the bacterial proton gradient and chromosome organization. *Nature Communications* 11, 3888.

2. Caremoli, F., Dong, T., Lagishetty, V., **Duong, T.L.**, Jacobs, J.P., De Giorgio, R., Sternini, C. 2019. Intestinal Epithelial Barrier Abnormalities and Changes in Microbiome As Early Events in Diet-induced Obesity. *Gastroenterology* 156(6): S-494-S-495.

1. Parra, D., Hsu, C., Le, Q., Lam, K., Rosenberg, G., Jin, L., Hwang, J., Shen, D., Bergsma, J., Aquinde, M., Le, C., **Duong, T.**, Doherty, A., Dowiak, A., Fallon, R., Green, J., Lund, A., Bina, M., Reddi, K., Moberg-Parker, J., Garlena, R.A., Russell, D.A., Pope, W.H., Jacobs-Sera, D., Hendrix, R.W. and Hatfull, G.F. 2017. Mycobacterium Phage Phox, Complete Genome. *GenBank*, accession number: MF919527.5.

PRESENTATIONS

8. **Duong, L.**, Gross, S., Siryaporn, A. 2023. Histones: more than just basic DNA spools. Oral presentation in Systems Microbiology Seminar, Irvine, CA.

7. **Duong, L.**, Bru, J.L., Hurst, P., Patterson, J., Gross, S., Siryaporn, A. 2022. A novel and synergistic antimicrobial approach against *P. aeruginosa*. Abstract and oral presentation in Molecular Biology and Biochemistry Research in Progress Talks, Irvine, CA.

6. **Duong, L.**, Gross, S., Siryaporn, A. 2022. A novel antimicrobial strategy against *P. aeruginosa*. Abstract and oral presentation in Molecular Biology and Biochemistry Annual Retreat, Irvine, CA.

5. **Duong, L.**, Gross, S., Siryaporn, A. 2022. Lessons from innate immunity: A novel antimicrobial strategy against *P. aeruginosa*. Abstract and oral presentation in Molecular Genetics of Bacteria and Phages Meeting, Madison, WI.

4. **Duong, L.**, Gross, S., Siryaporn, A. 2022. Understanding how histones and antimicrobial peptides synergize against bacteria. Oral presentation in Systems Microbiology Seminar, Irvine, CA.

3. **Duong, L.**, Gross, S., Siryaporn, A. 2021. Unraveling synergistic antimicrobial mechanisms of histones with pore-forming antimicrobials. Oral presentation in Systems Microbiology Seminar, Irvine, CA.

2. **Duong, L.**, Gross, S., Siryaporn, A. 2020. A novel antimicrobial approach: histones and pore-forming antimicrobial peptides. Abstract and oral presentation in the American Association of Immunologists (AAI)'s 18th Annual Immunology Fair at UCI: COVID-19, Irvine, CA.

1. Aquinde, M., Bergsma, J., **Duong, T.**, Le, C., Bina, M., Lund, A., Reddi, K., Moberg-Parker, J. 2017. Lysogenic Properties of Novel Mycobacteriophages Phallon and Phox to Elucidate Potential Antibacterial Applications. Poster presented at the annual Microbiology, Immunology, and Molecular Genetics Undergraduate Research Poster Symposium, Los Angeles, CA.

HONORS AND AWARDS

Molecular Biology and Biochemistry Annual Retreat, Oral Presentation Award	September 2022
Molecular Biology and Biochemistry Outstanding Student Award	September 2021
National Science Foundation Graduate Research Fellow	June 2021—June 2024
Ford Predoctoral Fellowship, Honorable Mention	March 2021
University of California Irvine Supply Fellowship	January 2021
UCI AAI Immunology Fair at UCI, Oral Presentation Award	December 2020
Associate Graduate Students Social Wellness Grant	July 2020
Associate Graduate Students Emergency Travel Grant	June 2020

CERTIFICATES

Ensembl Browser and REST API Course	November 2022
Narrative Tools for Researchers Nature Masterclasses Online Courses	September 2022
Interpreting Scientific Results, Nature Masterclasses Online Courses	August 2022
Scientific Writing and Publishing, Nature Masterclasses Online Courses	August 2022
Public Speaking by Activate to Captivate, UCI Graduate Division	March 2022
Mentorship Excellence Program, UCI Graduate Division	February 2022
Course Design Program, UCI Division of Teaching Excellence and Innovation	September 2020

ABSTRACT OF THE DISSERTATION

Characterizing antimicrobial synergy between histones and
pore-forming antimicrobials in bacterial and fungal pathogens

by

Leora Duong

Doctor of Philosophy in Biological Sciences

University of California, Irvine, 2024

Professor Albert Siryaporn, Chair

To combat the growing threat of antibiotic resistance, new antimicrobial strategies are urgently needed. Here, I describe a strategy and mechanism that combines antimicrobial peptides (AMPs) with histones, which can be used to treat pathogenic *Pseudomonas aeruginosa* and *Staphylococcus aureu*s bacteria, and *Aspergillus fumigatus* fungi. When combined in Gram-negative bacteria, AMPs target the outer membranes of bacteria and enable histones to pass the lipopolysaccharide-rich outer membrane. Here, histones can increase the number and size of membrane pores by targeting bacterial membranes that have significantly less lipopolysaccharide, including the bacterial inner membrane and inner leaflet of the outer membrane, and contribute to bacterial membrane damage from the inside. Consistent with this, histones increase the efficacy of the antibiotic and AMP polymyxin B to treat *P. aeruginosa*. Altogether, this strategy of combining histones with antimicrobial peptides is an effective alternative antimicrobial mechanism against Gram-negative bacteria and can also be extended to clinically-relevant Gram-positive bacteria and fungi. This research can be used to improve the efficacy of current antimicrobials and guide the development of novel antibiotic strategies against various microbes.

INTRODUCTION

The simultaneous overuse of current antibiotics, and underdevelopment of new antibiotics, contributes to millions of untreatable, and oftentimes lethal, microbial infections each year[1]. To combat the growing threat of antibiotic resistance, new antimicrobial drugs and therapeutic approaches are urgently needed. My research approaches this problem by studying histones, particularly how they work synergistically with other known antimicrobials to inhibit microbial growth. Understanding how naturally abundant antimicrobials, such as histones[2], work together with currently available antimicrobials could unravel novel mechanisms, ultimately guiding antibiotic development efforts and novel therapeutic approaches.

Histones are commonly known for their roles in eukaryotic chromosomal condensation[3]; however, they were first discovered to have antimicrobial roles[4]. *In vivo*, histones possess antimicrobial properties in neutrophil extracellular traps[2] and lipid droplets[5]. Despite this, the antimicrobial mechanisms of histones were previously unclear due to a curious lack of antimicrobial activity *in vitro*, particularly at physiological magnesium levels[6]. Recent work demonstrates that although histones alone are not effective at killing bacteria, the combination of histones and antimicrobial peptides (AMPs) synergistically inhibits bacterial growth[6], where synergy is defined as a greater combined effect than the sum of each constituent's individual effects. In this model, AMPs induce pores in bacterial membranes, which are then enhanced by histones, leading to a loss of bacterial cytoplasm and destruction of bacterial proton gradients. Additionally, the AMP-induced bacterial pores also enable histone entry into bacterial cells, causing internal damage by restructuring chromosomes and limiting transcription, all of which results in bacterial cell death[6].

Previous work also shows that although bacteria can recover from AMP-induced pores, they cannot recover from pores created when both histones and AMPs are present[6]. This work was initially studied in *E. coli*; however, little was known regarding synergistic effects of histones and pore-forming antimicrobials against common drug-resistant microbes, including clinically relevant bacterial species *P. aeruginosa* and methicillin-resistant *S. aureus* (MRSA), and fungal species *A. fumigatus*[7–9]. How histones work together with pore-forming antimicrobials, including AMPs and antibiotics, to keep bacterial pores open also remains unclear. Assessing the synergistic effects of histones with various pore-forming AMPs and antibiotics *in vitro* and *in vivo*, particularly against common drug-resistant and pathogenic microbes, will better define the currently proposed mechanisms and establish whether such mechanisms are conserved in various microbial species. The clarification of these antimicrobial mechanisms will help guide the potential utilization of histones as part of a novel antibiotic regimen in clinical settings.

Introduction References

1. Talaat, M. *et al.* Increasing Antimicrobial Resistance in World Health Organization Eastern Mediterranean Region, 2017–2019. *Emerg. Infect. Dis.* **28**, (2022).

2. Brinkmann, V. *et al.* Neutrophil Extracellular Traps Kill Bacteria. *Science* **303**, 1532–1535 (2004).

3. Hewish, D. R. & Burgoyne, L. A. Chromatin sub-structure. The digestion of chromatin DNA at regularly spaced sites by a nuclear deoxyribonuclease. *Biochem. Biophys. Res. Commun.* **52**, 504–510 (1973).

4. Miller, B. F., Abrams, R., Dorfman, A. & Klein, M. Antibacterial Properties of Protamine and Histone. *Science* **96**, 428–430 (1942).

5. Anand, P. *et al.* A novel role for lipid droplets in the organismal antibacterial response. *eLife* **1**, e00003 (2012).

6. Doolin, T. *et al.* Mammalian histones facilitate antimicrobial synergy by disrupting the bacterial proton gradient and chromosome organization. *Nat Comm* (2020) doi:http://doi.org/10.1038/s41467-020-17699-z.

7. Pang, Z., Raudonis, R., Glick, B. R., Lin, T.-J. & Cheng, Z. Antibiotic resistance in Pseudomonas aeruginosa: mechanisms and alternative therapeutic strategies. *Biotechnol. Adv.* **37**, 177–192 (2019).

8. Turner, N. A. *et al.* Methicillin-resistant Staphylococcus aureus: an overview of basic and clinical research. *Nat. Rev. Microbiol.* **17**, 203–218 (2019).

9. Toyotome, T., Hagiwara, D., Takahashi, H., Watanabe, A. & Kamei, K. Emerging Antifungal Drug Resistance in Aspergillus fumigatus and Among Other Species of Aspergillus. *Curr. Fungal Infect. Rep.* **12**, 105–111 (2018).

CHAPTER 1: DEVELOPING SYNERGY WITH ANTIMICROBIAL PEPTIDES (AMPS)

1.1 Synopsis

Antimicrobial peptides (AMPs) have been extensively studied due to their vast natural abundance and ability to kill microbes. In an era critically lacking in new antibiotics, manipulating AMPs for therapeutic application is a promising option. However, bacterial pathogens resistant to AMPs remain problematic. To improve AMPs antimicrobial efficacy, their use in conjunction with other antimicrobials has been proposed. How might this work? AMPs are positively charged and kill bacteria by forming pores in bacterial membranes or by inhibiting bacterial macromolecular functions. What remains unknown is the duration for which AMPs keep bacterial pores open, and the extent to which bacteria can recover by repairing these pores. In this chapter, various antimicrobial synergies with AMPs are discussed. Such synergies might arise if the antimicrobial agents helped to keep bacterial pores open for longer periods of time, prevented pore repair, perturbed bacterial intracellular functions at greater levels, or performed other independent bacterial killing mechanisms. We first discuss combinations of AMPs, and then focus on histones, which have antimicrobial activity and co-localize with AMPs on lipid droplets and neutrophil extracellular traps (NETs). Recent work has demonstrated that histones can enhance AMP-induced membrane permeation. It is possible that histones, histone fragments, and histone-like peptides could amplify the antimicrobial effects of AMPs, giving rise to antimicrobial synergy. If so,

clarifying these mechanisms will thus improve our overall understanding of the antimicrobial processes and potentially contribute to improved drug design.

1.2 Role of AMPs in Antimicrobial Resistance

Bacterial infections are an increasing threat to global health, due to both an increase in bacterial resistance to current therapeutics and a decline in new antibiotic development. This results in rising numbers of untreatable health complications and deaths worldwide[1]. There is thus an urgent need to identify new antibacterial strategies to effectively treat drug-resistant pathogens. The demand for such new strategies has encouraged scientists to investigate biologically-abundant antimicrobial tools that can be manipulated to kill bacteria. Repurposing and modifying known natural antimicrobial proteins may contribute to successful development of new therapeutic strategies.

Antimicrobial peptides (AMPs) have broad spectrum antimicrobial activity and are found ubiquitously in nature. They have been extensively studied as a promising option to combat multidrug-resistant bacteria. However, the rapid ability of bacteria to evolve requires new approaches to limit potential bacterial resistance to AMPs[2–4]. Here, we discuss the use of AMPs in conjunction with other antimicrobials to form antimicrobial synergy, in which the combined antimicrobial effect is greater than the sum of either treatment alone. Antimicrobial synergy could potentially reduce the rise of bacterial resistance. A number of synergistic approaches using AMPs have been sought, with 300 reports made during the last 5 years as determined by PubMed. We examine and propose potential mechanisms that give rise to antimicrobial synergy with AMPs.

1.3 Physiological Roles

AMPs are ubiquitously observed in nature and are known for their physiological antimicrobial roles. They are produced by both prokaryotic and eukaryotic organisms, ranging from bacteria[5,6], insects[7–9], amphibians[10–12], and humans[13–16]. AMPs protect organisms from microbial harm and thus play vital roles in innate immunity[17] by directly or indirectly killing microbes. AMPs directly kill microbes by acting at the bacterial membrane[18,19] or eliciting bacterial cell death via inhibition of macromolecular functions[20]. AMPs indirectly kill microbes by directing cytokines to sites of infection for increased immunological responses in hosts[21]. Neutrophils, the first line of innate immune defense, have dense granules that are packed with AMPs that are used to defend against microbial infections[22]. When stimulated, neutrophils can also release their intracellular contents to form neutrophil extracellular traps (NETs). These web-like structures, consisting of DNA, AMPs, and other antimicrobial agents, can entrap and kill bacteria[23,24]. Similar to neutrophil elastases, AMPs have vital roles in NETs in controlling microbial threats[25]. A recent report indicates that AMPs also localize to cellular lipid droplets with histones[26] and contribute to lipid-droplet based cellular immunity.

1.4 Structure and Function

AMPs are typically small peptides, ranging from about 5 to 50 amino acids, but can be as large as over 100 amino acids[27]. Most AMPs are positively charged (+2 to +9) due to their high proportions of arginine and lysine residues[28], though negatively charged AMPs do also exist[29,30,21]. Structures of AMPs include α-helix, β-sheet, extended, and loop[31], with α-helix and β-sheet structures being the most common. More complex structures also exist, including cyclic and lasso peptides[32]. AMPs are known for their amphipathic nature, typically consisting 50% of hydrophobic

residues including alanine, glycine, and leucine[28,33]. The biophysical properties of AMPs contribute to their potent antimicrobial activity. Cationic (positively charged) AMPs can bind to anionic (negatively charged) lipopolysaccharide (LPS) and lipoteichoic acid (LTA), which are major components of bacterial membranes[34]. The amphipathic nature of AMPs also enables them to interact with and insert into bacterial cell membranes.

Many reports attribute the antimicrobial activity of AMPs to the formation of pores within bacterial membranes, which can elicit cell damage and death. Several different classes of AMP-induced membrane pores have been proposed, including barrel-stave, toroidal, and carpet[20]. In a barrel-stave model, peptide monomers form a transmembrane channel that is parallel to bacterial membrane phospholipids. A toroidal model proposes that AMPs insert into bacterial cell membranes and force membrane lipid structures to change in conformation, as opposed to pore insertion through an intact membrane like that of the barrel-stave model. The carpet model suggests that AMPs do not form transmembrane pores but instead localize to the bacterial membrane surface, where they disrupt membrane organization and integrity[35]. These membrane disruptions can cause loss of bacterial membrane proton gradient, cell leakage, and eventually cell death[19]. Alternative models to pore formation in membranes have also been proposed, with pore formation and cell leakage being attributed to the high concentrations of AMPs that are typically used in membrane pore formation studies[35]. In particular, the entry of AMPs into bacterial cells may induce intracellular damage, including disruption of bacterial nucleic acid synthesis, protein synthesis, cell wall synthesis, and cell division[20].

1.5 Bacterial Resistance to AMPs

LPS in Gram-negative bacterial membranes and LTA in Gram-positive cell walls contribute to overall negative charges of bacterial cell exteriors. Negatively charged membranes, which are conserved among bacteria, provide cytoplasmic rigidity and proper cationic gradients that are necessary for bacterial survival[36]. However, cationic AMPs can easily bind to anionic components of bacterial membranes via electrostatic interactions to elicit cell damage. Complete bacterial resistance to AMPs is unlikely because evolving a bacterial membrane that possesses an outer neutral or positive charge simply for the purpose of avoiding AMPs would be too evolutionarily costly[37,38]. Still, many studies have shown that bacteria can have intrinsic resistance or evolve resistance to AMPs[2–4,39,40].

A vast array of bacterial resistance and defense mechanisms against AMPs exist, including the utilization of efflux pumps[41–43], modifications to cell membrane charge[38], expression of protective barriers around bacterial membranes [44], inhibition of antimicrobials via peptide cleavage[45,46], and potential membrane healing and recovery post-damage[47]. Both multidrug-resistant Gram-negative and Gram-positive bacteria utilize efflux pump mechanisms to actively pump AMPs back out into the extracellular environment to prevent cell damage[41,42]. In Gram-negative *S.* Typhimurium and *P. aeruginosa*, the lipid A portion of LPS is modified with the addition of 4-amino-4-deoxy-L-arabinose, which reduces the overall negative charge and thus reduces the binding affinity of positively charged AMPs, including azurocidin, polymyxin B (PMB), indolicidin, and LL-37[48–50]. In Gram-positive *S. aureus*, lysine is added to membrane phospholipids, reducing the overall anionic charge and affinity to defensin-like cationic AMPs[51]. Colanic acid is a polysaccharide which functions as a protective capsule around many *Enterobacteriaceae*[52] and may prevent AMP-mediated activity. It has been suggested that these

capsular polysaccharides play a role in bacterial resistance[40,53] and virulence[54,55]; capsular polysaccharides increase resistance of *K. pneumoniae*, *S. pneumoniae*, and *P. aeruginosa* to both PMB and human neutrophil alpha-defensin 1[53]. Additionally, increased slime production by *S. epidermidis* in medical catheters has been reported when bacterial capsular polysaccharides are expressed[54,55]. Bacterial species like *E. coli* and *S.* Typhimurium also release proteases to cleave and inhibit antimicrobials that threaten their survival, particularly protamine and alpha helical cationic AMPs, respectively[45,46].

Recent work suggests that bacteria can recover from pores formed by LL-37[47]. However, the duration in which AMPs can keep bacterial pores open and the extent to which bacteria can repair these pores is unknown. It is possible that efflux pumps are used to eject AMPs out of the membrane to allow for bacterial lipid bilayers to reform. Additionally, bacterial cell wall biosynthesis may be upregulated for the purpose of membrane repair.

1.6 Antimicrobial Synergies with AMPs

1.6.1 AMP Synergy Could Reduce Antimicrobial Resistance

To optimize the use of antibiotics, it is important to mitigate potential bacterial resistance mechanisms. Many AMPs have been tested in clinical trials due their potent antimicrobial activity[56,57]. However, as with any antibiotic, using AMPs is associated with the risk of ever-evolving bacterial resistance that could negate their effects. A potential way to reduce the risk of drug-resistance to AMPs in clinical settings is to use AMPs in conjunction with other antimicrobials, focusing on combinations that lead to effective antimicrobial synergies. Synergistic combinations that have multiple targets in independent pathways could require two independent

and simultaneous sets of mutations to address both challenges. Synergy could also be more lethal, decreasing the likelihood that bacteria can escape and develop resistance.

It has been suggested that bacteria are less likely to evolve resistance to antibiotic cocktails than to a single antimicrobial[58,59]. Consistent with this is the fact that multiple AMPs are released during immune responses *in vivo*, making it difficult for bacteria to develop resistance[60]. Therefore, using AMP cocktails, especially ones that convey antimicrobial synergy, could be an effective strategy. Synergistic antibacterial combinations with AMPs could enable bacterial pores to stay open for longer durations, prevent pore repair, increase perturbation of bacterial intracellular functions, or convey other independent but complementary bacterial killing mechanisms. These mechanisms may potentially increase antimicrobial efficacy, decrease resistance, and reduce host toxicity if only low concentrations of each antimicrobial component are needed to carry out a large antimicrobial effect[61]. The abundance of antimicrobial synergies discovered with AMPs presents exciting possibilities for the potential use of synergistic AMP combinations in clinical settings.

1.6.2 Synergy with Other AMPs

Numerous reports indicate that AMPs synergize with other AMPs. We discuss antimicrobial synergies of AMPs from organisms like insects, amphibians, and mammals, suggesting that synergistic interactions are common between AMPs within the animal kingdom.

The insect AMPs, diptericins and attacins, show synergistic killing against *P. burhodogranariea* in flies[62]. A combination of the synthetic AMP pexiganan and bumblebee AMP melittin show *S. aureus* killing effects comparable to that of Vancomycin, a last line of defense antibiotic[39]. Additionally, the antimicrobial activity of a bumblebee AMP, abaecin, is

synergistically enhanced by the presence of a pore forming AMP, hymenoptaecin[63]. In this example, hymenoptaecin forms membrane pores, potentially causing cell leakage or lytic cell death and enabling the entry of abaecin into bacterial cells. The hymenoptaecin-induced pores may increase the ability for abaecin to access and bind to DnaK, a molecular chaperone, to inhibit bacterial replication[63]. Thus, the two AMPs work together to kill bacteria on both a membrane and intracellular level.

AMPs can potentially bind to other AMPs to form more potent antibacterial agents. For example, the amphibian AMPs magainin-2 and peptidyl-glycylleucine-carboxyamide (PGLa) work synergistically to inhibit *E. coli* growth[11]. When magainin-2 and PGLa are added together, they form a "supramolecule" to quickly induce bacterial membrane pores and mediate pore stabilization[64]. Moreover, it has been reported that PGLa forms an antiparallel dimer that spans the cell membrane where it binds to magainin-2 at the C-terminus[65], forming toroidal pore structures [66]. These results are consistent with an additional report in which fused AMPs induce greater killing activities in *S. mutans* than on their own[67]. These findings suggest that AMPs can bind other AMPs or other types of antimicrobials to give rise to antimicrobial synergy.

The mammalian AMP protegrin 1 has been reported to exhibit synergistic killing activity with indolicidin, LL-37, and bactenecin against *P. aeruginosa* and *E. coli*[68]. Additionally, the combination of indolicidin and bactenecin gives rise to antimicrobial synergy against *E. coli*[68]. The combinations of protegrin 1 with LL-37, bactenecin with LL-37, and protegrin 1 with bactenecin are also synergistic against *E. faecalis*[68]. Lastly, human platelet-derived synthetic AMP combinations of PD1 through PD4 and Arg-Trp repeats RW1 through RW5 are synergistically antimicrobial in platelets[69].

AMPs can be effective when their mechanisms are complementary, such as in the case of the AMPs coleoptericin and defensin. Coleoptericin contributes to the survival of the mealworm beetle, *Tenebrio molitor*, but does not reduce bacterial load. In contrast, defensin does not improve host survival but reduces bacterial load[70]. Their combined use both significantly increases host survival and reduces bacterial load[70]. Using multiple AMPs together can thus maintain the independent functions of each AMP, resulting in a more effective treatment strategy.

While many studies demonstrate robust antimicrobial synergies with just two AMPs, synergies with three AMPs reveal even greater effects. For example, while apidaecin functions antagonistically with either pexiganan or LL 19-27 (an analog of LL-37), the triple combination of apidaecin, pexiganan, and LL 19-27 demonstrate strong synergism[58]. Synergy was also observed from the combination of human β-defensin, LL-37, and lysozyme, which are produced on the skin, against *S. aureus* and *E. coli*[13]. The observation of synergy between these antimicrobials is an example in which natural defense molecules have greater activity in combination rather than individually. Thus, combining natural antimicrobials could yield further discoveries of synergy.

1.6.3 Synergy with Antibiotics

AMPs can also synergize with antibiotics, and in some cases, overcoming antibiotic resistance. The use of AMPs to increase the efficacy of already approved antibiotics appears to be a promising option to combat commonly drug-resistant pathogens. The human AMPs, LL-37 and human β-defensin 3 (HBD3), have antimicrobial synergy with the antibiotics tigecycline, moxifloxacin, piperacillin-tazobactam, and meropenem. Specifically, antibiotic killing against *C. difficile* is improved when both LL-37 and HBD3 are present[71]. Lastly, LL 17-29 establishes

antimicrobial synergy with the antibiotic chloramphenicol against highly virulent bacterial strains, including methicillin-resistant *S. aureus* and multidrug-resistant *P. aeruginosa*[59].

In addition, combining the AMPs nisin Z, pediocin, or colistin with various antibiotics, including penicillin, ampicillin, or rifampicin, is effective in overcoming antibiotic-resistance in *P. fluorescens*[72]. Also, the AMP melamine has synergistic killing activities when paired with ciprofloxacin, a fluoroquinolone antibiotic, against antibiotic-resistant strains of *P. aeruginosa*. This combination may aid in overcoming *P. aeruginosa* resistance to fluoroquinolone antibiotics[73]. Synergistic combinations of AMPs with PMB (originally discovered as an AMP), erythromycin, and tetracycline have also been shown. In particular, variants of the AMP indolicidin synergize with the antibiotics PMB, tobramycin, gentamycin, and amikacin[74].

One of the mechanisms by which AMPs improve antibiotic function is by disrupting bacterial membranes to aid in the delivery of antibiotics into the bacterial cytoplasm, where antibiotics can act on intracellular targets. For example, the AMP arenicin-1 synergistically functions with antibiotics including ampicillin, erythromycin, and chloramphenicol to kill *S. aureus*, *S. epidermis*, *P. aeruginosa*, and *E. coli*[75]. Arenicin-1 assists in the uptake of antibiotics into cells and inhibits bacterial growth via hydroxyl radical formation[75], which suggests complementary mechanisms are at play.

1.6.4 Synergy with Histones

Histones, more commonly known for their roles in condensing eukaryotic DNA, have antibacterial properties[76,77]. However, the mechanisms by which histones kill bacteria have not previously been understood[78]. Since histones are positively charged and have similar structures to that of AMPs, it has been suggested that histones and AMPs have redundant antibacterial roles[79,80].

Histones and AMPs colocalize in innate immunity components, including on cellular lipid droplets and in NETs, suggesting that they could work together to kill microbes[81,82,26,83]. For fish in particular, fractions of salmon histone H1 have reported antimicrobial synergy with lysozyme and a flounder AMP, pleurocidin[84]. Recent work demonstrates that histones H2A and H3 can function with the pore-forming AMPs LL-37 and magainin-2 to produce antibacterial synergy against Gram-positive and Gram-negative bacteria[47]. Additionally, H2A and the pore-forming antimicrobial PMB synergistically work together to completely inhibit *E. coli* growth over 24 hours[47]. It is important to note that histones must be paired with pore forming AMPs in order for this synergistic model to be effective; histones alone have minimal antimicrobial effects at physiological conditions[47]. It is possible that other histones, histone fragments, and histone-like peptides also amplify the antimicrobial effects of AMPs and give rise to antimicrobial synergy.

The mechanism of synergy between AMPs and histones is due the ability of AMPs to form pores in bacterial membranes, enabling histones to enter the bacterial cytoplasm[47,85]. Here, histones inhibit global transcription and reorganize bacterial chromosomes. Furthermore, histones enhance AMP-mediated pores that bacteria otherwise would be able to recover from, leading to reduced cell sizes and increased cytoplasmic leakage[47]. The uptake of AMPs and histones into bacterial cells elicits an effective antimicrobial response consistent with a positive feedback loop[47]. Importantly, if bacterial intracellular functions, like transcription and translation, are inhibited, this could reduce bacterial cell membrane integrity and repair.

Another potential effect of histones is that they may induce stress on bacterial membranes. This membrane stress could aid AMPs to more effectively form bacterial membrane pores. Altered membrane physiology, revealed through scanning electron microscopy (SEM), suggests that when bacteria are treated with only an individual AMP or histone, the membrane largely remains intact

(**Fig. 1.1**). However, the treatment with both AMPs and histones induces gross cell deformation and leakage of cytoplasmic contents (**Fig. 1.1**). The reduced membrane integrity from the AMP and histone treatment also inhibits *E. coli* from maintaining their proton gradient, which is necessary for ATP production[47]. Thus, membrane damage caused by synergistic combinations with AMPs may lead to lack of recovery from AMP-mediated pores, rapid loss of cytoplasmic content, failure to produce ATP, and ultimately bacterial cell death. In response to histone exposure, the *rcs* gene responsible for colanic acid expression is upregulated in *E. coli*[47]. The bacterial upregulation of colanic acid, which functions as a bacterial membrane protective capsule, suggests that there is an active microbial attempt to mitigate potential membrane stress effects due to histones.
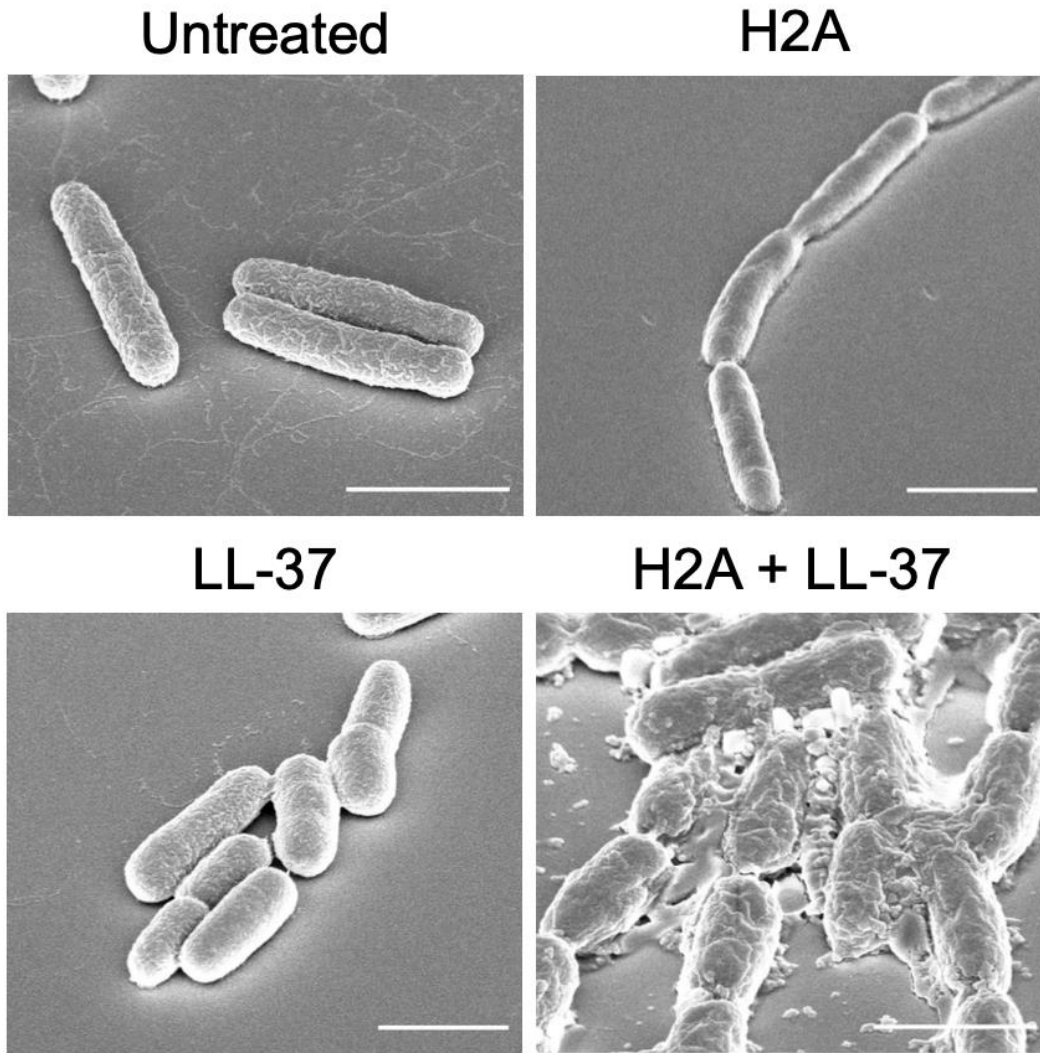
Figure 1.1. Scanning Electron Micrographs of Untreated *E. coli* or *E. coli* treated with H2A, LL-37, or Both. *E. coli* that are treated with both H2A and LL-37 demonstrate extensive cellular damage. Scale bars indicate 2 µm.

1.6.5 Synergy with Other Antimicrobial Agents

AMPs also synergize with other antimicrobial agents. For example, silver nitrate and silver nanoparticles can synergize with PMB and Gramicidin S, enhancing their intracellular antimicrobial effects in Gram-negative bacteria[86]. Additionally, peptoid analogs of AMPs are known to have effective and specific antimicrobial activity[87]. AMPs can synergize with peptoids against Gram-negative bacteria [88]. The AMP *Galleria mellonella* anionic peptide 2 and antimicrobial enzyme lysozyme are also synergistic against Gram-negative bacteria[89].

1.7 Conclusion

The combination of AMPs with current antimicrobial strategies can produce synergy through a number of distinct mechanisms (**Fig. 1.2**). The introduction of antibiotics inside bacteria has often been a challenge. However, AMPs can address this challenge by forming membrane pores, thus facilitating entry of antibiotics into the cytoplasm, where the antibiotics can bind to their intracellular targets. The combination of AMPs with antibiotics could thus be an effective antibacterial strategy. This strategy could limit bacterial resistance because defense from the multifaceted attack could be significantly more difficult to achieve.

If the ability for AMPs to synergize with other AMPs or antimicrobials is a conserved characteristic, then relatively low doses of each antimicrobial can be used as antibiotic treatments to exhibit large antimicrobial effects. Lower drug concentrations might also limit harmful side effects. For example, PMB is now an FDA-approved and potent last-resort antibiotic; however, PMB is also highly toxic to the nephrotic and nervous systems[90,91]. Using PMB in a synergistic antimicrobial combination, like with indolicidin or histones, would potentially require lower doses of each antimicrobial agent, potentially reducing host toxicity, while maintaining effective

antimicrobial activity. Since the production of peptides can be costly, taking advantage of lower antimicrobial doses needed for synergistic treatments may also reduce production expenses. If toxicity remains an issue even with the low doses required in synergistic antimicrobial combinations, changing amino acids on AMPs has been shown to have strong effects on synergy[74]. Moreover, AMPs that can synergize with preexisting AMPs in hosts could be especially potent *in vivo*, due to the activation of natural AMP release by the immune system. In innate immunity, humans express LL-37; therefore, synergies that arise with LL-37, like histones and protegrin 1, would be especially critical to consider for antibiotic applications.

Synergistic antimicrobial combinations are promising candidates that reduce potential bacterial resistance, overcome preexisting resistance to current antibiotics, prevent host toxicity, and increase antimicrobial efficacy. Thus, an improved understanding of mechanisms by which AMPs synergize with other antimicrobials is necessary. Moving forward, the synergistic interactions between AMPs and other antimicrobials will provide promising options to be explored in the development of new antibiotics.
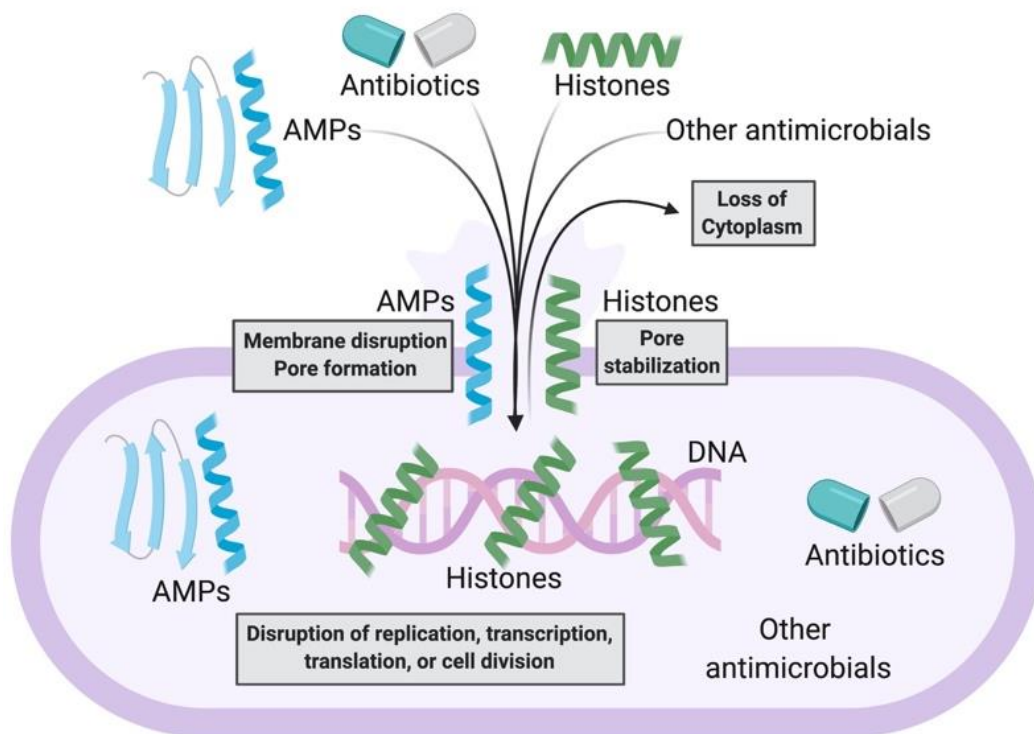
Figure 1.2. Model of Antimicrobial Synergy Between AMPs and Other AMPs, Antibiotics, Histones, and Other Antimicrobials. AMPs form bacterial membrane pores or disrupt bacterial membranes. This enables the entry of more AMPs, antibiotics, histones, or other antimicrobials into bacteria. As a result, there is loss of bacterial cytoplasm and disruption of bacterial macromolecular functions. Histones potentially stabilize AMP-induced pores that enable further synergistic antimicrobial activity.

1.8 References

1. Ventola, C. L. The Antibiotic Resistance Crisis. *Pharm. Ther.* **40**, 277–283 (2015).

2. El Shazely, B., Yu, G., Johnston, P. R. & Rolff, J. Resistance Evolution Against Antimicrobial Peptides in Staphylococcus aureus Alters Pharmacodynamics Beyond the MIC. *Front. Microbiol.* **11**, (2020).

3. Bauer, M. E. & Shafer, W. M. On the in vivo significance of bacterial resistance to antimicrobial peptides. *Biochim. Biophys. Acta* **1848**, 3101–3111 (2015).

4. Anaya-López, J. L., López-Meza, J. E. & Ochoa-Zarzosa, A. Bacterial resistance to cationic antimicrobial peptides. *Crit. Rev. Microbiol.* **39**, 180–195 (2013).

5. McCafferty, D. G., Cudic, P., Yu, M. K., Behenna, D. C. & Kruger, R. Synergy and duality in peptide antibiotic mechanisms. *Curr. Opin. Chem. Biol.* **3**, 672–680 (1999).

6. Nes, I. F., Diep, D. B. & Holo, H. Bacteriocin Diversity in Streptococcus and Enterococcus. *J. Bacteriol.* **189**, 1189–1198 (2007).

7. Choi, J. H. *et al.* Melittin, a honeybee venom-derived antimicrobial peptide, may target methicillin-resistant Staphylococcus aureus. *Mol. Med. Rep.* **12**, 6483–6490 (2015).

8. Romanelli, A. *et al.* Peptides from Royal Jelly: studies on the antimicrobial activity of jelleins, jelleins analogs and synergy with temporins. *J. Pept. Sci.* **17**, 348–352 (2011).

9. Wu, Q., Patočka, J. & Kuča, K. Insect Antimicrobial Peptides, a Mini Review. *Toxins* **10**, (2018).

10. Mor, A., Hani, K. & Nicolas, P. The vertebrate peptide antibiotics dermaseptins have overlapping structural features but target specific microorganisms. *J. Biol. Chem.* **269**, 31635–31641 (1994).

11. Westerhoff, H. V. *et al.* Functional Synergism of the Magainins PGLa and Magainin-2 in Escherichia coli, Tumor Cells and Liposomes. *Eur. J. Biochem.* **228**, 257–264 (1995).

12. Patocka, J., Nepovimova, E., Klimova, B., Wu, Q. & Kuca, K. Antimicrobial Peptides: Amphibian Host Defense Peptides. *Curr. Med. Chem.* **26**, 5924–5946 (2019).

13. Chen, X. *et al.* Synergistic effect of antibacterial agents human beta-defensins, cathelicidin LL-37 and lysozyme against Staphylococcus aureus and Escherichia coli. *J. Dermatol. Sci.* **40**, 123–132 (2005).

14. Singh, P. K., Tack, B. F., McCray, P. B. & Welsh, M. J. Synergistic and additive killing by antimicrobial factors found in human airway surface liquid. *Am. J. Physiol. Lung Cell. Mol. Physiol.* **279**, L799-805 (2000).

15. Tollin, M. *et al.* Antimicrobial peptides in the first line defence of human colon mucosa. *Peptides* **24**, 523–530 (2003).

16. Wang, G. Human Antimicrobial Peptides and Proteins. *Pharmaceuticals* **7**, 545–594 (2014).

17. Diamond, G., Beckloff, N., Weinberg, A. & Kisich, K. O. The Roles of Antimicrobial Peptides in Innate Host Defense. *Curr. Pharm. Des.* **15**, 2377–2392 (2009).

18. Lehrer, R. I. *et al.* Interaction of human defensins with Escherichia coli. Mechanism of bactericidal activity. *J. Clin. Invest.* **84**, 553–561 (1989).

19. Shai, Y. Mode of action of membrane active antimicrobial peptides. *Biopolymers* **66**, 236–248 (2002).

20. Le, C.-F., Fang, C.-M. & Sekaran, S. D. Intracellular Targeting Mechanisms by Antimicrobial Peptides. *Antimicrob. Agents Chemother.* **61**, (2017).

21. Lai, Y. & Gallo, R. L. AMPed Up immunity: how antimicrobial peptides have multiple roles in immune defense. *Trends Immunol.* **30**, 131–141 (2009).

22. Wetering, S. van, Tjabringa, G. S. & Hiemstra, P. S. Interactions between neutrophil-derived antimicrobial peptides and airway epithelial cells. *J. Leukoc. Biol.* **77**, 444–450 (2005).

23. Fuchs, T. A. *et al.* Novel cell death program leads to neutrophil extracellular traps. *J. Cell Biol.* **176**, 231–241 (2007).

24. Brinkmann, V. *et al.* Neutrophil Extracellular Traps Kill Bacteria. *Science* **303**, 1532–1535 (2004).

25. Rocha, J. D. B. *et al.* Capsular polysaccharides from Cryptococcus neoformans modulate production of neutrophil extracellular traps (NETs) by human neutrophils. *Sci. Rep.* **5**, (2015).

26. Bosch, M. *et al.* Mammalian lipid droplets are innate immune hubs integrating cell metabolism and host defense. *Science* **370**, (2020).

27. Bahar, A. A. & Ren, D. Antimicrobial Peptides. *Pharmaceuticals* **6**, 1543–1575 (2013).

28. Yeaman, M. R. & Yount, N. Y. Mechanisms of Antimicrobial Peptide Action and Resistance. *Pharmacol. Rev.* **55**, 27–55 (2003).

29. Brogden, K. A. Antimicrobial peptides: pore formers or metabolic inhibitors in bacteria? *Nat. Rev. Microbiol.* **3**, 238–250 (2005).

30. Steffen, H. *et al.* Naturally processed dermcidin-derived peptides do not permeabilize bacterial membranes and kill microorganisms irrespective of their charge. *Antimicrob. Agents Chemother.* **50**, 2608–2620 (2006).

31. Powers, J.-P. S. & Hancock, R. E. W. The relationship between peptide structure and antibacterial activity. *Peptides* **24**, 1681–1691 (2003).

32. Koehbach, J. & Craik, D. J. The Vast Structural Diversity of Antimicrobial Peptides. *Trends Pharmacol. Sci.* **40**, 517–528 (2019).

33. Wang, G., Li, X. & Wang, Z. APD2: the updated antimicrobial peptide database and its application in peptide design. *Nucleic Acids Res.* **37**, D933-937 (2009).

34. Sitaram, N. & Nagaraj, R. Interaction of antimicrobial peptides with biological and model membranes: structural and charge requirements for activity. *Biochim. Biophys. Acta BBA - Biomembr.* **1462**, 29–54 (1999).

35. Wimley, W. C. Describing the Mechanism of Antimicrobial Peptide Action with the Interfacial Activity Model. *ACS Chem. Biol.* **5**, 905–917 (2010).

36. Farha, M. A., Verschoor, C. P., Bowdish, D. & Brown, E. D. Collapsing the Proton Motive Force to Identify Synergistic Combinations against Staphylococcus aureus. *Chem. Biol.* **20**, 1168–1178 (2013).

37. Yu, G., Baeder, D. Y., Regoes, R. R. & Rolff, J. Predicting drug resistance evolution: insights from antimicrobial peptides and antibiotics. *Proc. R. Soc. B Biol. Sci.* **285**, 20172687 (2018).

38. Andersson, D. I., Hughes, D. & Kubicek-Sutherland, J. Z. Mechanisms and consequences of bacterial resistance to antimicrobial peptides. *Drug Resist. Updat.* **26**, 43–57 (2016).

39. Dobson, A. J., Purves, J., Kamysz, W. & Rolff, J. Comparing Selection on S. aureus between Antimicrobial Peptides and Common Antibiotics. *PLoS ONE* **8**, (2013).

40. Campos, M. A. *et al.* Capsule polysaccharide mediates bacterial resistance to antimicrobial peptides. *Infect. Immun.* **72**, 7107–7114 (2004).

41. Schindler, B. D. & Kaatz, G. W. Multidrug efflux pumps of Gram-positive bacteria. *Drug Resist. Updat. Rev. Comment. Antimicrob. Anticancer Chemother.* **27**, 1–13 (2016).

42. Otrębska-Machaj, E. *et al.* Efflux Pump Blockers in Gram-Negative Bacteria: The New Generation of Hydantoin Based-Modulators to Improve Antibiotic Activity. *Front. Microbiol.* **7**, (2016).

43. Nikaido, H. Multidrug efflux pumps of gram-negative bacteria. *J. Bacteriol.* **178**, 5853–5859 (1996).

44. Pando, J. M., Karlinsey, J. E., Lara, J. C., Libby, S. J. & Fang, F. C. The Rcs-Regulated Colanic Acid Capsule Maintains Membrane Potential in Salmonella enterica serovar Typhimurium. *mBio* **8**, (2017).

45. Stumpe, S., Schmid, R., Stephens, D. L., Georgiou, G. & Bakker, E. P. Identification of OmpT as the Protease That Hydrolyzes the Antimicrobial Peptide Protamine before It Enters Growing Cells ofEscherichia coli. *J. Bacteriol.* **180**, 4002–4006 (1998).

46. Guina, T., Yi, E. C., Wang, H., Hackett, M. & Miller, S. I. A PhoP-regulated outer membrane protease of Salmonella enterica serovar typhimurium promotes resistance to alpha-helical antimicrobial peptides. *J. Bacteriol.* **182**, 4077–4086 (2000).

47. Doolin, T. *et al.* Mammalian histones facilitate antimicrobial synergy by disrupting the bacterial proton gradient and chromosome organization. *Nat. Commun.* **11**, 3888 (2020).

48. Gunn, J. S. *et al.* PmrA-PmrB-regulated genes necessary for 4-aminoarabinose lipid A modification and polymyxin resistance. *Mol. Microbiol.* **27**, 1171–1182 (1998).

49. Gunn, J. S., Ryan, S. S., Van Velkinburgh, J. C., Ernst, R. K. & Miller, S. I. Genetic and Functional Analysis of a PmrA-PmrB-Regulated Locus Necessary for Lipopolysaccharide Modification, Antimicrobial Peptide Resistance, and Oral Virulence of Salmonella enterica Serovar Typhimurium. *Infect. Immun.* **68**, 6139–6146 (2000).

50. McPhee, J. B., Lewenza, S. & Hancock, R. E. W. Cationic antimicrobial peptides activate a two-component regulatory system, PmrA-PmrB, that regulates resistance to polymyxin B and cationic antimicrobial peptides in Pseudomonas aeruginosa. *Mol. Microbiol.* **50**, 205–217 (2003).

51. Ernst, C. M. *et al.* The Bacterial Defensin Resistance Protein MprF Consists of Separable Domains for Lipid Lysinylation and Antimicrobial Peptide Repulsion. *PLOS Pathog.* **5**, e1000660 (2009).

52. Grant, W. D., Sutherland, I. W. & Wilkinson, J. F. Exopolysaccharide colanic acid and its occurrence in the Enterobacteriaceae. *J. Bacteriol.* **100**, 1187–1193 (1969).

53. Llobet, E., Tomás, J. M. & Bengoechea, J. A. Capsule polysaccharide is a bacterial decoy for antimicrobial peptides. *Microbiol. Read. Engl.* **154**, 3877–3886 (2008).

54. Christensen, G. D., Simpson, W. A., Bisno, A. L. & Beachey, E. H. Adherence of slime-producing strains of Staphylococcus epidermidis to smooth surfaces. *Infect. Immun.* **37**, 318–326 (1982).

55. Davenport, D. S. *et al.* Usefulness of a test for slime production as a marker for clinically significant infections with coagulase-negative staphylococci. *J. Infect. Dis.* **153**, 332–339 (1986).

56. Koo, H. B. & Seo, J. Antimicrobial peptides under clinical investigation. *Pept. Sci.* **111**, e24122 (2019).

57. Greber, K. E. & Dawgul, M. Antimicrobial Peptides Under Clinical Trials. *Curr. Top. Med. Chem.* **17**, 620–628 (2017).

58. Yu, G., Baeder, D. Y., Regoes, R. R. & Rolff, J. Combination Effects of Antimicrobial Peptides. *Antimicrob. Agents Chemother.* **60**, 1717–1724 (2016).

59. Rajasekaran, G., Kim, E. Y. & Shin, S. Y. LL-37-derived membrane-active FK-13 analogs possessing cell selectivity, anti-biofilm activity and synergy with chloramphenicol and anti-inflammatory activity. *Biochim. Biophys. Acta Biomembr.* **1859**, 722–733 (2017).

60. Pasupuleti, M., Schmidtchen, A. & Malmsten, M. Antimicrobial peptides: key components of the innate immune system. *Crit. Rev. Biotechnol.* **32**, 143–171 (2012).

61. Xu, X. *et al.* Synergistic combination of two antimicrobial agents closing each other's mutant selection windows to prevent antimicrobial resistance. *Sci. Rep.* **8**, 7237 (2018).

62. Hanson, M. A. *et al.* Synergy and remarkable specificity of antimicrobial peptides in vivo using a systematic knockout approach. *eLife* **8**, e44341 (2019).

63. Rahnamaeian, M. *et al.* Insect antimicrobial peptides show potentiating functional interactions against Gram-negative bacteria. *Proc. R. Soc. B Biol. Sci.* **282**, (2015).

64. Matsuzaki, K. *et al.* Mechanism of synergism between antimicrobial peptides magainin 2 and PGLa. *Biochemistry* **37**, 15144–15153 (1998).

65. Zerweck, J. *et al.* Molecular mechanism of synergy between the antimicrobial peptides PGLa and magainin 2. *Sci. Rep.* **7**, 13153 (2017).

66. Tremouilhac, P., Strandberg, E., Wadhwani, P. & Ulrich, A. S. Synergistic Transmembrane Alignment of the Antimicrobial Heterodimer PGLa/Magainin. *J. Biol. Chem.* **281**, 32089–32094 (2006).

67. He, J. *et al.* Novel Synthetic Antimicrobial Peptides against Streptococcus mutans. *Antimicrob. Agents Chemother.* **51**, 1351–1358 (2007).

68. Yan, H. & Hancock, R. E. W. Synergistic Interactions between Mammalian Antimicrobial Defense Peptides. *Antimicrob. Agents Chemother.* **45**, 1558–1560 (2001).

69. Mohan, K. V. K., Rao, S. S., Gao, Y. & Atreya, C. D. Enhanced antimicrobial activity of peptide-cocktails against common bacterial contaminants of ex vivo stored platelets. *Clin. Microbiol. Infect. Off. Publ. Eur. Soc. Clin. Microbiol. Infect. Dis.* **20**, O39-46 (2014).

70. Zanchi, C., Johnston, P. R. & Rolff, J. Evolution of defence cocktails: Antimicrobial peptide combinations reduce mortality and persistent infection. *Mol. Ecol.* **26**, 5334–5343 (2017).

71. Naghmouchi, K., Le Lay, C., Baah, J. & Drider, D. Antibiotic and antimicrobial peptide combinations: synergistic inhibition of Pseudomonas fluorescens and antibiotic-resistant variants. *Res. Microbiol.* **163**, 101–108 (2012).

72. Kampshoff, F., Willcox, M. D. P. & Dutta, D. A Pilot Study of the Synergy between Two Antimicrobial Peptides and Two Common Antibiotics. *Antibiotics* **8**, 60 (2019).

73. Ruden, S. *et al.* Synergy Pattern of Short Cationic Antimicrobial Peptides Against Multidrug-Resistant Pseudomonas aeruginosa. *Front. Microbiol.* **10**, (2019).

74. Choi, H. & Lee, D. G. Synergistic effect of antimicrobial peptide arenicin-1 in combination with antibiotics against pathogenic bacteria. *Res. Microbiol.* **163**, 479–486 (2012).

75. Nuding, S., Frasch, T., Schaller, M., Stange, E. F. & Zabel, L. T. Synergistic Effects of Antimicrobial Peptides and Antibiotics against Clostridium difficile. *Antimicrob. Agents Chemother.* **58**, 5719–5725 (2014).

76. Miller, B. F., Abrams, R., Dorfman, A. & Klein, M. ANTIBACTERIAL PROPERTIES OF PROTAMINE AND HISTONE. *Science* **96**, 428–430 (1942).

77. Hirsch, J. G. Bactericidal action of histone. *J. Exp. Med.* **108**, 925–944 (1958).

78. Doolin, T., Gross, S. & Siryaporn, A. Physical Mechanisms of Bacterial Killing by Histones. in *Physical Microbiology* (eds. Duménil, G. & van Teeffelen, S.) 117–133 (Springer International Publishing, 2020). doi:10.1007/978-3-030-46886-6_7.

79. Kawasaki, H., Isaacson, T., Iwamuro, S. & Conlon, J. M. A protein with antimicrobial activity in the skin of Schlegel's green tree frog Rhacophorus schlegelii (Rhacophoridae) identified as histone H2B. *Biochem. Biophys. Res. Commun.* **312**, 1082–1086 (2003).

80. Pavia, K. E., Spinella, S. A. & Elmore, D. E. Novel Histone-Derived Antimicrobial Peptides Use Different Antimicrobial Mechanisms. *Biochim. Biophys. Acta* **1818**, 869–876 (2012).

81. Cermelli, S., Guo, Y., Gross, S. P. & Welte, M. A. The Lipid-Droplet Proteome Reveals that Droplets Are a Protein-Storage Depot. *Curr. Biol.* **16**, 1783–1795 (2006).

82. Anand, P. *et al.* A novel role for lipid droplets in the organismal antibacterial response. *eLife* **1**, (2012).

83. Brinkmann, V. & Zychlinsky, A. Neutrophil extracellular traps: Is immunity the second function of chromatin? *J. Cell Biol.* **198**, 773–783 (2012).

84. Patrzykat, A., Zhang, L., Mendoza, V., Iwama, G. K. & Hancock, R. E. W. Synergy of Histone-Derived Peptides of Coho Salmon with Lysozyme and Flounder Pleurocidin. *Antimicrob. Agents Chemother.* **45**, 1337–1342 (2001).

85. Duong, L., Gross, S. P. & Siryaporn, A. A novel antibacterial strategy: histone and antimicrobial peptide synergy. *Microb. Cell* **7**, 309–311 (2020).

86. Ruden, S., Hilpert, K., Berditsch, M., Wadhwani, P. & Ulrich, A. S. Synergistic Interaction between Silver Nanoparticles and Membrane-Permeabilizing Antimicrobial Peptides. *Antimicrob. Agents Chemother.* **53**, 3538–3540 (2009).

87. Chongsiriwatana, N. P. *et al.* Peptoids that mimic the structure, function, and mechanism of helical antimicrobial peptides. *Proc. Natl. Acad. Sci. U. S. A.* **105**, 2794–2799 (2008).

88. Chongsiriwatana, N. P., Wetzler, M. & Barron, A. E. Functional synergy between antimicrobial peptoids and peptides against Gram-negative bacteria. *Antimicrob. Agents Chemother.* **55**, 5399–5402 (2011).

89. Zdybicka-Barabas, A. *et al.* Synergistic action of Galleria mellonella anionic peptide 2 and lysozyme against Gram-negative bacteria. *Biochim. Biophys. Acta BBA - Biomembr.* **1818**, 2623–2635 (2012).

90. Falagas, M. E. & Kasiakou, S. K. Toxicity of polymyxins: a systematic review of the evidence from old and recent studies. *Crit. Care* **10**, R27 (2006).

91. Zavascki, A. P. & Nation, R. L. Nephrotoxicity of Polymyxins: Is There Any Difference between Colistimethate and Polymyxin B? *Antimicrob. Agents Chemother.* **61**, e02319-16 (2017).

CHAPTER 2: HISTONE AND AMP ANTIMICROBIAL SYNERGY

Originally published in: Leora Duong, Steven P. Gross, and Albert Siryaporn (2020). A novel antibacterial strategy: histone and antimicrobial peptide synergy. Microbial Cell 7(11): 309-311.

2.1 Introduction

The rate at which antibiotics are discovered and developed has stagnated; meanwhile, antibacterial resistance continually increases and leads to a plethora of untreatable and deadly infections worldwide. Therefore, there is a critical need to develop new antimicrobial strategies to combat this alarming reality. One approach is to understand natural antimicrobial defense mechanisms that higher-level organisms employ in order to kill bacteria, potentially leading to novel antibiotic therapeutic approaches. Mammalian histones have long been reported to have antibiotic activity, with the first observation of their antibacterial properties reported in 1942[1]. However, there have been doubts about whether histones could truly have any such role in the animal, predominantly based on two issues: they are found in the nucleus (so are not in a position to encounter bacteria), and their antibiotic activity *in vitro* has been relatively weak in physiological conditions. More recent studies have addressed both sets of concerns. Histones are released from cells as part of neutrophil extracellular traps (NETs)[2] and are thus able to encounter extracellular bacteria. Histones are also present intracellularly in the cytoplasm attached to lipid droplets, positioning them to encounter cytosolic bacteria. Our recent work[3], which is discussed here, shows that histones have synergistic antimicrobial activities when they are paired with antimicrobial peptides (AMPs), which form pores in bacterial membranes and co-localize with histones in NETs. The work demonstrates that histones enhance AMP-mediated pores, impair

30

bacterial membrane recovery, depolarize the bacterial proton gradient, and enter the bacterial cytoplasm, where they restructure the chromosome and inhibit transcription. Here, we examine potential mechanisms that are responsible for these outcomes.

At physiological ionic concentrations *in vitro*, histones by themselves have little impact on bacterial growth. The work sought to address an outstanding question in the field: why do histones exhibit relatively weak antimicrobial activity *in vitro* despite having clear antimicrobial activity *in vivo*? The work provides a potential answer to this by recognizing that *in vivo*, histones are not by themselves but are instead surrounded by other antimicrobial molecules. In both NETs and lipid droplets[4], histones co-localize with pore-forming AMPs[5,6]. By themselves, pore-forming AMPs, including LL-37, magainin-2, and polymyxin B, have inhibitory effects on bacterial growth. However, when these AMPs are paired with histones, the inhibitory effect is amplified and synergistic[3]. That is, the combined inhibitory effect of AMPs and histones on bacterial growth is greater than the sum of the individual effects.

Such synergistic antimicrobial interactions could improve the efficacy of new and existing antimicrobial agents. How does the synergy between histones and AMPs arise? The study focuses on the activity of histone H2A, one of the four core histone proteins, and the cathelicidin-derived AMP LL-37[7]. Both H2A and LL-37 are comparable in size (14 and 18 kDa, respectively), are cationic, contain a high proportion of hydrophobic amino acids, and possess the ability to form alpha helices. The overlapping similarities suggest that both molecules have similar impacts on bacterial physiology. The work reveals, however, that the molecules perform distinct functions and that the complementarity of the mechanisms give rise to synergistic antimicrobial activity. For example, whereas LL-37 alone increases membrane permeability, H2A alone has little impact. While H2A binds DNA and condenses chromosomes, LL-37 has no such function. When LL-37

and H2A are paired together, these functions combine and produce irreparable damage by targeting two sites: the bacterial membrane and the cytoplasm. Other AMPs, including magainin-2 and polymyxin-B, exhibit similar antimicrobial synergies with H2A. How exactly does this enhancement by histones work?

2.2 Histones Enhance Membrane Permeation

LL-37 has previously been reported to inhibit growth by forming pores in bacterial membranes[8]. Our study demonstrates that bacteria recover from the pore-forming effects of LL-37 after the molecule is removed. Remarkably, when bacteria are treated with both LL-37 and H2A, the pore-forming effects to the membrane are persistent and irrecoverable[9]. The persistence of membrane pores facilitates the leakage of components out of the cytoplasm and enables the entry of additional histones and LL-37 into the cell. This suggests that H2A stabilizes LL-37-induced pores (**Fig. 2.1**).

How histones could stabilize AMP-induced pores is unknown. The stabilization could arise through indirect interactions between histone and AMP mechanisms in which histones may alter the chemical or physical properties of membranes. Our fluorescence imaging shows that histones significantly increase the recruitment of LL-37 to the membrane, where LL-37 could create greater membrane stress and a greater number of or larger pores. In addition, our scanning electron microscopy images indicate that histones cause membrane surfaces to appear rough, which suggests that histones alter the mechanical properties of the membrane[10]. A significant increase in membrane tension due to histones could facilitate pore formation by AMPs and likewise, would increase the barriers against closing any AMP-induced pores. Alternatively, histones could stabilize pores through direct interaction with AMPs. Such interactions could result in the creation

of new complexes that widen AMP-induced pores, hold open pores for longer periods of time, obstruct membrane repair, inhibit drug efflux pumps, or a combination of these mechanisms.

The data suggest a combination of these mechanisms contribute to increasing the pore-forming action of AMPs, which impedes the ability of bacteria to recover. Future experiments that probe the localization and binding of histones and AMPs, measure the binding affinities between histones and AMPs, and probe membrane mechanics will address the extent to which each mechanism is involved. Regardless of the how histones stabilize pores, the impact of pore stabilization is clear: the bacterial membrane proton gradient is destroyed. This gradient is necessary for ATP energy production and without it, bacteria cannot carry out essential cellular functions.
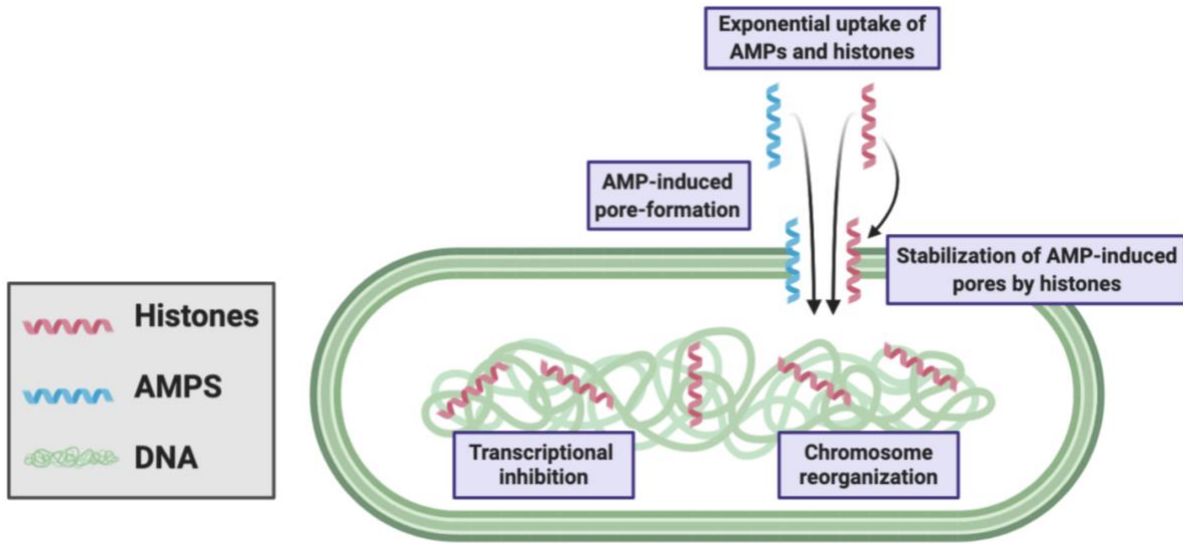
Figure 2.1. **Model of Antibacterial Synergy Between Mammalian Histones and Pore-forming AMPs.** AMPs induce pore formation, which facilitates the entry of histones. Histones stabilize AMP-induced pores, re-organize the chromosome, and inhibit transcription.

2.3 Chromosomal Reorganization

In eukaryotes, histones bind to and regulate chromosomes. In bacteria, histone-like nucleoid structuring (H-NS) proteins regulate chromosomal structure and transcription[11]. However, when membrane pores are formed, the facilitated entry of eukaryotic histones into the bacterial cytoplasm causes dysregulation of functions associated with H-NS. Histone H2A binds to bacterial DNA, reorganizes the structure of bacterial chromosomes, and inhibits transcription (**Fig. 2.1**). Thus, in addition to the damaging effects of histones at the membrane, histones attack bacteria via intracellular targets. As a result, bacteria are unable to maintain the expression of genes that are essential for growth and duplication and are unable to express genes that could repair membrane pores, such as those that produce lipid components. Transcriptional inhibition also suppresses genes that could provide resistance to AMPs and histones, including drug efflux pumps and membrane charge-modifying components. It remains to be explored the extent to which bacterial defense mechanisms are suppressed by the histones. Many questions remain about the effects of histones on bacterial chromosomes, including how they affect the function of H-NS proteins, how the accessibility to transcription sites by DNA or RNA polymerase is affected, and the existence of high affinity histone-binding sites in the chromosome.

2.4 Synergy Through a Positive Feedback Loop

A notable effect of histones and AMPs is their ability to increase the uptake of the partner molecule into bacteria: H2A increases the uptake of LL-37 and LL-37 increases the uptake of H2A[9]. These dynamics give rise to a positive feedback loop that exponentially increases the intracellular concentration of both molecules. The individual use of histones or AMPs results in little uptake and relatively weak antimicrobial activity. In contrast, their combination gives rise to

a synergistic mechanism in which both drugs are taken up into the cytoplasm at significantly greater concentrations, resulting in greater antimicrobial activity. These results suggest that the incorporation of a positive feedback loop into the design strategy of antimicrobial drugs could greatly increase their efficacy.

2.5 Conclusion

The dual treatment strategy described in this work can be used to invigorate current antibiotics that are under development. Possible therapeutic strategies include manipulating the release of histones and AMPs in NETs or lipid droplets to regulate levels of free histones to inhibit bacterial growth. On the other hand, safer and more efficient analogs of histones and AMPs can also be developed to treat an array of infections. Topical treatments can also be made from the synergistic treatments, where histone toxicity is less of a concern. The ability of the combined antimicrobial treatment to act via multiple distinct modes of action potentially increases the barrier for the development of bacterial resistance to the treatment. The targeting of both bacterial membranes and intracellular functions positions the histones and AMP dual treatment as a potentially effective antimicrobial strategy against both Gram-negative and Gram-positive bacteria. This antimicrobial approach provides a refreshing perspective toward the revitalization of current antibiotic development strategies.

2.6 References

1. Miller, B. F., Abrams, R., Dorfman, A. & Klein, M. Antibacterial Properties of Protamine and Histone. *Science* **96**, 428–430 (1942).

2. Brinkmann, V. *et al.* Neutrophil Extracellular Traps Kill Bacteria. *Science* **303**, 1532–1535 (2004).

3. Doolin, T. *et al.* Mammalian histones facilitate antimicrobial synergy by disrupting the bacterial proton gradient and chromosome organization. *Nat. Commun.* **11**, 3888 (2020).

4. Cermelli, S., Guo, Y., Gross, S. P. & Welte, M. A. The lipid-droplet proteome reveals that droplets are a protein-storage depot. *Curr. Biol. CB* **16**, 1783–1795 (2006).

5. Anand, P. *et al.* A novel role for lipid droplets in the organismal antibacterial response. *eLife* **1**, e00003 (2012).

6. Bosch, M *et al.* Mammalian lipid droplets are innate immune hubs integrating cell metabolism and host defense. *Science* (2020).

7. Dürr, U. H. N., Sudheendra, U. S. & Ramamoorthy, A. LL-37, the only human member of the cathelicidin family of antimicrobial peptides. *Biochim. Biophys. Acta* **1758**, 1408–1425 (2006).

8. Lee, C.-C., Sun, Y., Qian, S. & Huang, H. W. Transmembrane pores formed by human antimicrobial peptide LL-37. *Biophys. J.* **100**, 1688–1696 (2011).

9. Doolin, T. *et al.* Mammalian histones facilitate antimicrobial synergy by disrupting the bacterial proton gradient and chromosome organization. *Nat Comm* (2020) doi:http://doi.org/10.1038/s41467-020-17699-z.

10. Doolin, T., Gross, S.P., & Siryaporn, A. Physical Mechanisms of Bacterial Killing by Histones. in *Physical Microbiology* (https://doi.org/10.1007/978-3-030-46886-6_7, In press.).

11. Grainger, D. C. Structure and function of bacterial H-NS protein. *Biochem. Soc. Trans.* **44**, 1561–1569 (2016).

CHAPTER 3: HISTONE ANTIMICROBIAL MECHANISM

IN GRAM-NEGATIVE BACTERIA

3.1 Synopsis

To combat the growing threat of antibiotic resistance, new antimicrobial strategies are urgently needed. In Gram-negative bacteria, the presence of dual membrane layers can significantly restrict the activity of antimicrobials. Lipopolysaccharides (LPS) are highly abundant in the bacterial outer membrane (OM) but not in the inner membrane (IM). This asymmetry creates distinct membrane environments such that a single molecule with high specificity cannot target both membranes. In particular, antimicrobial peptides (AMPs) LL-37 and polymyxin B (PMB) have high specificity towards LPS, resulting in greater activity towards the OM rather than the IM. In innate immune responses, histones have antimicrobial synergy with LL-37. However, the mechanism that gives rise to this synergy has not been understood. Here, we show that AMPs enable histone H2A to bypass the LPS-rich OM into the periplasmic space, where H2A permeabilizes membrane leaflets that contain far less LPS. Synergistic differential targeting by H2A and PMB in particular is potent against *Escherichia coli* and the opportunistic pathogen *Pseudomonas aeruginosa*, creating large membrane pore structures and irreversible membrane damage within minutes of their introduction. This combination reduces *P. aeruginosa* infection in wax moth larvae and in murine corneas, demonstrating clinical relevance of the differential membrane targeting mechanism.

3.2 Introduction

The rapid rise of antibiotic resistance necessitates an urgent need for novel resistance-proof antimicrobial approaches. Antimicrobial peptide (AMP) LL-37 (cathelicidin) and histones are critical components of innate immunity and produce potent antimicrobial activity and synergy[1–5]. The use of synergistic antimicrobial agents are less likely to induce resistance due to having multiple targets[2,6–9]. We seek to understand the underlying mechanisms of synergy between AMPs and histones to identify bacterial vulnerabilities, better understand an innate immunity antimicrobial mechanism, and guide the development of antibiotics.

Pseudomonas aeruginosa is a Gram-negative opportunistic pathogen that causes a broad range of diseases including corneal infections and severe lung infections, including in cystic fibrosis patients[10,11]. Antimicrobial agents need to penetrate multiple barriers before they can reach intracellular targets. On the outer surface of the cell, negatively-charged lipopolysaccharides (LPS) function as a protective barrier against extracellular stressors[12]. The outer membrane (OM), the cell wall, and the inner membrane (IM) provide additional barriers against the entry of antimicrobials (**Fig. 3.1a**)[13].

Antimicrobial peptides, including human LL-37 and bacterially-derived polymyxin B (PMB) and polymyxin E (colistin), increase bacterial permeability by targeting the OM[14,15]. PMB and colistin in particular are used as last-resort antibiotics to treat infections and have high clinical relevance[16]. LL-37 forms toroidal pores in membranes whereas PMB and colistin target the LPS component lipid A and rearranges LPS into rigid crystalline structures[17–21]. While the antimicrobial mechanisms of these AMPs differ, their greatest impacts are towards the OM rather than the IM, which contains far less LPS[22,23].

Histones have a regulatory role in eukaryotic chromosome condensation and an additional role as an antimicrobial agent in diverse immune systems, including amphibians, drosophila, salmon, shrimp, and humans[24]. In mammals, histones are integral parts of innate immunity in neutrophil extracellular traps (NETs) and cellular lipid droplets (LDs), where they co-localize with LL-37[4,25,26]. Histones alone cause minimal damage to *E. coli* membranes in physiological conditions[1]. However, when paired with LL-37, histone H2A produces synergistic effects, destroying the bacterial proton gradient, permeabilizing both the OM and IM, and causing the loss of bacterial cytoplasm components[1] (schematic in **Fig. 3.1a**). The mechanism(s) underlying this synergy and the extent that each molecule damages the OM and IM have yet to be determined.

Here, we find that synergy between histone H2A and AMPs involves differential membrane targeting. H2A entry and activity towards the OM is blocked by LPS. AMPs LL-37 and PMB are effective at permeabilizing the OM, which enables the uptake of H2A into the periplasm, where H2A has membrane-permeating activity towards the OM inner leaflet and IM outer leaflet. The combination of PMB+H2A increases bacterial membrane damage through the formation of large pores in both the OM and IM. The mechanism of differential membrane targeting identifies a significant bacterial vulnerability that could be exploited as a potential antibiotic strategy.

3.3 Materials and Methods

3.3.1 Bacterial Strains, Growth Conditions, and Reagents

Bacterial strains were streaked onto LB-Miller (BD Biosciences, Franklin Lakes, NJ) petri dishes containing 2% Bacto agar (BD Biosciences) and incubated at 37 °C to obtain single colonies. Single colonies were inoculated into MinA minimal medium[46] (4.5 g KH_2PO_4, 10.5 g K_2HPO_4 1 g $(NH_4)_2SO_4$, and 0.5 g sodium citrate • $2H_2O$ per 1 L water; 1 mM $MgSO_4$)

supplemented with 0.2% glucose and 0.1% casamino acids, herein referred to as MinA+ medium. Liquid cultures were grown overnight to stationary phase at 37 °C on a roller drum at 18 rpm. Overnight cultures were diluted 1:100 into fresh media and sub-cultured to an optical density at 600 nm (OD_{600}) of 0.3 to 0.4, which is referred to here as mid-exponential phase.

E. coli experiments were performed using the wild-type *E. coli* strain MG1655 seq[47]. The *E. coli* MG1655 Δ*waaC* strain, which contains truncated LPS, was a gift from the Hiller lab[21]. *P. aeruginosa* P2m (PAmFLR02[48]) is a mucoid cystic fibrosis clinical isolate. *P. aeruginosa* experiments otherwise were performed using the wild-type strain PAO1F[41,49].

The antimicrobial agents calf thymus histone H2A (Sigma-Aldrich, St. Louis, MO), human cathelicidin LL-37 (Anaspec, Fremont, CA), and polymyxin B sulfate salt (Sigma-Aldrich) were prepared fresh before experiments and used at indicated concentrations. Typical MICs for kanamycin, gentamicin, and tetracycline were estimated using the EUCAST antimicrobial wild type distributions of microorganisms database[30].

Histone H2A was fluorescently labeled by mixing 10 mg/ml Alexa Fluor 488 NHS Ester or Alexa Fluor 647 NHS Ester (Invitrogen, Waltham, MA) dissolved in DMSO with 10 mg/ml H2A in 0.1 M $NaHCO_3$ solution in a 1:20 ratio. LL-37 was labeled by mixing 2 mg/ml Atto 488 NHS Ester (Sigma-Aldrich) dissolved in DMSO with 2 mg/ml LL-37 in 0.1 M $NaHCO_3$ solution in a 1:8.33 ratio. All solutions were stirred continuously in the dark at room temperature for 1 hr, passed through PD MidiTrap G-25 columns (GE Healthcare Life Sciences, Pittsburgh, PA) to remove unreacted dye, aliquoted, and frozen at -80 ºC. Labeled molecules were thawed and used only once. To avoid saturation effects during imaging, labeled H2A and LL-37 were mixed with unlabeled species. The final Alexa Fluor 488-labeled H2A solution (AF488-H2A) contains 20% Alexa Fluor 488-labeled H2A and 80% unlabeled H2A. The final Alexa Fluor 647-labeled H2A

solution (AF647-H2A) contains 5% Alexa Fluor 647-labeled H2A and 95% unlabeled H2A. The final Atto 488-labeled LL-37 solution (AT488-LL-37) contains 3% Atto 488-labeled LL-37 and 97% unlabeled LL-37.

3.3.2 Growth Curves, Checkerboard Assays, and CFU Assays

Strains were cultured overnight in MinA+ medium to mid-exponential phase, diluted 1:20 into fresh medium, and treated with antimicrobial agents. For growth curves, 200 µl of bacterial cultures were immediately transferred to 96-well microplates (Corning, Corning, NY) that were sterile, tissue-culture treated, clear bottom, and composed of black polystyrene. Growth measurements were acquired every 15 min for up to 24 h using a BioTek Synergy HTX multi-mode plate reader (Agilent, Santa Clara, CA) at 37 °C. The reader was set to continuous orbital shaking mode at a frequency of 282 cpm (3 mm) with a 100 msec delay and 8 OD_{600} measurements taken per data point.

To calculate checkerboard fractional inhibitory concentrations, MICs were determined through OD_{600} measurements and the following equation was used: $FIC = (A/MIC_A) + (B/MIC_B)$, where A and B are the MICs of each antimicrobial agent when used in combination, and MIC_A and MIC_B are MICs of each agent when used individually[29,50]. Indexes of $FIC \leq 0.5$, $FIC \geq 4$, and $0.5 < FIC < 4$ were considered synergistic, antagonistic, and additive, respectively[29,50].

For colony forming unit (CFU) assays, following a 1:20 dilution into fresh medium, cultures were treated with antimicrobial agents for 1 h at 37 ºC on a roller drum, diluted in ten-fold serial dilutions into non-selective fresh media, plated as 10 µl droplets onto non-selective LB-Miller agar plates, incubated for 16-18 h at 37 °C, and counted for single colonies.

3.3.3 Fluorescence Microscopy

Phase contrast and fluorescence images were acquired using a Nikon Eclipse Ti-E microscope (Nikon, Melville, NY) containing a Nikon 40X and 100X Plan Apo (1.45 N.A.) objective, a 1.5X magnifier, a Sola light engine (Lumencor, Beaverton, OR), an LED-DA/FI/TX filter set (Semrock, Rochester, NY) containing a 409/493/596 dichroic, a Hamamatsu Orca Flash 4.0 V2 camera (Hamamatsu, Bridgewater, NJ), and an Andor DU-897 EMCCD camera (Andor Technology, Belfast, Northern Ireland). The 474/27 nm and 525/45 nm excitation and emission filters, respectively, were used to visualize Alexa Fluor 488 and FITC-DEAE-Dextran. The 575/25 nm and 641/75 nm excitation and emission filters, respectively, were used to visualize propidium iodide (PI) fluorescence. A Cy5 filter (Chroma, Bellows Falls, VT) containing 640/30 nm and 690/50 nm excitation and emission filters, respectively, and a T660lpxr dichroic was used to visualize Alex Fluor 647 fluorescence. Images were acquired using Nikon NIS-Elements version 4.5 and analyzed using AVIassembleGUI[51,52] version 1.2c written in MATLAB R2017a (MathWorks, Natick, MA) (see 'Code Availability' section for code). After treating bacteria with antimicrobial agents, 5 µl of culture was placed on 1% agarose-minimal medium pads and imaged immediately, as described previously[53]. A minimum of 100 bacterial cells were imaged and analyzed for each experiment.

For direct stochastic optical reconstruction microscopy (dSTORM), mid-exponential cultures in MinA+ medium were diluted 1:4 into fresh medium, and treated with H2A, LL-37, or both for 40 minutes at 37 °C on a roller drum. H2A treatments were performed at a concentration of 10 mg/ml and consisted of 95% unlabeled H2A and 5% Alex Fluor 647-labeled H2A. LL-37 treatments were performed at a concentration of 20 µg/ml and consisted of 97% unlabeled LL-37

and 3% Atto 488-labeled LL-37. Following treatment, cells were washed and resuspended in STORM buffer[54], which contains 143 mM beta-mercaptoethanol (Sigma-Aldrich), 10% glucose, 50 mM Tris NaCl pH 8.0, 10 mM NaCl, 0.56 mg/ml glucose oxidase (Sigma-Aldrich), and 0.034 mg/ml of catalase from *Aspergillus niger* (Sigma-Aldrich), and loaded into microchamber slides containing 0.5 mm-wide channels, which were constructed by coating cover glass with 0.1% (w/v) poly-L-lysine solution (Sigma-Aldrich) that was diluted 1:100 in ethanol for 20 minutes, drying at 100 ºC for 10 minutes, and attaching to slides using double-sided tape. Fresh STORM buffer was flowed in after 5 minutes to wash away cells that were not adhered to the cover glass surface.

dSTORM imaging was performed using a custom total internal refection (TIRF) Nikon TE200 microscope containing a Nikon 100X Apo TIRF (1.49 N.A.) objective, Ti:Sapphire 488 nm or 640 nm laser (Coherent, Santa Clara, CA), QuantEM 512SC EMCCD camera (Photometrics, Tucson, Arizona), a 432/515/595/681/809 nm penta-band bandpass filter, and 405/488/561/635 nm dichroic beamsplitter (Semrock). For each cell, 2,000 frames were acquired and reconstructed into a single image using RapidSTORM software version 3.0[55] using an input pixel size of 150 nm, 500 nm PSF FWHM, and an output resolution of 10 nm/pixel, consistent with previous analyses[56,57]. For images in Fig. 2, the output pixels sizes were set to represent 1 nm/pixel. Quantification of fluorescent spots was performed using scripts that were written in Python. We utilized the libraries skimage (v0.19.3), scipy (v1.10.0), pandas (v1.5.3), numpy (v1.23.5), matplotlib (v3.7.0) and PIT (v9.4.0) for image processing and plotting (see 'Data Availability' section for code).

3.3.4 Visualization of Bacterial Membrane Permeability using PI and Dextran

To visualize bacterial membrane permeability, mid-exponential cells cultured in MinA+ medium were diluted 1:20 into fresh medium, treated with antimicrobial agents for 1 h at 37 °C, supplemented with 30 µM PI for 15 min, immobilized on 1% agarose pads containing MinA+ medium, and imaged immediately using fluorescence microscopy. To estimate bacterial pore sizes, mid-exponential strains cultured in MinA+ medium were diluted 1:20 into fresh medium, treated with antimicrobial agents for 45 min at 37 °C on a roller drum, mixed with 0.25 mg/ml of 40 kDa or 150 kDa FITC-DEAE-Dextran (Sigma-Aldrich) for 15 min, washed twice in MinA+ medium, immobilized onto 1% agarose pads containing MinA+ medium, and immediately visualized using fluorescence microscopy. Dextran diameters were based on Stokes' radii reported in the manufacturer's technical documents[31], with 40 kDa and 150 kDa dextrans corresponding to 9 and 17 nm pores, respectively.

3.3.5 Electroporation of Histones into E. coli

Electrocompetent *E. coli* were prepared by culturing in SOB medium[58] to mid-exponential phase, washing with 10% glycerol four times, resuspending to an OD_{600} of 0.2, and freezing at −80 °C. *E. coli* were thawed, supplemented with 1 µM $MgSO_4$, electroporated with 10 µg/ml of H2A using a Bio-Rad Micropulser (Bio-Rad, Hercules, CA), resuspended in cold MinA+ medium, incubated for 10 minutes at room temperature, supplemented with 30 µM PI, immobilized on 1% agarose pads containing MinA+ medium, and imaged immediately using fluorescence microscopy.

3.3.6 Bacterial Spheroplast Time-lapses

Bacterial spheroplasts were prepared based on previous protocols[23,35]. Briefly, *E. coli* were cultured for 18 hours in LB-Miller Broth (BD Biosciences), washed twice in Cation-Adjusted

Mueller Hinton Broth (CA-MHB) (BD Biosciences), resuspended in CA-MHB, incubated for 2 hours at 37°C with shaking at 180 rpm, washed using 0.03 M Tris-HCl pH 8.0 (Tris buffer), washed additionally using Tris buffer containing 20% sucrose, resuspended in Tris buffer containing 20% sucrose, 0.012 mg/ml ethylenediaminetetraacetic acid (EDTA) and 0.02 mg/ml lysozyme (Sigma-Aldrich), incubated at 30°C for 1 hour with shaking at 180 rpm, and resuspended in Tris buffer containing 20% sucrose. Immediately before imaging, spheroplasts were diluted 1:10 into Tris buffer containing 20% sucrose, 1 mM $MgSO_4$, and 10 µM PI, injected into 0.5 x 2.4 cm microchannels that were assembled using cover glass and double-sided tape, centrifuged at 70 g for 3 minutes, and imaged immediately. Phase contrast and fluorescence images were acquired at room temperature every 3 minutes for 21 minutes. Following the initial 5 minutes, Tris buffer containing 20% sucrose, 1 mM $MgSO_4$, 10 µM PI, and antimicrobial agents were pulsed into the channel. Images were analyzed using AVIassembleGUI[51,52] version 1.3 written in MATLAB R2023b (see 'Code Availability' section for code).

3.3.7 Transmission Electron Microscopy and Cryogenic Transmission Electron Microscopy

For TEM, strains were cultured to mid-exponential phase in MinA+ medium, treated with antimicrobial agents at room temperature for 10 minutes and adhered to formvar-coated copper electron microscopy grids (Electron Microscopy Sciences, Hatfield, PA). Grids were washed twice in water, stained with 2% uranyl acetate for 2 minutes, washed again in water, and dried at room temperature overnight. Samples were imaged in a JEOL JEM-2800 transmission electron microscope containing a Schottky-type field-emission gun operating at 200 keV and a Gatan OneView CMOS camera at 4k × 4k resolution. Images were acquired using DigitalMicrograph software (Gatan Inc., Pleasanton, CA).

For cryoTEM, strains were cultured to mid-exponential phase in MinA+ medium, diluted 1:2 into fresh medium, and treated with antimicrobial agents at 37 ºC. *E. coli* and *P. aeruginosa* samples were treated for 15 minutes and 30 minutes, respectively, added to Lacey Carbon films on copper grids (Electron Microscopy Sciences, Hatfield, PA) that were previously glow-discharged for 70 seconds, and placed in a Leica EM GP2 automatic plunge freezer (Leica Microsystems, Wetzlar, Germany) that reached 95-99% humidity. Grids were blotted for 3 s prior to plunging into liquid propane. Vitrified samples were imaged on a JEOL JEM-2100F transmission electron microscope using a Schottky-type field-emission gun operating at 200 keV, and a Gatan OneView CMOS camera at 4k × 4k resolution. Images were acquired using SerialEM software[59] v3.4 in low dose imaging mode. Bacterial membrane deformation and pore widths were measured along a line tangent to the membrane using ImageJ v1.53a (NIH, Bethesda, MD).

3.3.8 Predictive Model of AMP-Histone Synergy

We constructed a predictive model that describes the dynamics of AMPs and histones in a Gram-negative bacterium, which is derived in full detail in the Extended Data Synergy Model section. Briefly, AMPs and histones are initially present in the extracellular space and translocate to the periplasm and cytoplasm through membrane pores. We distinguish between two types of membrane surfaces: LPS membranes, in particular the outer leaflet of the OM; and the inner leaflet of the OM and the outer and inner leaflets of the IM, referred to as non-LPS membranes. The synergy score is computed based on the concentrations of AMPs and histones in the cytoplasm following a fixed simulation time and compares the concentrations of AMPs and histones when cells are treated with the molecules individually or in combination:

$$S = \frac{[A_c]_{combined} + [H_c]_{combined}}{[A_c]_{individual} + [H_c]_{individual}},$$

where $[A_c]$ and $[H_c]$ refer to AMPs or histones in the cytoplasm, respectively, and individual and combined refer to the AMPs or histones that are supplied individually or in combination in the initial conditions, respectively. The concentration is assessed in the cytoplasm because their presence here decreases cell viability[1]. If the concentrations inside the cytoplasm are greater in combination than individually, a synergy score of greater than one results. Higher scores represent greater levels of synergy. Synergy was assessed for a broad range of histone and AMP pore formation rates towards LPS and non-LPS membranes.

3.3.9 Galleria mellonella (Wax Moth Larvae) Infection Model

The impact of antimicrobial agents on *P. aeruginosa* infection was assessed in a *Galleria mellonella* (wax moth larvae) model as described previously[60]. *Galleria mellonella* larvae (Speedy Worm, Alexandria, MN) that were about ¾" in length were maintained at room temperature, fed with bedding that came with the shipment, and were used within one week of shipment arrival. *P. aeruginosa* was cultured to mid-exponential phase in MinA+ medium, resuspended and diluted 1:20 into PBS, mixed with antimicrobial agents, and injected immediately into wax moth larvae at the junction of the rear left leg. Larval survival was assessed every 24 hours, with live and healthy larvae showing yellow or tan coloration and visible movement, and deceased larvae exhibiting dark pigmentation, black bodily patches, and lack of movement.

3.3.10 Murine Corneal Infection Model

The impact of antimicrobial agents on *P. aeruginosa* infection was assessed in a murine corneal infection model as described previously[40,61]. Briefly, *P. aeruginosa* cells were grown to mid-exponential phase in MinA+ medium, resuspended and diluted 1:4 in PBS. The corneal

epithelium of C57BL/6J mice aged 6-8 weeks (Jackson Laboratory, Bar Harbor, ME) was abraded and a 2 µl solution corresponding to 5×10^4 CFUs was applied topically. Approximately equal numbers of male and female mice were used per experimental group. Antimicrobial treatments were applied 3 times per day using 10 µl droplets over the course of 48 hours. The dosage of PMB was determined by identifying the minimum amount that caused a statistically significant reduction in CFUs after 48 hours. H2A was supplied in a molar ratio to PMB that was comparable to *in vitro* experiments. Mice were euthanized by CO_2 asphyxiation at 48 hours post-infection.

Corneal opacity and corneal colonization were measured using a Leica MZ10 F Modular Stereo Microscope (Lecia Microsystems), gooseneck fiber optic light source, and a Leica DFC450 C camera (Lecia Microsystems). Images were captured using the Leica Application Suite version 4.5 (Leica Microsystems). Opacity was quantified as performed previously[61] using ImageJ v1.53a (NIH). The percent opacity was defined as the average pixel intensity above that for eyes with no apparent disease divided by the maximum pixel intensity in the image series and normalized by cornea area. Areas of glare were removed from the analysis process. Corneal CFUs were measured by homogenizing mouse eyes in PBS using a TissueLyser II (Qiagen, Hilden, Germany) at 30 Hz for 3 minutes, plating in ten-fold serial dilutions onto non-selective LB-Miller agar (BD Biosciences), incubating for 16-18 hours at 37 °C, and counting CFUs.

Mouse experiments were approved in protocol AUP-21-123 by the University of California Irvine's Institutional Animal Care and Use Committee (UCI IACUC). Mice were monitored at least twice per day for signs of distress or discomfort. Any mice determined to be in distress were humanely euthanized by CO_2 asphyxiation followed by cervical dislocation, as approved by UCI IACUC.

3.3.11 Statistical Analyses

Statistical analysis was performed using unpaired one- or two-tailed (Welch's) t-tests with unequal variances using GraphPad Prism version 9.5 or R version 4.3.1. Statistical significance was defined as a p-value of < 0.05.

3.3.12 Code Availability

The custom MATLAB scripts used for processing and analyzing the fluorescence microscopy data and the custom Python scripts used for dSTORM analyses are available at Github at https://github.com/asirya/AVIassembleGUI.git.

3.4 Results

3.4.1 Membrane Permeabilization and Antimicrobial Synergy Accompany AMP and Histone Localization

To determine if PMB increases membrane permeability similar to LL-37, *E. coli* was incubated with PMB at a sub-minimal inhibitory concentration (MIC) concentration of 1 µg/ml (6.4 µM)[27] and assessed for uptake of propidium iodide (PI), a fluorescent molecule that does not cross intact membranes. PMB significantly increased PI fluorescence (**Fig. 3.1b-c**), indicating that like LL-37[1], PMB at sub-MIC concentrations increases membrane permeability. We assessed histone uptake using fluorescently-labeled histones. Histone H2A alone at 10 µg/ml (0.7 µM), a concentration below that in blood plasma following *E. coli* infection[28], produced little H2A entry (**Fig. 3.1d-e**). PMB significantly increased H2A uptake, indicating that PMB permeabilizes the membrane and facilitates H2A entry into bacteria.

We quantified PMB+H2A synergy through checkerboard assays, which yielded a fractional inhibitory concentration (FIC) index of 0.16 (**Fig. 3f**). FIC indexes below 0.5 are synergistic[29]. PMB+H2A treatment reduced bacterial viability by over 7 orders of magnitude of colony forming units (CFUs) and completely suppressed liquid culture growth for at least 24 hours (**Fig. 3.1g-h**). The significant CFU reduction, which was assessed on non-selective media after 1 hour of treatment, suggests that PMB+H2A is bactericidal. The synergistic potency is underscored by the significant (10-fold) reduction in MIC of PMB, from 2 µg/ml to 0.2 µg/ml, due to H2A addition. The PMB+H2A inhibitory effect was more potent than the aminoglycosides kanamycin and gentamicin and the broad-spectrum protein synthesis inhibitor tetracycline at standard reported MIC concentrations[30] (**Fig. 3.1i**). The LL-37+H2A combination was synergistic but weaker, with an FIC index of 0.27, decreasing bacterial viability by 3 orders of magnitude, and inhibiting bacterial growth by 5 hours longer than LL-37 alone (**Fig. 3.1j-l**).

We assessed membrane permeability near the lowest PMB concentration that antimicrobial synergy was observed (0.25 µg/ml) (**Fig. 3.1m**). PMB alone increased cytoplasmic PI fluorescence to a just-discernable level, indicating marginal membrane permeabilization (**Fig. 3.1m**). H2A alone had no impact on fluorescence, consistent with no change in membrane permeability. The PMB+H2A combination increased PI fluorescence by 16-fold compared to PMB treatment alone, indicating significant membrane permeabilization (**Fig. 3.1m-n**). This increased fluorescence was greater than higher concentrations of PMB alone (**Fig. 3.1m**), underscoring the magnitude of the synergistic effect and suggesting that H2A enhances PMB-induced membrane permeability. Thus, inducing membrane permeability that enables histone uptake is sufficient to produce potent antimicrobial synergy; LL-37 or PMB induces initial membrane permeability and H2A strongly enhances it.

To determine how H2A enhances membrane permeability, we tracked the single molecule localization of fluorescently-labeled LL-37 (AT488-LL-37) via direct stochastic optical reconstruction microscopy (dSTORM). H2A increased the number of fluorescent spots up to 30 nm in diameter, suggesting that H2A increases localization of LL-37 to the cell (**Fig. 3.2a-c**). We also fluorescently labeled H2A (AF647-H2A) to track the effect of LL-37 on H2A. Fluorescent spots up to 30 nm were observed when H2A was supplied alone (**Fig. 3.2d-e**). Co-treatment with LL-37 increased the number of H2A spots and also caused H2A to localize in large clusters greater than 110 nm in diameter (**Fig. 3.2d-g**). Similar results were observed by co-treating with PMB in place of LL-37 (**Fig. 3.2d-g**). The average H2A spot diameters due to the combination with LL-37 and PMB were 19.5 and 18.7 nm, respectively (**Fig. 3.2h**). Thus, combining H2A with LL-37 increased the localization of LL-37 and H2A spots and triggered larger H2A cluster formation. The LL-37 and H2A localization likely reflects binding of these molecules to the membrane and could reflect the formation of membrane pores associated with membrane permeabilization.
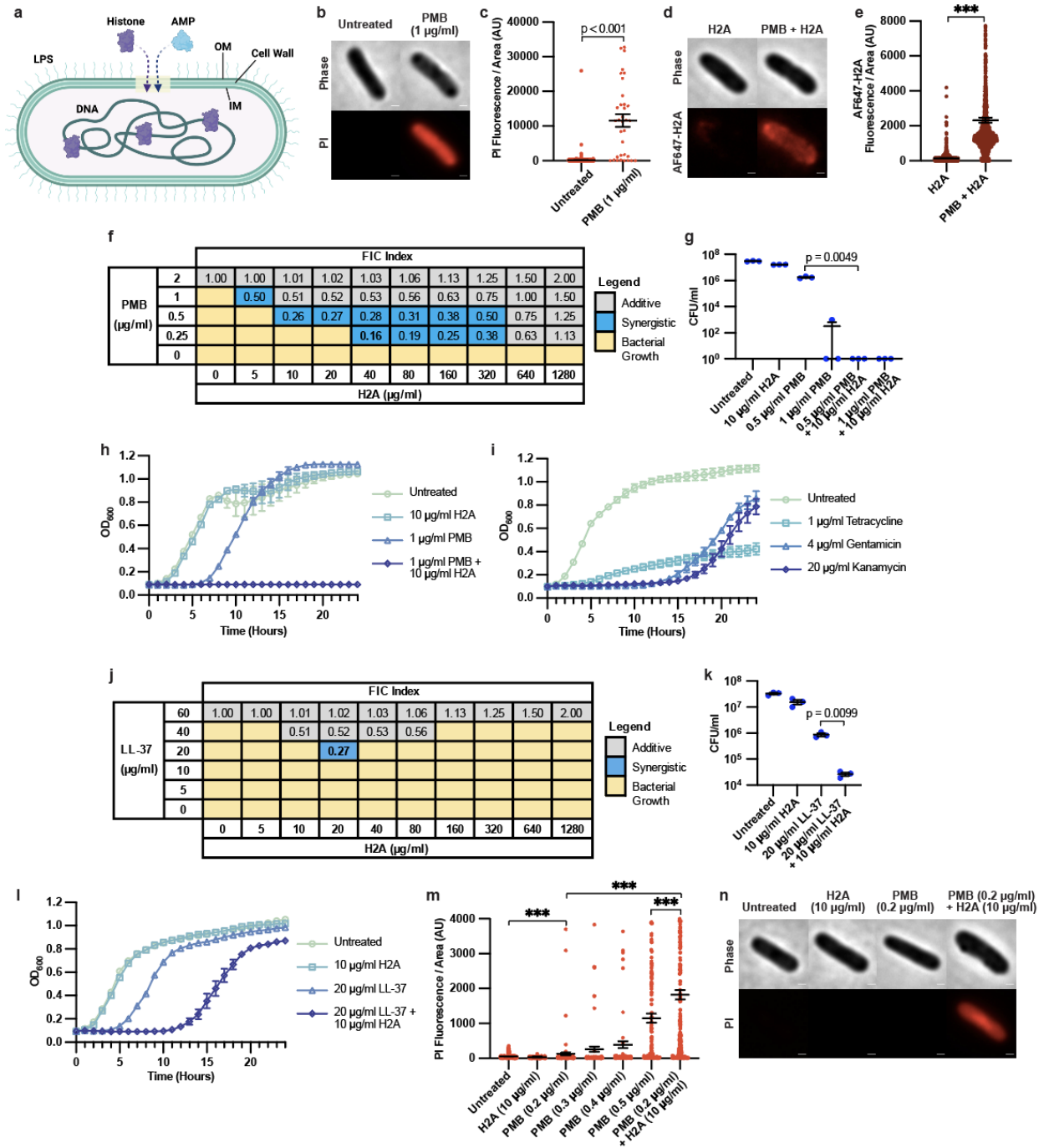
Figure 3.1. Polymyxin B (PMB) Increases Bacterial Uptake of Histone H2A, Leading to Increased Membrane Damage. (a) Schematic summarizing model in which histones enter the bacterial cytoplasm through AMP-induced bacterial membrane pores and alter chromatin. OM = outer membrane; IM = inner membrane; LPS = lipopolysaccharides; AMP = antimicrobial peptide.

(b) Representative phase-contrast and fluorescence images of intracellular propidium iodide (PI) in *E. coli* following a 1-hour treatment of PMB (1 µg/ml). Scale bars represent 500 nm. (c) Distribution and mean intracellular PI fluorescence of individual *E. coli* following a 1-hour treatment of PMB (1 µg/ml). (d) Representative phase-contrast and fluorescence images of intracellular fluorescently-labeled H2A (AF647-H2A) in *E. coli* following a 1-hour treatment of AF647-H2A (10 µg/ml) or a combination of AF647-H2A (10 µg/ml) and PMB (1 µg/ml). Scale bars represent 500 nm. (e) Distribution and mean intracellular AF647-H2A in individual *E. coli* following a 1-hour treatment of PMB (1 µg/ml) or a combination of AF647-H2A (10 µg/ml) and PMB (1 µg/ml). (f) Checkerboard assay to assess antimicrobial synergy between PMB and H2A towards *E. coli*. FIC values are displayed for conditions in which no growth was observed after 24 hours. (g) Colony forming units (CFUs) *E. coli* that were treated for 1 hour or untreated, plated on non-selective LB agar, and incubated for 18 hours. Each data point represents a biological replicate. (h) Optical densities (OD_{600}) of *E. coli* treated with PMB, H2A, or both, or untreated (n = 4 for each condition, error bars indicating SEM). (i) Optical densities of *E. coli* treated with kanamycin, tetracycline, or gentamicin, or untreated (n = 4 for each condition, error bars indicating SEM). (j) Checkerboard assays, (k) CFUs, and (l) growth profiles of *E. coli* treated with H2A, LL-37, or both or untreated (n = 4 for each condition). (m) Distribution and mean intracellular PI fluorescence of *E. coli* following a 1-hour treatment of H2A, PMB, or a combination of H2A and PMB at indicated concentrations. (n) Representative phase-contrast and fluorescence images of intracellular PI in *E. coli* following a 1-hour treatment of H2A, PMB or a combination of H2A and PMB at indicated concentrations. Scale bars represent 500 nm. Fluorescence was quantified in arbitrary units (AU). In panels e and m, a minor subset of data points are above the vertical axis maximum and are not displayed. In panels c, e, and m, data points represent individual bacterial

cells. Mean and standard error of the mean (SEM) are shown. Two-tailed Welch's t-tests were performed, with p-values indicated in graphs or indicated as "ns" for nonsignificant. Different fluorescence acquisition times were used in panels c and m.
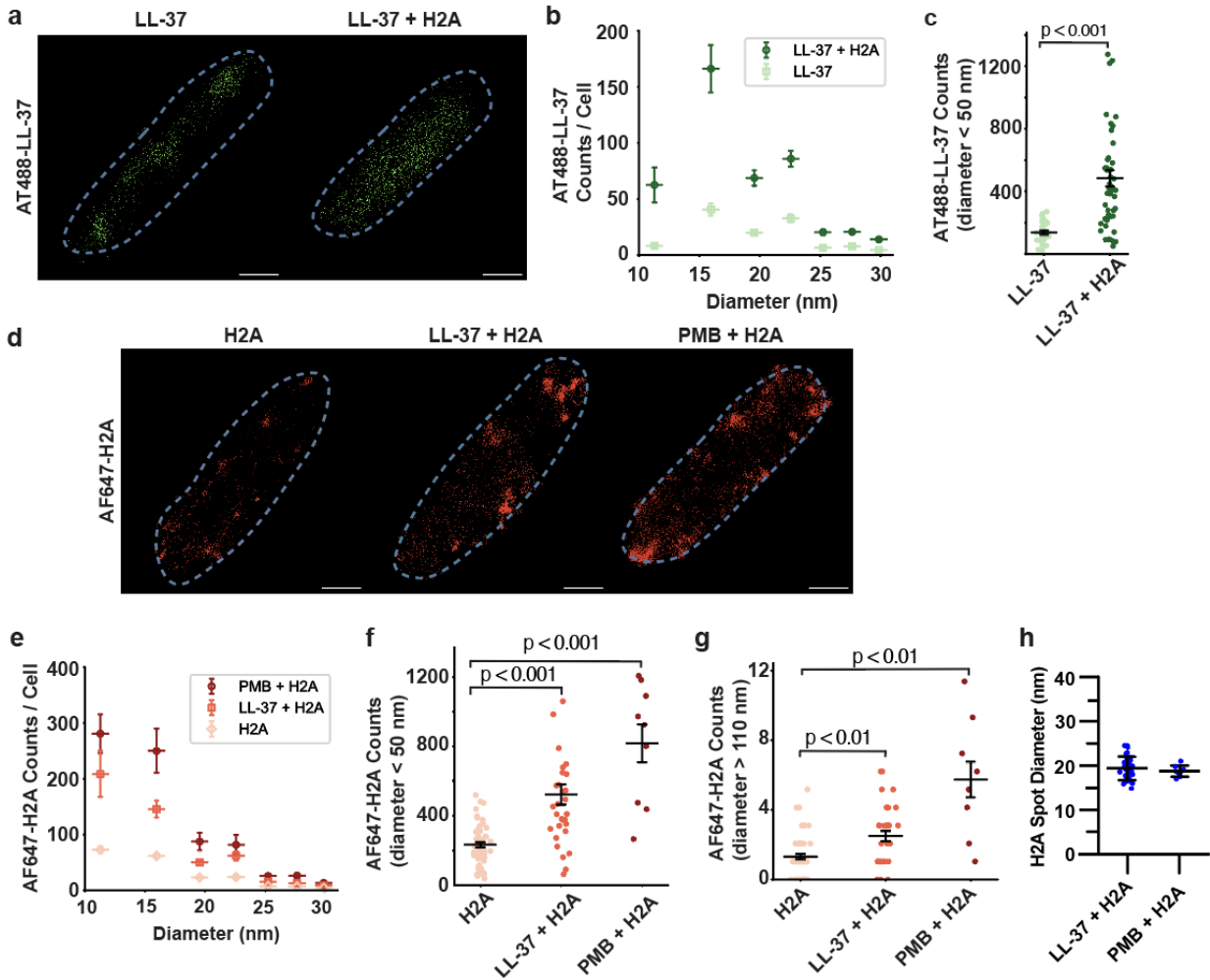
Figure 3.2. Combining H2A and AMPs Increases their Localization and Triggers the Formation of H2A Clusters in *E. coli*. (a) Representative dSTORM images of *E. coli* treated with 20 µg/ml of Atto 488-labeled LL-37 (AT488-LL-37) alone, or 20 µg/ml AT488-LL-37 with 10 µg/ml H2A. Scale bars represent 500 nm. (b) Distribution of AT488-LL-37 spots per cell. (c) Number of AT488-LL-37 fluorescent spots observed in each cell that were less than 50 nm in diameter. (d) Representative dSTORM images of *E. coli* treated with 10 µg/ml Alexa Fluor 647-labeled H2A (AF647-H2A) alone or in combination with 20 µg/ml LL-37 or 1 µg/ml PMB. Scale bars represent 500 nm. (e) Distribution of AF647-H2A spots per cell. Number of AF647-H2A fluorescent spots in each cell that had diameters (f) less than 50 nm or (g) greater than 110 nm.

Each data point in panels c, f, and g represents individual bacterial cells for experiments that were performed in at least biological triplicate. (h) Distribution and mean diameters of AF647-H2A spots in dSTORM images up to 50 nm. Data points indicate the average of spot diameters within an individual cell. Mean and SEM are shown. Two-tailed Welch's tests were performed, with p-values indicated in graphs or indicated as "ns" for nonsignificant.

3.4.2 Histones Induce OM Deformations and Increase Uptake of Dextran Molecules

Based on the observations that combining H2A with PMB or LL-37 increases membrane permeability and H2A localization, we hypothesized that histones increase both the size and number of membrane pores. Transmission electron microscopy (TEM) was used to directly characterize membranes. Minor changes in membrane smoothness were observed in cells treated with H2A or LL-37 alone (**Fig. 3.3a**). In contrast, LL-37+H2A induced deformations that were greater in contrast, typically round, and concentrated near cell poles (**Fig. 3.3a**). PMB+H2A similarly induced prominent round deformations near the poles while no obvious membrane deformations were observed with PMB treatment alone (**Fig. 3.3a**). The average diameters of the round membrane deformations due to LL-37+H2A and PMB+H2A were 17.0 and 17.1 nm, respectively (Extended Data Figure 1i). It is possible that smaller deformations were present but below the resolution limit (< 5 nm).

To assess the functional impact of the deformations, we measured their effective size using fluorescently-labeled dextrans (FITC-dextrans) to enter the cell. We first used 40 kDa dextrans, which are approximately 9 nm in diameter[31]. Minimal FITC-dextran fluorescence was detected in untreated and H2A-treated cells (**Fig. 3.3b-c**), consistent with the interpretation that H2A does not induce membrane pores. In contrast, PMB significantly increased FITC-dextran fluorescence and PMB+H2A further increased dextran entry (**Fig. 3.3b-c**). The dextran entry correlates with the prominent round deformations (**Fig. 3.3a iv, vi**), suggesting these deformations could be pores at least 9 nm in diameter. We then used 150 kDa dextrans (17 nm in diameter[31]) and observed FITC-dextran fluorescence in cells treated with PMB+H2A (**Fig. 3.3d-e**), suggesting that PMB+H2A deformations (**Fig. 3.3a vi**) are likely pores at least 17 nm in diameter.

PMB+H2A only slightly increased (1.3x) the uptake of 9 nm dextrans compared to PMB alone (**Fig. 3.3f**). In contrast, PMB+H2A significantly increased the uptake of larger 17 nm dextrans (2.5x) (**Fig. 3.3f**). This result suggests that PMB-only pores are less restrictive towards the 9 nm molecules but are partly restrictive towards 17 nm dextrans; addition of H2A relieves this restriction. H2A could increase uptake of larger dextrans by increasing the size of existing pores established by PMB or by combining with the function of PMB to create larger pores.
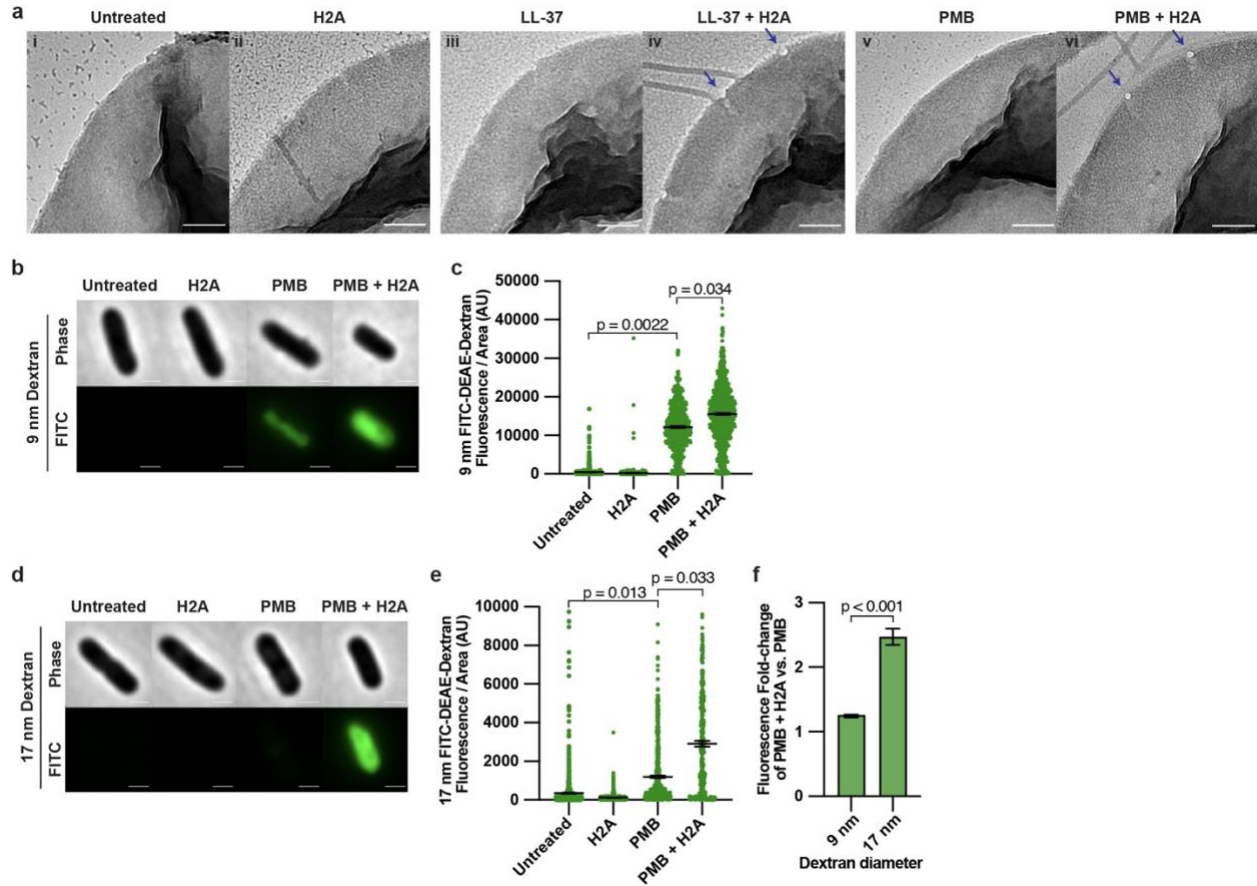
Figure 3.3. Membrane Deformations and Increased Dextran Uptake are Induced by the Combination of PMB and H2A. (a) Representative transmission electron microscopy (TEM) images of *E. coli* (i) without treatment or following treatment of (ii) 10 µg/ml H2A, (iii) 20 µg/ml LL-37, (iv) LL-37 and H2A, (v) 1 µg/ml PMB, or (vi) PMB with H2A. Arrows point towards high contrast round membrane deformations. Scale bars represent 100 nm. Representative phase-contrast and fluorescence images of (b) 9 nm or (d) 17 nm FITC-DEAE-dextran with *E. coli* following treatments of 10 µg/ml H2A, 0.2 µg/ml PMB, or a combination of H2A and PMB. Scale bars represent 1 µm. Distribution and mean intracellular fluorescence of (c) 9 nm or (e) 17 nm FITC-DEAE-dextran in individual *E. coli* following treatment of PMB or a combination of H2A and PMB. A minor subset of data points are above the vertical axis maximum and are not displayed; full data are in Source Data. (f) Fold-change of FITC-DEAE-Dextran fluorescence

61

following treatment with PMB and H2A compared to PMB alone. Fluorescence was quantified in arbitrary units (AU). The mean and SEM of three independent experiments are shown. Two-tailed Welch's tests were performed, with p-values indicated in graphs.

3.4.3 Synergistic Combination Induces Pore Formation in the OM and IM

We visualized bacterial membranes using cryogenic TEM (cryoEM), which better preserves membrane structures and enables visualization of both the OM and IM. Cells were treated for only 15 minutes due to complete lysis of most cells by PMB+H2A co-treatment beyond this time. This short treatment time enabled us to capture potential early-stage membrane deformation events and detect pores. H2A or PMB treatment alone created no obvious deformation of either membrane for most cells (**Fig. 3.4a**). However, PMB+H2A co-treatment caused significant disruptions of the OM and IM (**Fig. 3.4a**). Since the PMB+H2A treatment increased membrane permeability and the uptake of histones and larger dextran molecules (**Fig. 3.1d-e, Fig 3.1m-n, and Fig. 3.3d-e**), we interpret the OM and IM disruptions to be membrane pores.

Cells treated with PMB+H2A contained up to 15 pores per cell, with pore sizes averaging 25.8 nm in length (**Fig. 3.4b-c**). No pores in the OM were observed in untreated cells. Few pores were observed in cells that were treated with H2A or PMB alone (**Fig. 3.4b-c**). In the rare cases that pores were observed, they were smaller, at 15.4 and 17 nm for H2A or PMB treatment, respectively (**Fig. 3.4b-c**). A fraction of PMB+H2A-treated cells did not contain pores, which is attributed to the brief treatment duration. IM disruption was only observed following combined PMB+H2A treatment (**Fig. 3.4a**), suggesting that H2A facilitates IM disruption in combination with PMB.

PMB alone increased uptake of small molecules including PI and smaller dextrans into the cytoplasm (**Fig. 3.1b-c and Fig. 3.3b-c**), which suggests that PMB permeabilizes both the OM and IM. The lack of obvious membrane disruptions in individual PMB or H2A treatments could reflect multiple causes, including that PMB pores may be transient or below our resolution limit. In contrast, H2A alone does not increase the uptake of PI, smaller dextrans, or H2A itself (**Fig.**

3.1m-n, Fig. 3.3b-c, and Fig. 3.1d-e), suggesting that H2A alone does not permeabilize either membrane.

3.4.4 Lipopolysaccharides Block the Membrane-permeabilization Activity of H2A

We next addressed why the OM is permeabilized by PMB and not H2A. PMB targets lipid A, which anchors LPS to the membrane and helps form a protective LPS layer on the outer leaflet of the OM[21,32,33]. H2A can bind to LPS[34] but could have higher activity towards other targets. We hypothesized that LPS blocks the membrane-permeating activity of H2A and assessed the impact of H2A on membrane permeability in a Δ*waaC* mutant, which contains lipid A but lacks the LPS outer core and a portion of the inner core[12]. The Δ*waaC* mutant exhibited significantly increased H2A uptake and slightly increased PI fluorescence in response to H2A at 10 µg/ml (**Fig. 3.4d-e**). These effects were further intensified at a higher H2A concentration (50 µg/ml). In contrast, H2A uptake and PI fluorescence did not increase in wild-type cells in response to either H2A concentration (**Fig. 3.4d-e**). Thus, LPS-deficient cell membranes are more susceptible to the membrane-permeabilizing effects of H2A.

Membrane permeabilization by H2A should hinder cell growth. Indeed, treatment of the Δ*waaC* mutant with lower H2A concentrations partially delayed exponential growth and fully inhibited growth at a higher concentration (**Fig. 3.4f**). No growth delays were observed for the wild-type strain treated at the same H2A concentrations, although final cell density was decreased. Thus, LPS inhibits the membrane-permeabilizing activity and growth-inhibitory effects of H2A.

The ability of H2A to permeabilize the OM of the Δ*waaC* mutant suggests histones could have pore-forming activity towards membranes lacking LPS. In *E. coli*, the bulk of the LPS is contained on the OM outer leaflet, with significantly less LPS on either IM leaflet. We assessed

the pore-forming activity of PMB and H2A on bacterial spheroplasts, produced by removing the OM and cell wall, leaving predominantly the IM and cytoplasm[35]. Tracking changes in PI fluorescence in at least 6000 individual spheroplasts over the course of 12 minutes, we found that H2A treatment significantly increased PI uptake and membrane permeability (**Fig. 3.5a-b**). In particular, H2A induced a larger change in PI uptake than PMB (**Fig. 3.5b-c**). Thus, H2A alone permeabilizes the IM but does not permeabilize the OM outer leaflet, as evidenced by the inability of H2A to induce the uptake of PI, small dextrans, or H2A itself in cells containing intact OMs and LPS (**Fig. 3.1m-n, Fig. 3.3b-c, and Fig. 3.1d-e**). Thus, histones have differential activity towards the outer leaflets of the OM and IM. The reduced LPS levels in the IM could facilitate membrane-permeabilizing activity towards the IM.

We hypothesized that H2A could also permeabilize the inner leaflets of both the OM and IM due to limited LPS in these leaflets. To test this hypothesis, we introduced fluorescently-labeled H2A (AF488-H2A) into the cytoplasm of wild-type cells via electroporation. AF488-H2A fluorescence confirmed H2A uptake into the electroporated cells. The presence of cytoplasmic H2A coincided with a significant increase in PI uptake (**Fig. 3.5d-e**), indicating that H2A increased permeation of both the IM and OM from within the cell. This membrane permeation effect was not due to electroporation alone, as PI was not detected in electroporated cells without H2A (**Fig. 3.5d-e**). The effect cannot be attributed solely to the inhibitory effects of histones on transcription, as the increase in PI uptake was observed within 10 minutes of H2A introduction. A modest level of H2A was detected in cells in which H2A was supplied but were not electroporated (**Fig. 3.5d-e**). However, only a small effect on PI uptake was observed, which we attribute to the increased susceptibility of cells to H2A due to the electrocompetent preparation procedure. Together, these

65

data support the hypothesis that H2A permeabilizes membranes that lack LPS, including the IM and OM inner leaflets.

Our findings support a model of AMP-histone synergy in which AMPs permeabilize the OM, which increases the uptake of AMPs and histones into the periplasmic space (**Fig. 3.5f**). Here, these molecules induce the formation of large pores (~26 nm in size) in the IM and OM that facilitate cell death. We developed a theoretical model to further understand how the membrane-permeating activities of AMPs and histones give rise to synergy. The model simulated the entry of AMPs and histones into bacteria using a system of differential equations (schematic in **Fig. 3.5g**; model derivation described in the Methods and Extended Data Synergy Model sections). We differentiated between pore formation activity towards two types of surfaces: the LPS-containing OM outer leaflet surface; and the OM inner leaflet and both IM leaflet surfaces, which contain far less LPS and are referred to here collectively as non-LPS surfaces. Antimicrobial synergy scores were computed, which are ratios that measure the relative cytoplasmic concentrations of AMPs and histones that are supplied extracellularly in combination or individually. The concentrations were assessed in the cytoplasm because these molecules have additional disruptive activity there[24,36]. Synergy scores were assessed for a broad range of pore-forming rates toward LPS and non-LPS membrane surfaces and plotted using dimensionless rate ratios to determine how changes in pore formation rates impact synergy (parameters in the Extended Data Synergy Model sections).

Synergy scores strongly increased with increasing histone activity towards non-LPS membranes and with decreasing activity towards LPS membranes (**Fig. 3.5h).** The maximum synergy was observed when histone activity towards LPS membranes was significantly lower than the value of AMP activity (vertical dashed line) and histone activity towards non-LPS membranes was significantly higher than AMPs (**Fig. 3.5h)**. In support of this model, our experimental data

indicate that H2A has relatively low pore-forming activity towards the LPS-rich OM compared to PMB (**Fig. 3.1d-e, Fig. 3.1m-n, and Fig. 3.3b-e**) and LL-37[1,24], and that H2A has higher pore-forming activity towards non-LPS membranes compared to PMB (**Fig. 3.4d-f and Fig. 3.5a-e**). These results indicate that synergy is highest when H2A and AMPs differentially target non-LPS and LPS membranes and suggest that the combination of H2A with either LL-37 or PMB is near a synergy maximum.

To further assess the validity of this model, we characterized PMB+H2A synergy in the Δ*waaC* LPS mutant. H2A has increased permeabilizing activity specifically towards the OM due to the truncation of LPS in the strain (**Fig. 3.4d-e**) but the activity towards the non-LPS membrane is unchanged. The LPS truncation did not have a significant impact on PMB activity (**Fig. 3.5i**). The model predicts that the increased activity of H2A towards the OM should decrease PMB+H2A synergy. Indeed, PMB+H2A gave an FIC index of 0.75 in the Δ*waaC* mutant, indicating an additive rather than synergistic effect (**Fig. 3.5i**).
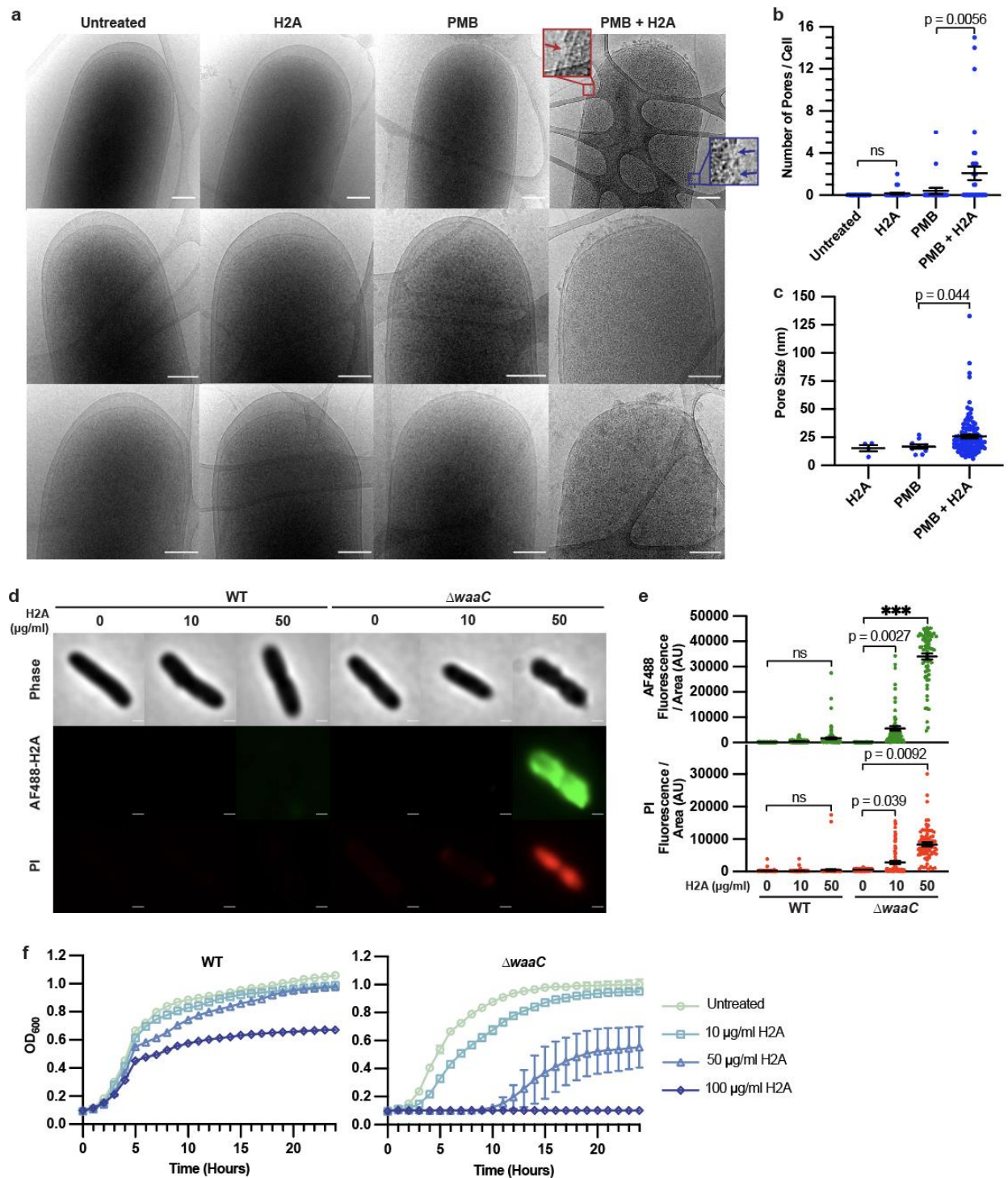
Figure 3.4. H2A Forms Membrane Pores in Combination with PMB and Permeabilizes Membranes that Lack LPS. (a) Representative cryoEM images of untreated *E. coli* or *E. coli* treated with 10 µg/ml H2A, 1 µg/ml PMB, or both, for 15 minutes. Scale bars represent 200 nm.

Insets show magnified portions of the OM and IM, with examples of OM disruption (red arrow) and both IM and OM disruption (blue arrows). (b) Distribution of OM pores per cell in cryoEM experiments, with each data point representing an individual bacterial cell. (c) Distribution of OM pore sizes in cryoEM experiments, with each data point representing an individual pore. Cells lacking pores were excluded from the analysis. (d) Representative phase-contrast and fluorescence images of wild-type (WT) and $\Delta waaC$ *E. coli* following treatment with AF488-H2A for 1 hour. Scale bars represent 500 nm. (e) Distribution and mean intracellular fluorescence of AF488-H2A and PI fluorescence for experiments in panel d. Means and SEM are shown for three independent experiments. Fluorescence quantifications are shown per thousands of arbitrary units (kAU). (f) Optical densities (OD_{600}) of WT (left) and $\Delta waaC$ (right) *E. coli* cultures treated with different concentrations of H2A. Data points represent the average of four independent experiments and error bars indicate the SEM. Two-tailed Welch's t-tests were performed, with p-values indicated in graphs or indicated as "ns" for nonsignificant.

3.4.5 Synergistic Activity of PMB and H2A is Effective Against the Opportunistic Pathogen

Pseudomonas aeruginosa

We hypothesized that the AMP+histone synergistic mechanism could be effective towards *P. aeruginosa*, a clinically significant pathogen with elevated antibiotic tolerance[37]. We used 1 µg/ml PMB and 10 µg/ml H2A, the same concentrations as used for *E. coli,* to determine relative antimicrobial efficacy (**Fig. 3.6**). Individual treatments of PMB or H2A had no significant impact on CFUs, indicating that these concentrations are sub-inhibitory towards *P. aeruginosa* (**Fig. 3.6a**). In contrast, PMB+H2A at these concentrations reduced *P. aeruginosa* CFUs by over 5 orders of magnitude on non-selective agar plates and inhibited growth for 15 hours (**Fig. 3.6a-b**). Checkerboard assays revealed an FIC index of 0.19 (**Fig. 3.6c**), supporting a strong synergistic effect[29]. Kanamycin, gentamicin, and tetracycline at the same concentrations as used against *E. coli* were ineffective at inhibiting *P. aeruginosa* growth (**Fig. 3.6d**). PMB+H2A also completely inhibited the growth of a cystic fibrosis clinical isolate *P. aeruginosa* (**Fig. 3.6e**), suggesting the strategy could be broadly effective. Together, these data indicate that PMB+H2A is bactericidal across multiple Gram-negative bacteria.

We hypothesized that AMP+histone also inhibit growth of *P. aeruginosa*. PMB moderately increased PI uptake in *P. aeruginosa* (**Fig. 3.6f-g**) while addition of H2A increased it further. High contrast membrane deformations were again observed using TEM for cells co-treated with the PMB+H2A combination, but not in individually treated cells (**Fig. 3.6h**). No pores were observed in the OM or IM of untreated, H2A-treated, or PMB-treated *P. aeruginosa* using cryoEM (**Fig. 3.6i-k**). However, multiple pores averaging 22.1 nm in size were observed in *P. aeruginosa* co-treated with PMB+H2A (**Fig. 3.6i-k**). The PMB+H2A co-treatment increased uptake of 9 and 17 nm fluorescent dextran molecules (**Fig. 3.6l-o**). The addition of H2A to PMB increased uptake of

17 nm dextrans compared to PMB-treated cells alone (2.6x), an effect which was diminished using 9 nm dextrans (1.9x) (**Fig. 3.6p**). These results indicate that PMB-induced pores are partly restrictive towards 17 nm dextrans and the addition of H2A significantly increases pore sizes compared to those established by PMB alone. Together, these results are consistent with the effects observed in *E. coli*, where combined PMB+H2A treatment induces formation of more and larger pores that enable uptake of large molecules.
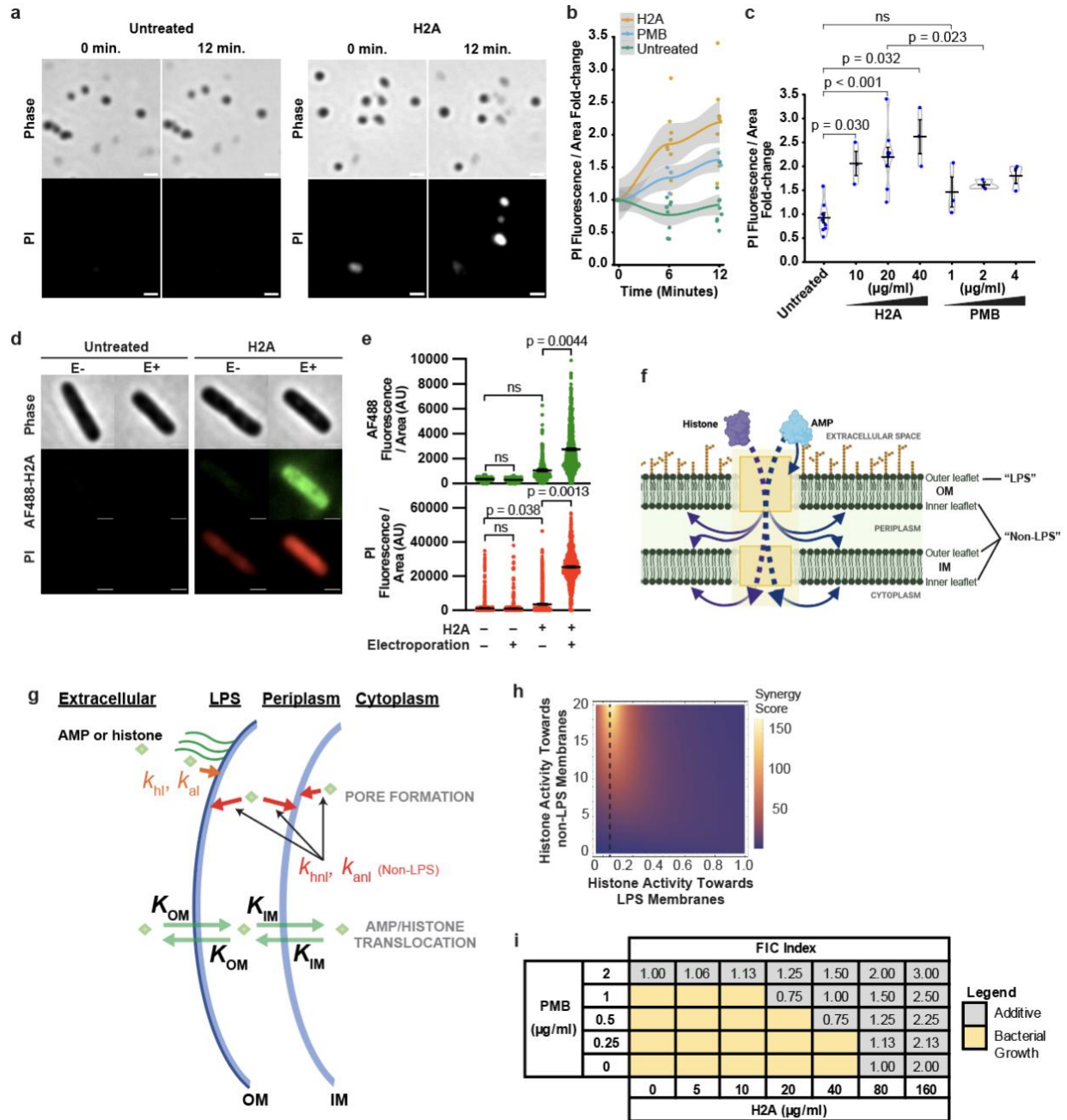
Figure 3.5. H2A Permeabilizes Non-LPS Membranes. (a) Representative phase contrast and PI fluorescence images of *E. coli* spheroplasts in microchannels at the indicated time points in which media containing 40 µg/ml H2A or no treatment was pulsed into the microchannels after 2 minutes. Scale bars represent 2 µm. (b) Fold-change in PI fluorescence relative to the value at 0 minutes in microchannel experiments using 20 µg/ml H2A and 2 µg/mL PMB is shown with a local

regression model using gaussian smoothing and a confidence interval of 95%. (c) PI fluorescence fold-change after 12 minutes for the indicated H2A and PMB concentrations. Violin plots indicate the distribution of the average of individual experiments using gaussian smoothing. Mean and SEM are shown. Each data point in panels b and c represents an independent experiment in which at least 2000 individual spheroplasts were analyzed. (d) Representative phase-contrast and fluorescence images of AF488-H2A and PI in *E. coli* at 10 minutes following electroporation (E+) or no electroporation (E-) with 25 µg/ml AF488-H2A. Scale bars represent 1 µm. (e) Distribution and mean intracellular fluorescence of AF488-H2A and PI from experiments in panel d, with each data point representing an individual cell. The mean and SEM of three independent experiments are shown. Fluorescence was quantified in arbitrary units (AU). (f) Proposed mechanistic model of antimicrobial synergy between histones and AMPs in which AMPs enable histones to translocate past the LPS layer, where histones can form pores in non-LPS membranes. (g) Schematic indicating bacterial compartments, membranes, and associated parameters of the predictive AMP-histone model. (h) Antimicrobial synergy scores for a range of histone pore formation rates against LPS and non-LPS membranes. Scores were computed using a theoretical model that determines the relative concentrations of AMPs and histones in cells that are treated with the molecules individually or in combination. The histone pore formation rates are normalized by a fixed AMP pore formation rate, yielding dimensionless parameters along the x and y axes (k_{hl}/k_{al} and k_{hnl}/k_{al}, respectively). The vertical dashed line indicates $k_{hl}/k_{al} = 0.1$. The full derivation, parameters, and discussion of model are given in the Methods and Supplementary Information Synergy Model sections. (i) Checkerboard assay to assess antimicrobial synergy between PMB and H2A towards the *E. coli* Δ*waaC* mutant after 24 hours. Two-tailed Welch's t-tests were performed, with p-values indicated in graphs or indicated as "ns" for not significant.

3.4.6 Combining PMB and H2A is Effective at Killing P. aeruginosa In Vivo

To determine if the PMB+H2A synergy is also effective *in vivo*, we first tested wax moth larvae (*Galleria mellonella*), which has been used as a model for *P. aeruginosa* infection[38,39]. *P. aeruginosa* were combined with treatments and immediately injected into *G. mellonella* larvae. H2A and PMB were supplied at the same concentrations as the *in vitro* experiments. No larvae injected with phosphate-buffered saline (PBS) or H2A alone survived after 24 hours (**Fig. 3.7a**). PMB treatment increased the survival of a small fraction of the larvae to 48 hours. Remarkably, all larvae treated with PMB+H2A survived for at least 5 days, comparable to the group treated with gentamicin. A high concentration of gentamicin (480 µg/ml) was necessary to achieve larvae survival for this duration, as a lower concentration (240 µg/ml) was not effective. These results suggest that the PMB+H2A combination is synergistic and effective in larvae.

We also assessed efficacy of PMB+H2A in a clinically relevant murine model of blinding *P. aeruginosa* corneal infection. Bacterial replication and infiltration of neutrophils leads to loss of corneal clarity that can be quantified by image analysis[40,41]. The corneal epithelium was abraded, and 5 x 10^4 *P. aeruginosa* strain PAO1 was added topically to initiate the infection. Mice were given topical PMB, H2A, PMB+H2A, or gentamicin three times per day over 48 hours as indicated (**Fig. 3.7b**). PMB dosage used was the minimum amount that caused a statistically significant reduction in CFUs; H2A dosage was the same molar ratio with PMB used *in vitro*. At 48 hours post-infection, we performed image analysis of corneal opacity, which quantifies total corneal disease, and eyes were homogenized and plated for CFU to quantify viable bacteria.

Consistent with previous reports, infection with *P. aeruginosa* resulted in severe corneal opacity, while corneas of gentamicin-treated mice remained clear (**Fig. 3.7c-d**). H2A-treated mice had the same percent corneal opacity as untreated (PBS) mice, while PMB alone partially inhibited

corneal opacity (**Fig. 3.7c-d**). In contrast, corneas of mice that were administered with PMB+H2A had reduced disease, significantly lower than PMB alone (**Fig. 3.7c-d).** Quantification of CFUs showed significant bacterial reduction following PMB+H2A treatment compared to PBS, H2A, or PMB alone (**Fig. 3.7e**). In particular, the effects on corneal opacity and CFU counts resembled those due to gentamicin treatment (**Fig. 3.7d-e**). Thus, combined PMB+H2A treatment is effective in two models of *P. aeruginosa* infection and inhibits corneal disease in a clinically relevant model of *P. aeruginosa* disease.
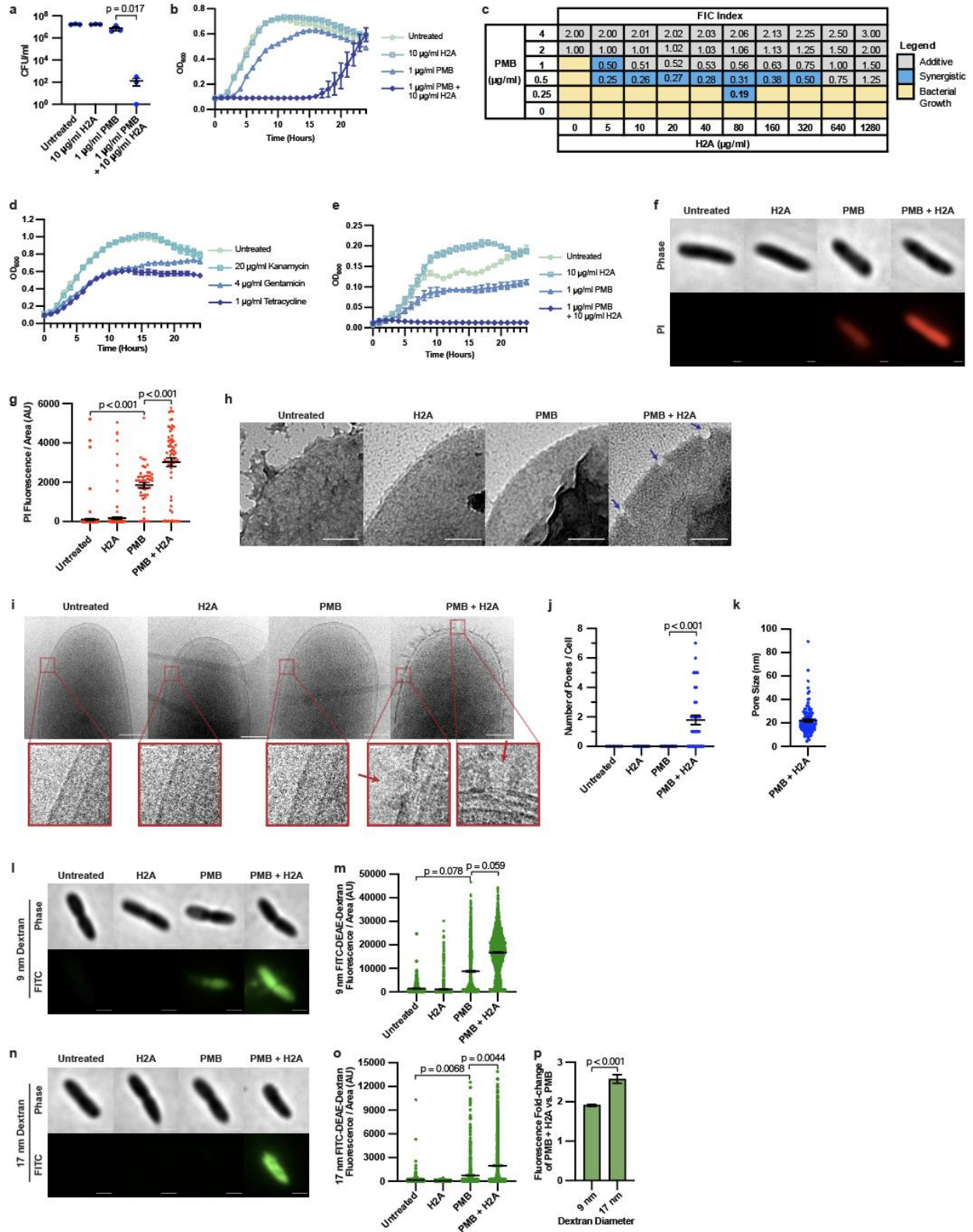
Figure 3.6. Synergy Between H2A and PMB Causes Membrane Pores in the Pathogen *P. aeruginosa*. (a) The effect of H2A and PMB on *P. aeruginosa* on colony forming units (CFU). Data points represent independent experiments. (b) Optical density (OD_{600}) of cultures with or without the same treatments as panel a. Data points indicate the average of 4 independent experiments and error bars indicate the SEM. (c) Checkerboard assay to assess antimicrobial synergy between PMB and H2A towards *P. aeruginosa* after 8 hours. (d) Optical densities (OD_{600}) of *P. aeruginosa* treated with kanamycin, tetracycline, and gentamicin or untreated ($n = 4$ for each condition, error bars indicating SEM). (e) Optical densities of the cystic fibrosis clinical isolate *P. aeruginosa* P2m treated with H2A, PMB, or both, or untreated ($n = 4$ for each condition, error bars indicating SEM). (f) Representative phase-contrast and PI fluorescence images and (g) associated intracellular PI fluorescence distributions of *P. aeruginosa* following a 1-hour treatment of 10 µg/ml H2A, 1 µg/ml PMB, a combination of H2A and PMB, or untreated. Scale bars represent 500 nm. Fluorescence was quantified in arbitrary units (AU). Each data point represents an individual cell. (h) Representative transmission electrom microscopy images of untreated *P. aeruginosa* or *P. aeruginosa* treated with 10 µg/ml H2A, 1 µg/ml PMB, or both. Arrows point towards high contrast round membrane deformations. Scale bars represent 100 nm. (i) Representative cryoEM images of *P. aeruginosa* that were either untreated or treated for 30 minutes with the indicated conditions. Scale bars represent 200 nm. The red boxes magnify a portion of the OM and IM, and the red arrows point to examples of OM disruption, with scale bars representing 25 nm. (j) OM pore number per cell in the full set of cryoEM data is shown, with each data point representing an individual cell. (k) Pore sizes due to the combination of H2A and PMB, with each data point representing an individual pore. (l) Representative phase-contrast and fluorescence images and (m) associated mean intracellular fluorescence distributions of 9 nm

diameter FITC-DEAE-dextrans with *P. aeruginosa* following treatments of 10 µg/ml H2A, 1 µg/ml PMB, a combination of H2A and PMB, or untreated. Scale bars represent 1 µm. (n) Representative phase-contrast and fluorescence images and (o) associated mean intracellular fluorescence distributions using the same conditions but 17 nm diameter FITC-DEAE-dextrans. Scale bars represent 1 µm. (p) Fold-change of FITC-DEAE-Dextran fluorescence in panels c through e following treatment with PMB and H2A compared to PMB alone. Data points in panels c and e represent individual bacterial cells. Fluorescence was quantified in arbitrary units (AU). Mean and SEM of three independent experiments are shown. Two-tailed Welch's t-tests were performed with p-values indicated in graphs.
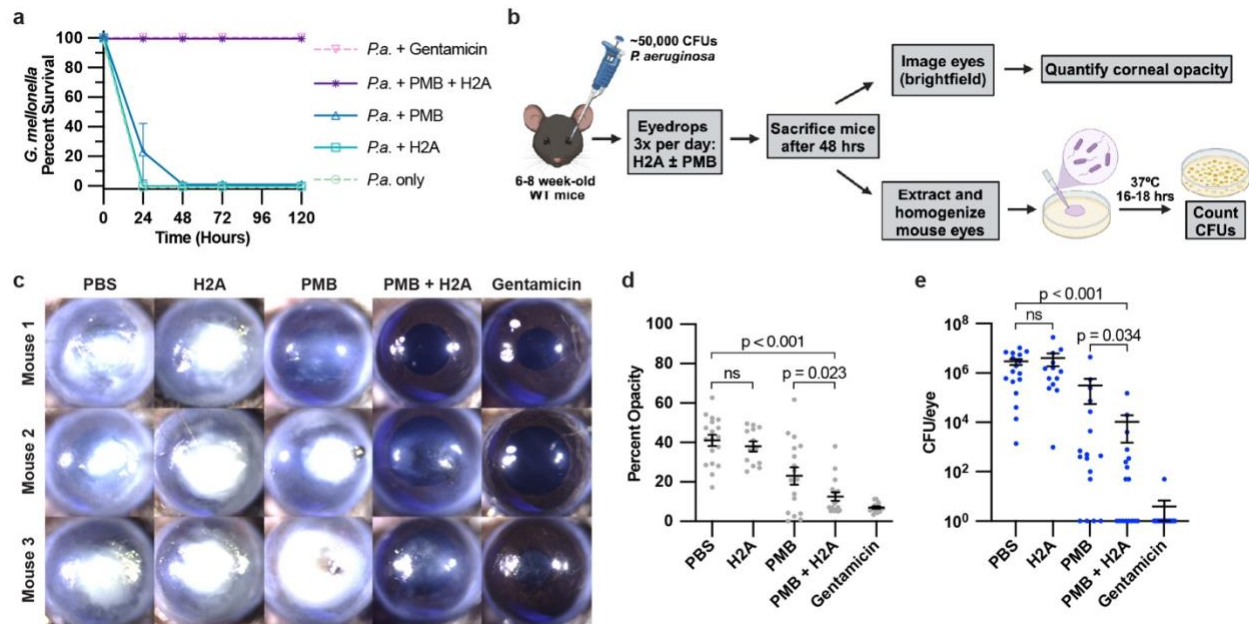
Figure 3.7. Combining PMB and H2A is Effective at Killing *P. aeruginosa* in Wax Moth Larvae and in a Murine Model of Corneal Infection. (a) Survival curve of wax moth larvae *G. mellonella* infected with untreated *P. aeruginosa* ("*P.a.*") or *P. aeruginosa* treated with 10 µg/ml H2A, 1 µg/ml PMB, both, or 480 µg/ml Gentamicin (n = 9 for each condition). (b) Schematic of mouse corneal infection experiments. (c) Representative brightfield images of mouse corneas 48 hours after infection with *P. aeruginosa* and treatment with either PBS, 10 µg H2A, 500 ng PMB, both PMB and H2A, or 30 µg Gentamicin. (d) Quantification of corneal opacity 48 hours post-infection, with each data point representing a single mouse cornea. (e) CFUs of *P. aeruginosa* from homogenized corneas in panel d, with each data point representing a single mouse cornea. Mean and SEM of all animals are shown. One-tailed Welch's t-tests were performed, with p-values indicated in graphs or indicated as "ns" for nonsignificant.

3.5 Conclusion

While antimicrobial synergies of AMPs and antibiotics have been reported[2,42], the mechanisms underlying the synergy are not well understood. Here, we have described the underlying mechanism of antimicrobial synergy between AMPs and histone H2A. We have shown that the synergy is due to AMPs targeting the LPS-containing OM whereas histones target membranes containing less LPS. This combination is bactericidal for *E. coli* and *P. aeruginosa* through membrane pore creation in both the OM and IM (**Fig. 3.5f**). Our results demonstrate that differential targeting of LPS and non-LPS membrane surfaces is a highly effective antimicrobial mechanism.

LPS functions as a barrier against the membrane-permeating effects of H2A, an interpretation supported by activity of H2A towards membrane leaflets that contain little LPS. H2A has little activity towards the OM outer leaflet, supported by the lack of H2A, PI or dextran uptake into the cytoplasm or periplasm of wild-type cells. In contrast, the introduction of H2A into the cytoplasm via electroporation increased uptake of extracellular PI and H2A increased PI uptake in spheroplasts. In addition, membrane permeabilization by H2A is observed towards the Δ*waaC* mutant, which has truncated LPS. Thus, LPS functions as a barrier that inhibits H2A activity against the outer leaflet of the OM. LPS domains are rearranged into hexagonal assemblies and scrambled by PMB, resulting in decreased membrane thickness and increased membrane permeability[19–21]. H2A's low activity towards the OM outer leaflet suggests it does not rearrange LPS in a similar way, even though H2A has greater affinity towards LPS than PMB[34]. Thus, the lack of outer leaflet OM-permeabilizing activity by H2A could reflect H2A binding to LPS rather than rearranging it. In this interpretation, LPS protects the membrane against H2A membrane-

permeabilizing activity by binding to it, possibly because LPS is highly negatively charged and histones have a positive charge.

The role of LPS as a barrier against H2A activity reveals a key aspect of PMB-H2A synergy: PMB facilitates entry of H2A into the periplasmic space, where H2A has activity towards phospholipid membranes. This interpretation is supported by our cryoEM studies that show H2A alone does not form OM or IM pores. PMB increases OM permeabilization, which enables H2A uptake into the periplasm where H2A can cause extensive damage by permeabilizing the OM inner leaflet and IM outer leaflet. In addition, H2A can translocate to the cytoplasm through IM pores, where H2A can permeabilize the IM inner leaflet. The activity of H2A towards the IM inner leaflet is supported by the membrane-permeabilizing effects of cytoplasmic H2A via electroporation. While our study focused on PMB and H2A, OM-permeabilizing activity and synergy were observed with LL-37 in place of PMB, suggesting that differential membrane targeting could arise between H2A and other AMPs. Additional support that synergy arises due to differential targeting by AMPs and H2A is provided by the predictive model, which found that synergy is maximized when histone activity is biased towards non-LPS membranes; increased histone activity towards LPS membranes counterintuitively decreases synergy. In support of the latter scenario, no PMB+H2A synergy was observed in the $\Delta waaC$ mutant, for which H2A has increased activity towards the OM outer leaflet.

The magnitude of the pores created by PMB+H2A is significantly larger than what has been described for other pore-forming antimicrobials[43,44]. The cryoEM data show that PMB+H2A pores are approximately 26 nm in diameter. The dSTORM, dextran, and TEM data are consistent with the observation of pores that are at least 17 nm in size. We propose that pores form through transient pore formation by PMB, which are stabilized or rapidly enlarged by H2A. This model is

supported by the absence of pores in *E. coli* and *P. aeruginosa* treated with PMB alone as shown by cryoEM and by the lack uptake of PI by PMB alone. These are significantly increased when H2A is combined with PMB, as supported by the PI, H2A, dextran uptake data and cryoEM studies. Since no PI uptake is observed using H2A alone, the converse model in which H2A creates transient pores is unlikely. In a second model, PMB and H2A cooperatively form a structure that is more effective at creating pores than either molecule alone. This cooperativity is predicted to give rise to synergy but requires molecular coordination between PMB and H2A, which has not been reported. Future work will need to address the stability of pores formed by PMB and H2A and molecular interactions between the two molecules.

The potent antimicrobial activity of dual PMB+H2A treatment could be effective at treating antibiotic resistant Gram-negative infections in clinical settings, supported by our *in vivo* studies using wax moth larvae and the murine corneal infection model. While the activity was more effective in co-treated animals than those given either reagent alone, PMB+H2A synergy in mice was not as effective as observed *in vitro*. Histones may have lower penetration through the corneal epithelial layer compared to smaller molecules such as PMB and gentamicin, thus limiting their synergistic effects *in vivo*. The synergistic effects may be improved by increasing the penetrative properties of H2A such as through liposomes or lipid droplets[45]. This is feasible as lipid droplets are reported to store high levels of H2A[25,26]. The combination of PMB with histones thus represents a novel treatment approach.

Collectively, we have reported that antimicrobial synergy exists between two agents with different membrane targets. Combining reagents that targets the OM with one that targets the IM is an effective approach for rupturing Gram-negative bacteria. Multi-component membrane

targeting could therefore be a general effective antimicrobial strategy, for which synergistic mechanisms could help address the problem of antimicrobial resistance.

3.6 References

1. Doolin, T. *et al.* Mammalian histones facilitate antimicrobial synergy by disrupting the bacterial proton gradient and chromosome organization. *Nat Comm* (2020) doi:http://doi.org/10.1038/s41467-020-17699-z.

2. Duong, L., Gross, S. P. & Siryaporn, A. Developing Antimicrobial Synergy With AMPs. *Front. Med. Technol.* **3**, 640981 (2021).

3. Duong, L., Gross, S. P. & Siryaporn, A. A novel antibacterial strategy: histone and antimicrobial peptide synergy. *Microb. Cell* **7**, 309–311 (2020).

4. Brinkmann, V. *et al.* Neutrophil Extracellular Traps Kill Bacteria. *Science* **303**, 1532–1535 (2004).

5. Cermelli, S., Guo, Y., Gross, S. P. & Welte, M. A. The lipid-droplet proteome reveals that droplets are a protein-storage depot. *Curr. Biol. CB* **16**, 1783–1795 (2006).

6. Bohlmann, L. *et al.* Chemical Synergy between Ionophore PBT2 and Zinc Reverses Antibiotic Resistance. *mBio* **9**, e02391-18 (2018).

7. Xu, X. *et al.* Synergistic combination of two antimicrobial agents closing each other's mutant selection windows to prevent antimicrobial resistance. *Sci. Rep.* **8**, 7237 (2018).

8. Singh, N. & Yeh, P. J. Suppressive drug combinations and their potential to combat antibiotic resistance. *J. Antibiot. (Tokyo)* **70**, 1033–1042 (2017).

9. Kumar, V. *et al.* Antibiotic adjuvants: synergistic tool to combat multi-drug resistant pathogens. *Front. Cell. Infect. Microbiol.* **13**, 1293633 (2023).

10. Hilliam, Y., Kaye, S. & Winstanley, C. Pseudomonas aeruginosa and microbial keratitis. *J. Med. Microbiol.* **69**, 3–13 (2020).

11. Gaspar, M. C., Couet, W., Olivier, J.-C., Pais, A. a. C. C. & Sousa, J. J. S. Pseudomonas aeruginosa infection in cystic fibrosis lung disease and new perspectives of treatment: a review. *Eur. J. Clin. Microbiol. Infect. Dis. Off. Publ. Eur. Soc. Clin. Microbiol.* **32**, 1231–1252 (2013).

12. Bertani, B. & Ruiz, N. Function and Biogenesis of Lipopolysaccharides. *EcoSal Plus* **8**, (2018).

13. Miller, S. I. Antibiotic Resistance and Regulation of the Gram-Negative Bacterial Outer Membrane Barrier by Host Innate Immune Molecules. *mBio* **7**, e01541-16 (2016).

14. Dürr, U. H. N., Sudheendra, U. S. & Ramamoorthy, A. LL-37, the only human member of the cathelicidin family of antimicrobial peptides. *Biochim. Biophys. Acta* **1758**, 1408–1425 (2006).

15. Li, J. *et al.* Membrane Active Antimicrobial Peptides: Translating Mechanistic Insights to Design. *Front. Neurosci.* **11**, 73 (2017).

16. Evans, M. E., Feola, D. J. & Rapp, R. P. Polymyxin B sulfate and colistin: old antibiotics for emerging multiresistant gram-negative bacteria. *Ann. Pharmacother.* **33**, 960–967 (1999).

17. Lee, C.-C., Sun, Y., Qian, S. & Huang, H. W. Transmembrane pores formed by human antimicrobial peptide LL-37. *Biophys. J.* **100**, 1688–1696 (2011).

18. Henzler Wildman, K. A., Lee, D.-K. & Ramamoorthy, A. Mechanism of lipid bilayer disruption by the human antimicrobial peptide, LL-37. *Biochemistry* **42**, 6545–6558 (2003).

19. Berglund, N. A. *et al.* Interaction of the antimicrobial peptide polymyxin B1 with both membranes of E. coli: a molecular dynamics study. *PLoS Comput. Biol.* **11**, e1004180 (2015).

20. Fu, L. *et al.* Polymyxins induce lipid scrambling and disrupt the homeostasis of Gram-negative bacteria membrane. *Biophys. J.* **121**, 3486–3498 (2022).

21. Manioglu, S. *et al.* Antibiotic polymyxin arranges lipopolysaccharide into crystalline structures to solidify the bacterial membrane. *Nat. Commun.* **13**, 6195 (2022).

22. Amos, S.-B. T. A. *et al.* Antimicrobial Peptide Potency is Facilitated by Greater Conformational Flexibility when Binding to Gram-negative Bacterial Inner Membranes. *Sci. Rep.* **6**, 37639 (2016).

23. Sabnis, A. *et al.* Colistin kills bacteria by targeting lipopolysaccharide in the cytoplasmic membrane. *eLife* **10**, e65836 (2021).

24. Doolin, T., Gross, S.P., & Siryaporn, A. Physical Mechanisms of Bacterial Killing by Histones. in *Physical Microbiology* (https://doi.org/10.1007/978-3-030-46886-6_7, In press.).

25. Anand, P. *et al.* A novel role for lipid droplets in the organismal antibacterial response. *eLife* **1**, e00003 (2012).

26. Bosch, M *et al.* Mammalian lipid droplets are innate immune hubs integrating cell metabolism and host defense. *Science* (2020).

27. Daugelavicius, R., Bakiene, E. & Bamford, D. H. Stages of polymyxin B interaction with the Escherichia coli cell envelope. *Antimicrob. Agents Chemother.* **44**, 2969–2978 (2000).

28. Xu, J. *et al.* Extracellular histones are major mediators of death in sepsis. *Nat. Med.* **15**, 1318–1321 (2009).

29. Hall, M. J., Middleton, R. F. & Westmacott, D. The fractional inhibitory concentration (FIC) index as a measure of synergy. *J. Antimicrob. Chemother.* **11**, 427–433 (1983).

30. Leclercq, R. *et al.* EUCAST expert rules in antimicrobial susceptibility testing. *Clin. Microbiol. Infect. Off. Publ. Eur. Soc. Clin. Microbiol. Infect. Dis.* **19**, 141–160 (2013).

31. Millipore Sigma. Supplier technical data: Fluorescein Isothiocyanate-Dextran. https://www.sigmaaldrich.com/US/en/technical-documents/technical-article/cell-culture-and-cell-culture-analysis/cell-based-assays/fluorescein-isothiocyanate-dextran.

32. Yin, N., Marshall, R. L., Matheson, S. & Savage, P. B. Synthesis of Lipid A Derivatives and Their Interactions with Polymyxin B and Polymyxin B Nonapeptide. *J. Am. Chem. Soc.* **125**, 2426–2435 (2003).

33. Morrison, D. C. & Jacobs, D. M. Binding of polymyxin B to the lipid A portion of bacterial lipopolysaccharides. *Immunochemistry* **13**, 813–818 (1976).

34. Augusto, L. A. *et al.* Histones: A Novel Class of Lipopolysaccharide-Binding Molecules. *Biochemistry* **42**, 3929–3938 (2003).

35. Figueroa, D. M., Wade, H. M., Montales, K. P., Elmore, D. E. & Darling, L. E. O. Production and Visualization of Bacterial Spheroplasts and Protoplasts to Characterize Antimicrobial Peptide Localization. *J. Vis. Exp.* 57904 (2018) doi:10.3791/57904.

36. Le, C.-F., Fang, C.-M. & Sekaran, S. D. Intracellular Targeting Mechanisms by Antimicrobial Peptides. *Antimicrob. Agents Chemother.* **61**, e02340-16 (2017).

37. Sindeldecker, D. & Stoodley, P. The many antibiotic resistance and tolerance strategies of Pseudomonas aeruginosa. *Biofilm* **3**, 100056 (2021).

38. Miyata, S., Casey, M., Frank, D. W., Ausubel, F. M. & Drenkard, E. Use of the Galleria mellonella caterpillar as a model host to study the role of the type III secretion system in Pseudomonas aeruginosa pathogenesis. *Infect. Immun.* **71**, 2404–2413 (2003).

39. Hill, L., Veli, N. & Coote, P. J. Evaluation of Galleria mellonella larvae for measuring the efficacy and pharmacokinetics of antibiotic therapies against Pseudomonas aeruginosa infection. *Int. J. Antimicrob. Agents* **43**, 254–261 (2014).

40. Sun, Y., Karmakar, M., Taylor, P. R., Rietsch, A. & Pearlman, E. ExoS and ExoT ADP Ribosyltransferase Activities Mediate *Pseudomonas aeruginosa* Keratitis by Promoting Neutrophil Apoptosis and Bacterial Survival. *J. Immunol.* **188**, 1884–1895 (2012).

41. Vareechon, C., Zmina, S. E., Karmakar, M., Pearlman, E. & Rietsch, A. Pseudomonas aeruginosa Effector ExoS Inhibits ROS Production in Human Neutrophils. *Cell Host Microbe* **21**, 611-618.e5 (2017).

42. Acar, J. F. ANTIBIOTIC SYNERGY AND ANTAGONISM. *Med. Clin. North Am.* **84**, 1391–1406 (2000).

43. Xhindoli, D. *et al.* New aspects of the structure and mode of action of the human cathelicidin LL-37 revealed by the intrinsic probe p-cyanophenylalanine. *Biochem. J.* **465**, 443–457 (2015).

44. Zakharova, A. A., Efimova, S. S. & Ostroumova, O. S. Lipid Microenvironment Modulates the Pore-Forming Ability of Polymyxin B. *Antibiot. Basel Switz.* **11**, 1445 (2022).

45. Liu, P., Chen, G. & Zhang, J. A Review of Liposomes as a Drug Delivery System: Current Status of Approved Products, Regulatory Environments, and Future Perspectives. *Mol. Basel Switz.* **27**, 1372 (2022).

46. Miller, J. H. *A Short Course in Bacterial Genetics: A Laboratory Manual and Handbook for Escherichia Coli and Related Bacteria. Laboratory Manual*. (Cold Spring Harbor Laboratory Press, 1992).

47. Blattner, F. R. *et al.* The Complete Genome Sequence of *Escherichia coli* K-12. *Science* **277**, 1453–1462 (1997).

48. Quinn, R. A. *et al.* Microbial, host and xenobiotic diversity in the cystic fibrosis sputum metabolome. *ISME J.* **10**, 1483–1498 (2016).

49. Vance, R. E., Rietsch, A. & Mekalanos, J. J. Role of the type III secreted exoenzymes S, T, and Y in systemic spread of Pseudomonas aeruginosa PAO1 in vivo. *Infect. Immun.* **73**, 1706–1713 (2005).

50. Orhan, G., Bayram, A., Zer, Y. & Balci, I. Synergy Tests by E Test and Checkerboard Methods of Antimicrobial Combinations against *Brucella melitensis*. *J. Clin. Microbiol.* **43**, 140–143 (2005).

51. Siryaporn, A., Kuchma, S. L., O'Toole, G. A. & Gitai, Z. Surface attachment induces *Pseudomonas aeruginosa* virulence. *Proc. Natl. Acad. Sci.* **111**, 16860–16865 (2014).

52. Perinbam, K., Chacko, J. V., Kannan, A., Digman, M. A. & Siryaporn, A. A Shift in Central Metabolism Accompanies Virulence Activation in Pseudomonas aeruginosa. *mBio* **11**, e02730-18 (2020).

53. Siryaporn, A., Perchuk, B. S., Laub, M. T. & Goulian, M. Evolving a robust signal transduction pathway from weak cross-talk. *Mol. Syst. Biol.* **6**, 452 (2010).

54. Dempsey, G. T., Vaughan, J. C., Chen, K. H., Bates, M. & Zhuang, X. Evaluation of fluorophores for optimal performance in localization-based super-resolution imaging. *Nat. Methods* **8**, 1027–1036 (2011).

55. Wolter, S. *et al.* rapidSTORM: accurate, fast open-source software for localization microscopy. *Nat. Methods* **9**, 1040–1041 (2012).

56. Xu, J., Ma, H. & Liu, Y. Stochastic Optical Reconstruction Microscopy (STORM). *Curr. Protoc. Cytom.* **81**, 12.46.1-12.46.27 (2017).

57. van de Linde, S. *et al.* Direct stochastic optical reconstruction microscopy with standard fluorescent probes. *Nat. Protoc.* **6**, 991–1009 (2011).

58. Green, M. R., Sambrook, J. & Sambrook, J. *Molecular Cloning: A Laboratory Manual*. (Cold Spring Harbor Laboratory Press, Cold Spring Harbor, N.Y, 2012).

59. Mastronarde, D. N. Automated electron microscope tomography using robust prediction of specimen movements. *J. Struct. Biol.* **152**, 36–51 (2005).

60. Harding, C. R., Schroeder, G. N., Collins, J. W. & Frankel, G. Use of Galleria mellonella as a model organism to study Legionella pneumophila infection. *J. Vis. Exp. JoVE* e50964 (2013) doi:10.3791/50964.

61. Minns, M. S. *et al.* NLRP3 selectively drives IL-1β secretion by Pseudomonas aeruginosa infected neutrophils and regulates corneal disease severity. *Nat. Commun.* **14**, 5832 (2023).

CHAPTER 4: HISTONE SYNERGY IN GRAM-POSITIVE

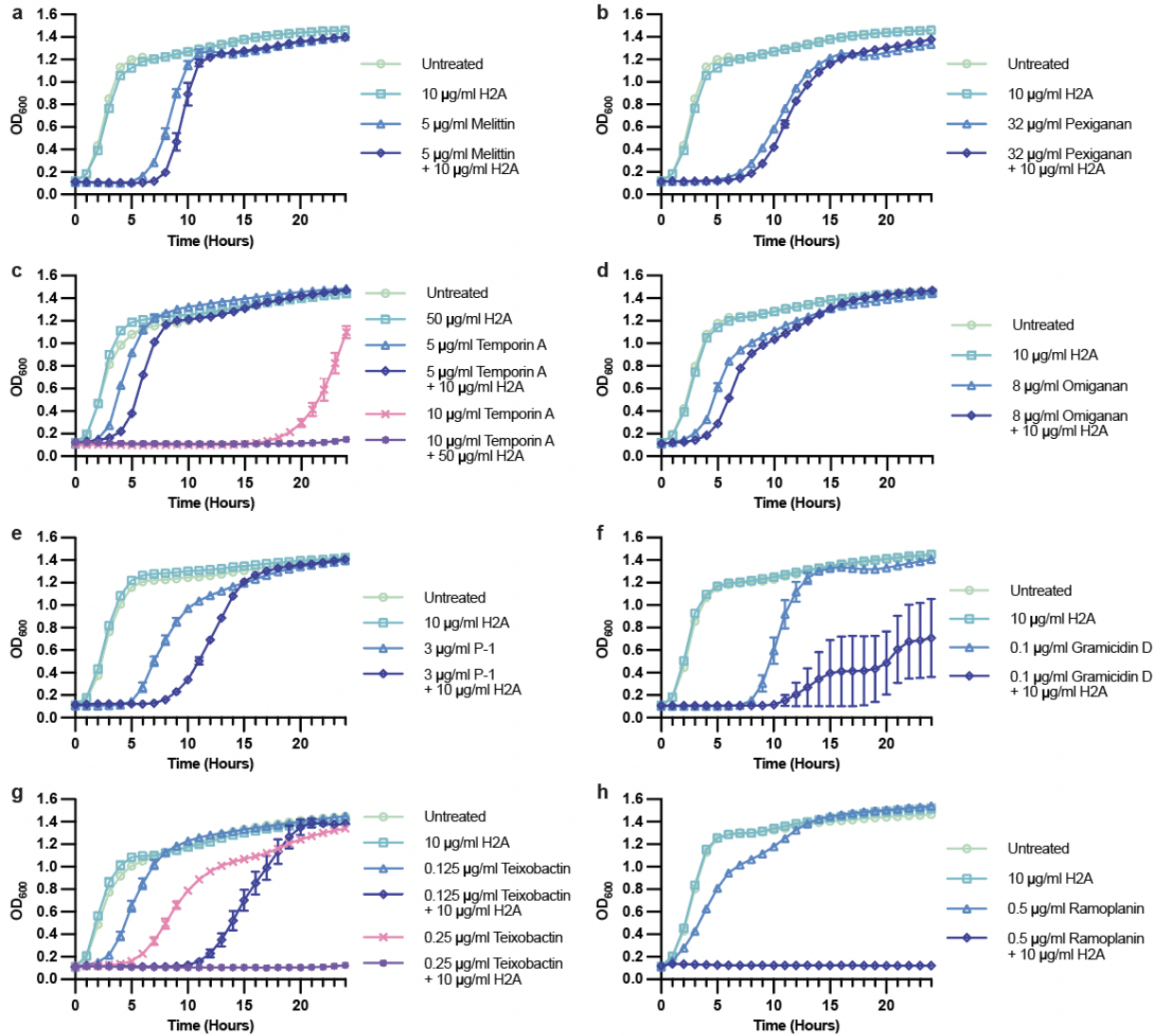# METHICILLIN-RESISTANT *STAPHYLOCOCCUS AUREUS*

4.1 Introduction

Although Gram-negative bacteria, including *P. aeruginosa,* pose a major threat to global health, a common bacterial species found alongside these life-threatening infections is Gram-positive *Staphylococcus aureus*[1]. For example, *S. aureus* is commonly found with *P. aeruginosa* bacteria in cystic fibrosis patients and in chronic skin wounds[2,3]. According to the World Health Organization, *S. aureus* bacteria are considered a serious threat. These opportunistic bacteria have evolved into several multi-drug resistant strains, such as methicillin-resistant *S. aureus* (MRSA), a strain that is insensitive to a majority of current antibiotics[4]. MRSA alone was responsible for over 100,000 deaths in 2019[5]. Thus, understanding alternative strategies against pathogenic Gram-positive bacteria is critical for addressing the increasing threat of antimicrobial resistance.

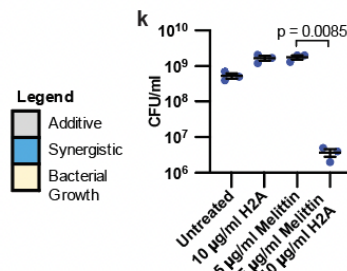## 4.2 Histones Synergize with AMPs in MRSA

Our lab has formerly reported that histone H2A and human AMP LL-37 can synergize in a laboratory strain of *Staphylococcus aureus*[6], suggesting a potentially effective strategy against this bacterial species. However, histone synergy with AMPs was not assessed in pathogenic MRSA. To assess antimicrobial synergy between AMPs with histones in MRSA, histone H2A was combined with the AMPs Melittin, Pexiganan, Temporin A, Omiganan, P-1[7], Gramicidin D, Teixobactin[8], and Ramoplanin. All AMP-histone combinations were found to produce antimicrobial synergy in MRSA, albeit with varying strengths of synergy (**Fig. 4.1a-h**). Of all the combinations tested, Teixobactin and Ramoplanin produced the strongest synergies with H2A

(**Fig. 4.1a-h**). In contrast, the single treatments of Teixobactin, Ramoplanin, or H2A show little to no inhibition of MRSA growth, but the dual treatments of each AMP with H2A inhibit bacterial growth over 24 hours (**Fig. 4.1a-h**). Synergy checkerboard assays confirmed antimicrobial synergy between Teixobactin and Ramoplanin with H2A, as demonstrated by FIC indexes less than or equal to 0.5[9] (**Fig. 4.1i-j**). When the AMPs Melittin and Ramoplanin were combined with H2A to assess bacterial viability post-treatment, the combination of Melittin or Ramoplanin with H2A resulted in 3-log-fold reductions in CFUs of MRSA, consistent with a bacteriostatic effect[10], while the single treatments were comparable to untreated cells (**Fig. 4.1k-l**).
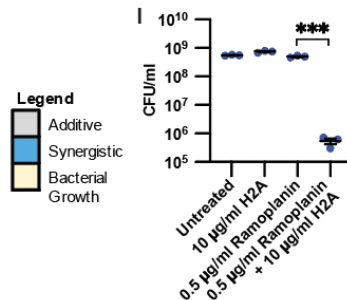
Figure 4.1. AMPs Synergize with H2A Against MRSA. Growth profile of untreated MRSA or MRSA treated with (a) H2A, Melittin, or both, (b) H2A, Pexiganan, or both, (c) H2A, Temporin A, or both, (d) H2A, Omiganan, or both, (e) H2A, P-1, or both, (f) H2A, Gramicidin D, or both, (g) H2A, Teixobactin, or both, (h) or H2A, Ramoplanin, or both. (i) Synergy checkerboard assay performed over 24 hours as an alternative method for assessing antimicrobial synergy between Teixobactin and H2A. (j) Synergy checkerboard assay performed over 24 hours as an alternative method for assessing antimicrobial synergy between Ramoplanin and H2A. (k) CFUs of untreated MRSA or MRSA treated with H2A, Melittin, or both for 1 hour and plated on non-selective LB agar at 37ºC for 18 hours. (l) CFUs of untreated MRSA or MRSA treated with H2A, Ramoplanin, or both for 1 hour and plated on non-selective LB agar at 37ºC for 18 hours. One-tailed Welch's t-tests were performed, with p-values indicated in graphs, or indicated as *** for $p < 0.001$.

4.3 Histones and AMPs Increase Membrane Damage in MRSA

Membrane-impermeable propidium iodide (PI) dye and fluorescence microscopy was used to assess how AMPs and histones may affect MRSA membrane permeability. If membranes are damaged, PI can enter bacterial cells. Higher levels of PI indicate greater membrane damage. Since Ramoplanin and H2A was the strongest synergistic combination found to date, we chose to focus on this combination for further experiments. Consistent with previous data in Gram-negative *E. coli* and *P. aeruginosa*, the dual treatment of Ramoplanin and H2A significantly increased MRSA membrane damage compared to Ramoplanin alone. In contrast, a single treatment of the same concentrations of H2A or Ramoplanin did not induce membrane damage at all, as indicated by the lack of PI fluorescence comparable to that of untreated MRSA (**Fig. 4.2a-b**). Even with up to 4 times greater concentrations of Ramoplanin, bacterial membrane permeability was still significantly less than the dual treatment of Ramoplanin and H2A (**Fig. 4.2b**). Consistent with AMP and histone membrane permeability effects in Gram-negative bacteria, these data suggest that the increased membrane damage from dual treatments of Ramoplanin with H2A is conserved in Gram-positive bacteria. Additionally, these data highlight that histones play a significant role in increasing bacterial membrane permeability when combined with the AMP Ramoplanin.
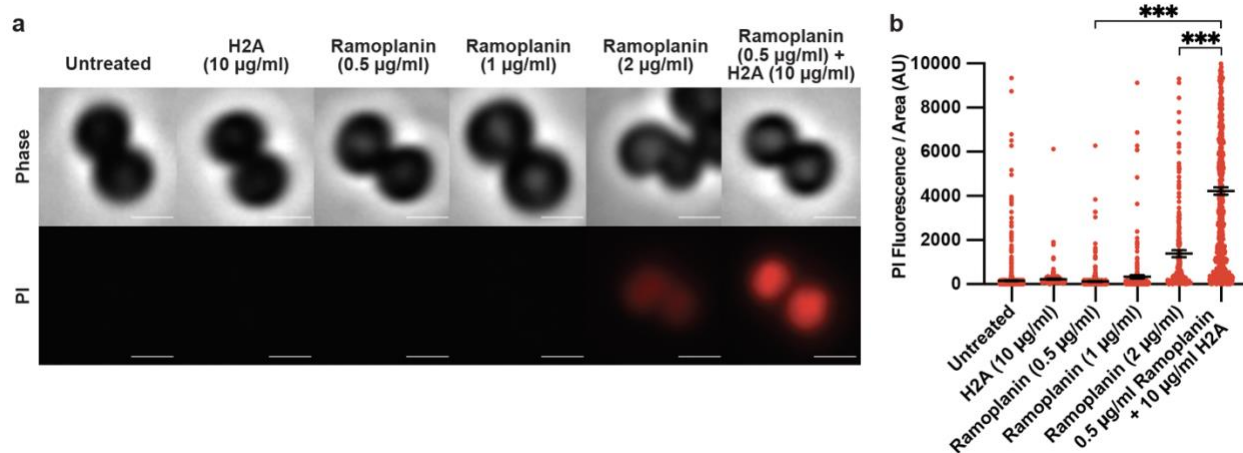
Figure 4.2. Combining Ramoplanin and H2A Increases Membrane Damage in MRSA. (a) Representative phase-contrast and fluorescence images of intracellular propidium iodide (PI) in MRSA following a 1-hour treatment of Ramoplanin, H2A, or both. Scale bars represent 500 nm. (b) Distribution and mean of intracellular PI fluorescence of MRSA following a 1-hour treatment of Ramoplanin, H2A, or both. One-tailed Mann-Whitney tests were performed, with p-values indicated as *** for $p < 0.001$.

4.4 Histone H2A Synergizes with Ramoplanin in a Murine Skin Infection Model

To assess potential the clinical application of using AMPs and histones against MRSA, it is critical to test their efficacy in a mammalian model. To prepare for *in vivo* experiments, treatment conditions were prepared to mimic conditions used in a murine skin infection model[11]. Since Teixobactin and Ramoplanin had the strongest synergies with H2A, *in vivo* experiments were focused on these two AMPs with H2A. Under these conditions, bacterial cells were resuspended in PBS and treated with H2A, Teixobactin, or both, or H2A, Ramoplanin, or both. Upon counting CFUs, the dual treatment of both Teixobactin (at the higher concentration of 16 µg/ml) and Ramoplanin (8 µg/ml) with H2A resulted in synergistic and complete killing of 10^7 CFU/ml of MRSA (**Fig. 4.3a-b**). Vancomycin was used as a positive control against MRSA[12]; however, it should be noted that the concentration used was at least 10 times greater than reported MICs of 0.5 to 2 µg/ml found on the European Committee on Antimicrobial Susceptibility Testing database[13] (**Fig. 4.3a-b**). The data suggest that the combination of Teixobactin or Ramoplanin with H2A is just as efficacious against MRSA as Vancomycin, a common last-resort antibiotic used to treat MRSA infections[12].

Since Teixobactin and Ramoplanin have similar mechanisms of action, in which both molecules negatively affect bacterial peptidoglycan production[14,15], we chose to first focus on treatments using Ramoplanin in combination with histones. As a proof of principle experiment, MRSA was prepared in the same way as in Fig. 4.3b, where bacterial cells were mixed with corresponding treatments, and injected intradermally into mice. After 3 days post-infection, mice were euthanized, and an 8 mm biopsy punch was utilized to collect MRSA-infected skin samples, as described[16]. The skin samples were homogenized, plated on LB agar plates, and incubated at 37 ºC overnight to count CFUs. Mice that were injected with untreated MRSA or MRSA treated with

H2A both showed comparably high amounts of CFUs. Mice injected with MRSA treated with Ramoplanin showed significantly less CFUs, suggesting that Ramoplanin by itself is highly effective *in vivo* (**Fig. 4.3c**). The dual treatment of Ramoplanin and H2A resulted in zero CFUs, suggesting that the treatment is synergistic and effective at killing MRSA *in vivo* (**Fig. 4.3c**). Vancomycin was used as a positive control but was not effective at killing MRSA *in vivo* as it was *in vitro*, despite being a much higher concentration than reported MICs[13]. Despite Vancomycin not being as effective as expected, the dual treatment of Ramoplanin and H2A had a significantly greater efficacy *in vivo* than a drug commonly used as a last line of defense antibiotic to treat MRSA (**Fig. 4.3c**). Using a higher concentration of H2A (20 µg/ml) and lower concentrations of Ramoplanin (4 and 6 µg/ml) did not seem to induce antimicrobial synergy in mice (**Fig. 4.3d**). However, only dual treatments of Ramoplanin and H2A resulted in zero CFUs for one data point, whereas this was not the case for single treatments of Ramoplanin (**Fig. 4.3d**). Additionally, blood samples were collected from mice in Fig. 4.3d to measure levels of bacteremia in mice that had MRSA skin infections. The blood samples were vortexed, spun down, and blood plasma supernatants were used for the CFU experiment. An overnight culture of MRSA was also used independently and added into a blood sample of a non-infected mouse as a positive control for MRSA detection in blood plasma. Interestingly, despite the high levels of MRSA CFUs in the mouse skin samples, MRSA was not detected in most of the blood samples; only one mouse showed less than 100 CFU/ml (**Fig. 4.3e**). These data show promising results that highlight the potential efficacy of synergistic combinations of AMPs with histones in mammalian systems.
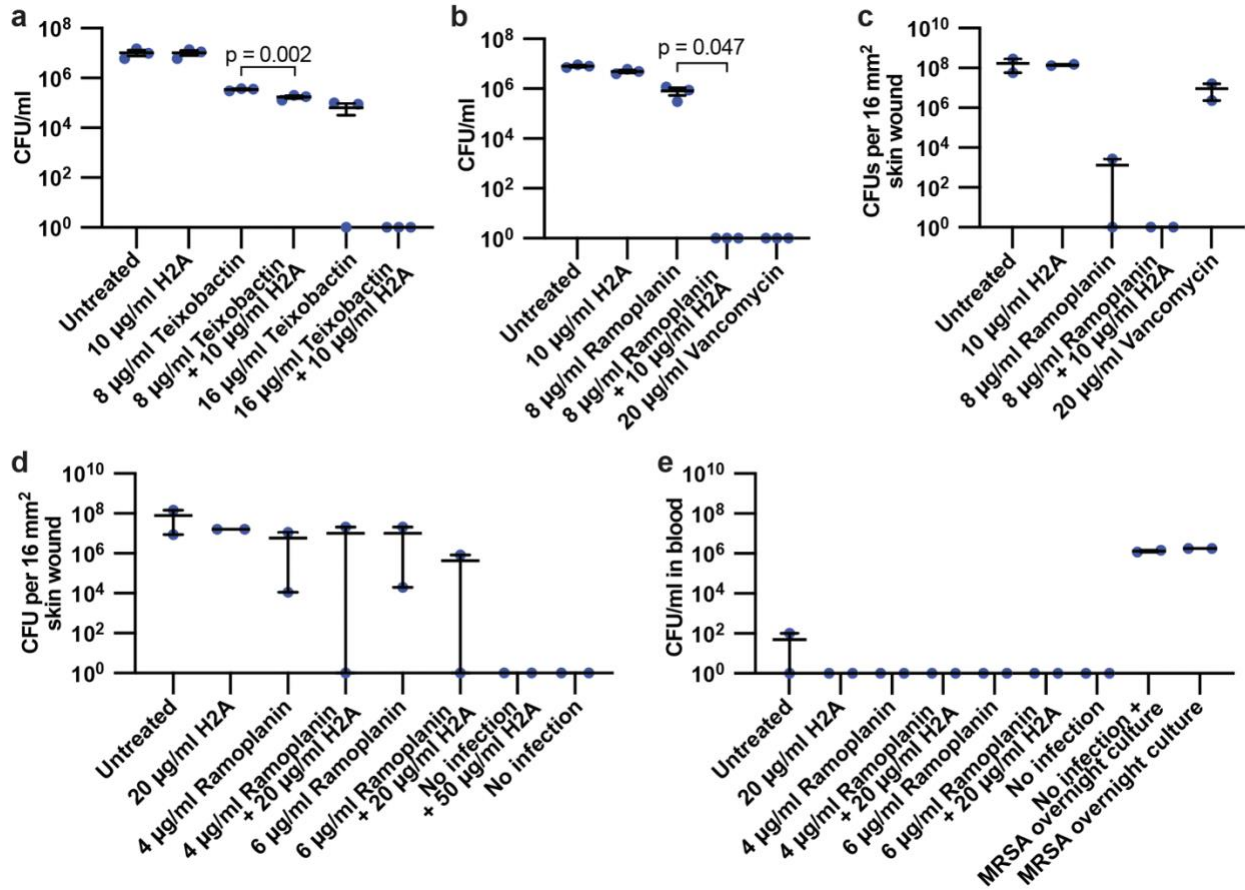
Figure 4.3. Preliminary Data for Ramoplanin and H2A Antimicrobial Synergy Against MRSA in a Murine Skin Infection Model. (a) CFUs of MRSA that was resuspended in PBS, treated with H2A, Teixobactin, or both, and immediately plated on LB agar for 18 hours at 37ºC to mimic infection conditions in a murine skin infection model. (b) CFUs of MRSA that was resuspended in PBS, treated with H2A, Ramoplanin, or both, and immediately plated on LB agar for 18 hours at 37ºC to mimic infection conditions in a murine skin infection model. (c, d) CFUs of homogenized murine skin samples after 3 days post-infection of untreated MRSA or MRSA treated with H2A, Ramoplanin, or both. (e) CFUs in blood plasma of mice after 3 days post-infection of untreated MRSA or MRSA treated with H2A, Ramoplanin, or both. Skin and blood samples were plated on non-selective LB agar at 37ºC for 18 hours. For c-e, n=2 mice. One-tailed Welch's t-tests were performed, with p-values indicated in graphs.

4.5 Conclusion

In summary, this chapter shows that histones could synergize with a range of AMPs against MRSA. However, the two AMPs that most strongly synergized with histones both target peptidoglycan synthesis in Gram-positive cell walls. Since we have recently found that histones target non-LPS cell membranes, it is possible that in order for histones to access the cell membrane in Gram-positive cells, the thick cell wall layer needs to be reduced. Further mechanistic and *in vivo* studies need to be performed to assess how to optimize AMP and histone synergy in Gram-positive bacteria and to treat such infections.

4.6 References

1. Ventola, C. L. The Antibiotic Resistance Crisis. *Pharm. Ther.* **40**, 277–283 (2015).

2. Briaud, P. *et al.* Coexistence with Pseudomonas aeruginosa alters Staphylococcus aureus transcriptome, antibiotic resistance and internalization into epithelial cells. *Sci. Rep.* **9**, 16564 (2019).

3. Serra, R. *et al.* Chronic wound infections: the role of Pseudomonas aeruginosa and Staphylococcus aureus. *Expert Rev. Anti Infect. Ther.* **13**, 605–613 (2015).

4. Klevens, R. M. *et al.* Invasive methicillin-resistant Staphylococcus aureus infections in the United States. *JAMA* **298**, 1763–1771 (2007).

5. Murray, C. J. L. *et al.* Global burden of bacterial antimicrobial resistance in 2019: a systematic analysis. *The Lancet* **399**, 629–655 (2022).

6. Doolin, T. *et al.* Mammalian histones facilitate antimicrobial synergy by disrupting the bacterial proton gradient and chromosome organization. *Nat. Commun.* **11**, 3888 (2020).

7. Oh, D. *et al.* Antibacterial Activities of Amphiphilic Cyclic Cell-Penetrating Peptides against Multidrug-Resistant Pathogens. *Mol. Pharm.* **11**, 3528–3536 (2014).

8. Ling, L. L. *et al.* A new antibiotic kills pathogens without detectable resistance. *Nature* **517**, 455–459 (2015).

9. Orhan, G., Bayram, A., Zer, Y. & Balci, I. Synergy Tests by E Test and Checkerboard Methods of Antimicrobial Combinations against Brucella melitensis. *J. Clin. Microbiol.* **43**, 140–143 (2005).

10. Pankey, G. A. & Sabath, L. D. Clinical Relevance of Bacteriostatic versus Bactericidal Mechanisms of Action in the Treatment of Gram-Positive Bacterial Infections. *Clin. Infect. Dis.* **38**, 864–870 (2004).

11. Zhang, L.-J. *et al.* Diet-induced obesity promotes infection by impairment of the innate antimicrobial defense function of dermal adipocyte progenitors. *Sci. Transl. Med.* **13**, eabb5280 (2021).

12. Yi, Y.-H., Wang, J.-L., Yin, W.-J. & Xu, W.-H. Vancomycin or Daptomycin Plus a β-Lactam Versus Vancomycin or Daptomycin Alone for Methicillin-Resistant Staphylococcus aureus Bloodstream Infections: A Systematic Review and Meta-Analysis. *Microb. Drug Resist. Larchmt. N* (2021) doi:10.1089/mdr.2020.0350.

13. Kahlmeter, G. *et al.* European harmonization of MIC breakpoints for antimicrobial susceptibility testing of bacteria. *J. Antimicrob. Chemother.* **52**, 145–148 (2003).

14. Shukla, R. *et al.* Mode of action of teixobactins in cellular membranes. *Nat. Commun.* **11**, 2848 (2020).

15. Fang, X. *et al.* The mechanism of action of ramoplanin and enduracidin. *Mol. Biosyst.* **2**, 69–76 (2006).

16. Zhang, L. *et al.* Innate immunity. Dermal adipocytes protect against invasive Staphylococcus aureus skin infection. *Science* **347**, 67–71 (2015).

CHAPTER 5: HISTONE SYNERGY IN *ASPERGILLUS* FUNGI

5.1 Introduction

Aspergillus fumigatus and *Fusarium oxysporum* are examples of two fungal species commonly known to cause infections in humans[1–3]. In particular, these pathogenic molds are responsible for fungal keratitis, a disease that causes visual impairment that could ultimately lead to blindness[4]. Due to their increased resistance to current antifungals and limited treatment options[5,6], the World Health organization considers *A. fumigatus* and *F. oxysporum* critical and high priority pathogens, respectively[7,8]. Thus, it is imperative that alternative antifungal methods are studied to address the lack of effective antifungals currently available.

5.2 Antifungal Amphotericin B is Strongly Synergistic with Histone H2A in *Aspergillus fumigatus* and *Fusarium oxysporum*

Since histones synergize with different antibacterial molecules, we wondered if histones could also synergize with current antifungals to increase their effectiveness against the pathogenic fungal species, *A. fumigatus* and *F. oxysporum*. Indeed, combining the membrane-permeating antifungal drug Amphotericin B[9] with histone H2A showed strong synergy against *A. fumigatus*. By measuring fungal growth over time, the dual treatment of Amphotericin B at sub-MIC (100 ng/ml) and H2A (10 µg/ml) showed an approximate 16-hour lag time, which is almost as effective as four-times the concentration used for Amphotericin B, whereas single treatments of Amphotericin B or H2A at the same concentrations were comparable to untreated *A. fumigatus* (**Fig. 5.1a**). However, when treating *A. fumigatus* with the cell wall synthesis inhibitor

Caspofungin[10] and H2A, antimicrobial synergy was not observed; the addition of H2A (10 µg/ml) to Caspofungin (32 µg/ml) did not increase fungal growth inhibition of Caspofungin (**Fig. 5.1b**).

Using a calcofluor white stain that binds to chitin components of fungal hyphae[11], the amount of fungal hyphae growth was imaged and measured after 16 hours following treatments of H2A, Amphotericin B, or both (**Fig. 5.1c**). These images and quantification of calcofluor white fluorescence were consistent with the growth profile of *A. fumigatus* in Fig. 5.1a, where the dual treatment of Amphotericin B (100 ng/ml) with H2A (10 µg/ml) show lack of fungal hyphae growth, but the single treatments show fungal hyphae growth comparable to untreated cells (**Fig. 5.1c-d**). In particular, fungal cells treated with only H2A or Amphotericin B were comparable to that of untreated *A. fumigatus*, but the dual treatment of Amphotericin B with H2A were comparable to the single treatment of 400 ng/ml Amphotericin B, which is the MIC that completely inhibits *A. fumigatus* growth 24 hours (**Fig. 5.1a, 5.1c-d**).

Similarly, when Amphotericin B and H2A were used to inhibit the growth of *F. oxysporum*, a synergistic effect was observed, albeit at a lower magnitude than as observed in *A. fumigatus*. The dual treatment of Amphotericin B (150 ng/ml) and H2A (10 µg/ml) showed an approximate 6-hour lag time, whereas single treatments of Amphotericin B or H2A at the same concentrations were comparable to untreated *A. fumigatus* (**Fig. 5.1e**). However, this growth inhibitory effect is still not comparable to the complete growth inhibition of positive-control Caspofungin (100 µg/ml). Just as in *A. fumigatus*, antimicrobial synergy was not observed between Caspofungin and H2A at the same concentrations (**Fig. 5.1f**).
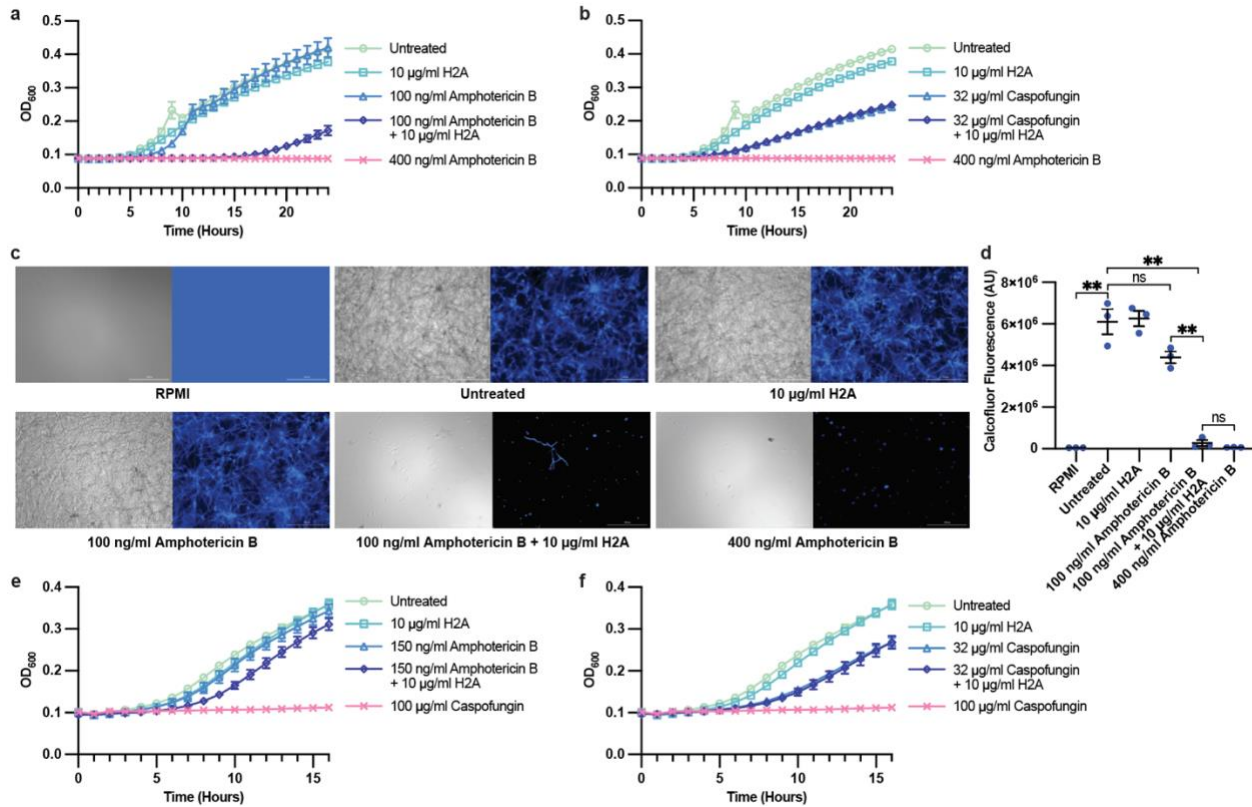
Figure 5.1. Amphotericin B, but Not Caspofungin, are Synergistic with H2A Against *Aspergillus fumigatus* **and** *Fusarium oxysporum*. Growth profile of untreated *A. fumigatus* or *A. fumigatus* treated with (a) H2A, Amphotericin B, or both, or (b) H2A, Caspofungin, or both. (c) Representative phase and calcofluor white-stained fluorescent microscopy images of *A. fumigatus* after treatment with H2A, Amphotericin B, or both for 16 hours at 37°C + 5% CO_2. (d) Quantification of calcofluor white fluorescence following antimicrobial treatments in c. Growth profile of untreated *F. oxysporum* or *F. oxysporum* treated with (a) H2A, Amphotericin B, or both, or (b) H2A, Caspofungin, or both. Error bars indicate SEM. Scale bars indicate 200 μm.

5.3 Antifungals Natamycin, Voriconazole, and Nystatin are Synergistic with Histone H2A in
Aspergillus fumigatus

Since membrane-active Amphotericin B synergizes strongly with H2A in *A. fumigatus*, but not cell-wall synthesis inhibitor Caspofungin, we hypothesized that other membrane active antifungals synergize with H2A against the same pathogen. Amphotericin B specifically binds to ergosterol[12], an essential component of fungal cell membranes, suggesting that this may be a critical prerequisite for synergy with H2A.

We tested three different membrane-active ergosterol-targeting antifungals, including Natamycin, Voriconazole, and Nystatin to test this hypothesis. Natamycin inhibits fungal growth by binding to ergosterol[13] and is commonly used to treat keratitis[14]. Voriconazole, a membrane-active triazole antifungal, decreases the concentration of ergosterol and damages the structure and function of fungal cell membranes by inhibiting 14-alpha-lanosterol demethylation[15,16]. Lastly, Nystatin, which is structurally similar to Amphotericin B[17], also binds to ergosterol and causes membrane damage similar to the mechanisms of Amphotericin B[18]. Thus, we hypothesized that Nystatin has the strongest synergy with H2A out of the three antifungals described and will demonstrate strong antifungal activity with H2A similar to that of Amphotericin B with H2A.

When assessing fungal growth over time, the dual treatment of Natamycin (4 µg/ml) and H2A (10 µg/ml) were weakly synergistic, showing the same lag time as Natamycin alone, however with an overall lower OD_{600} over time. The single treatment of H2A was consistent with previous growth curves, showing growth comparable to untreated *A. fumigatus* (**Fig. 5.2a**). Similarly, weak antimicrobial synergy was observed between Voriconazole (0.125 µg/ml) and H2A (10 µg/ml) (**Fig. 5.2b**). As hypothesized, Nystatin synergized the strongest with H2A of the three membrane-active antifungals described. The dual treatment of Nystatin (3.125 units/ml) and H2A (10 µg/ml)

showed an approximate 9-hour lag time, whereas single treatments of Amphotericin B or H2A at the same concentrations had shorter lag times of 3 hours and 1 hour, respectively. The dual treatment of Nystatin with H2A, though strongest of the three antifungals tested, is not as strong as the combination of Amphotericin B and H2A.
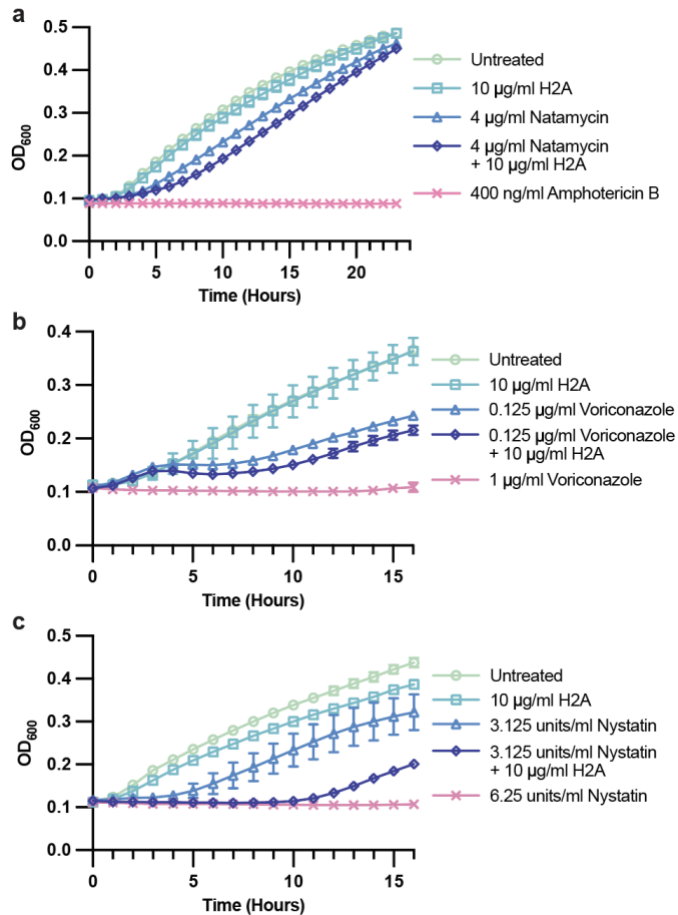
Figure 5.2. Natamycin, Voriconazole, and Nystatin, are Weakly Synergistic with H2A Against *Aspergillus fumigatus*. Growth profile of untreated *A. fumigatus* or *A. fumigatus* treated with (a) H2A, Natamycin, or both, (b) H2A, Voriconazole, or both, or (c) H2A, Nystatin, or both. Error bars indicate SEM.

5.4 Conclusion

This report is the first to show that histones are strongly synergistic with the membrane-active antifungal Amphotericin B, but not cell wall synthesis inhibitor Caspofungin, against *A. fumigatus* and *F. oxysporum*. Thus, it is possible that membrane permeating antifungals, specifically those that target fungal ergosterol, synergize more effectively with histones than cell wall inhibitors do not. Indeed, the ergosterol-targeting antifungals, Natamycin, Voriconazole, and Nystatin, all synergize with histone H2A to some extent against *A. fumigatus*. Nystatin, a molecule that is structurally most like Amphotericin B, showed the strongest synergy of the three aforementioned antifungals, suggesting that the specific polyene macrolide structure of Nystatin and Amphotericin B play a strong role in synergy with histones. Since Amphotericin B synergizes more strongly with histones than Natamycin, it is also possible that slight differences in their molecular structures are responsible for the differences in observed synergy effects.

In order to optimize this antifungal strategy using histones and membrane-active antifungals, it will be critical to understand the mechanisms of this synergy via experiments similar to histone synergy in bacteria. For example, propidium iodide and differentially sized dextran molecules can be used to understand how histones affect fungal cell membrane permeability and pore sizes when combined with Amphotericin B and Nystatin. Moreover, fluorescently-labeled histones can be utilized to assess histones localization in fungal cells when combined with synergistic antifungals. To assess potential clinical applications of combining histones with antifungals, a murine fungal keratitis model[19] will be informative. Following infection and treatments with Amphotericin B and histone H2A, analyzing corneal opacity, CFU counts, inflammatory markers via enzyme-linked immunosorbent assays, presence of immune cells via flow cytometry, and epithelial barrier defects via fluorescein strips will be essential.

5.5 References

1. Karthikeyan, R. S. *et al.* Expression of Innate and Adaptive Immune Mediators in Human Corneal Tissue Infected With Aspergillus or Fusarium. *J. Infect. Dis.* **204**, 942–950 (2011).

2. Leal, S. M. *et al.* Targeting Iron Acquisition Blocks Infection with the Fungal Pathogens Aspergillus fumigatus and Fusarium oxysporum. *PLoS Pathog.* **9**, e1003436 (2013).

3. Ortiz, S. C., Pennington, K., Thomson, D. D. & Bertuzzi, M. Novel Insights into Aspergillus fumigatus Pathogenesis and Host Response from State-of-the-Art Imaging of Host-Pathogen Interactions during Infection. *J. Fungi Basel Switz.* **8**, 264 (2022).

4. Ratitong, B. & Pearlman, E. Pathogenic Aspergillus and Fusarium as important causes of blinding corneal infections - the role of neutrophils in fungal killing, tissue damage and cytokine production. *Curr. Opin. Microbiol.* **63**, 195–203 (2021).

5. Fisher, M. C. *et al.* Tackling the emerging threat of antifungal resistance to human health. *Nat. Rev. Microbiol.* **20**, 557–571 (2022).

6. Batista, B. G., Chaves, M. A. de, Reginatto, P., Saraiva, O. J. & Fuentefria, A. M. Human fusariosis: An emerging infection that is difficult to treat. *Rev. Soc. Bras. Med. Trop.* **53**, e20200013 (2020).

7. Parums, D. V. Editorial: The World Health Organization (WHO) Fungal Priority Pathogens List in Response to Emerging Fungal Pathogens During the COVID-19 Pandemic. *Med. Sci. Monit. Int. Med. J. Exp. Clin. Res.* **28**, e939088 (2022).

8. Fisher, M. C. & Denning, D. W. The WHO fungal priority pathogens list as a game-changer. *Nat. Rev. Microbiol.* **21**, 211–212 (2023).

9. Mesa-Arango, A. C., Scorzoni, L. & Zaragoza, O. It only takes one to do many jobs: Amphotericin B as antifungal and immunomodulatory drug. *Front. Microbiol.* **3**, 286 (2012).

10. Walker, L. A., Lee, K. K., Munro, C. A. & Gow, N. A. R. Caspofungin Treatment of Aspergillus fumigatus Results in ChsG-Dependent Upregulation of Chitin Synthesis and the Formation of Chitin-Rich Microcolonies. *Antimicrob. Agents Chemother.* **59**, 5932–5941.

11. Monheit, J. E., Cowan, D. F. & Moore, D. G. Rapid detection of fungi in tissues using calcofluor white and fluorescence microscopy. *Arch. Pathol. Lab. Med.* **108**, 616–618 (1984).

12. Stone, N. R. H., Bicanic, T., Salim, R. & Hope, W. Liposomal Amphotericin B (AmBisome(®)): A Review of the Pharmacokinetics, Pharmacodynamics, Clinical Experience and Future Directions. *Drugs* **76**, 485–500 (2016).

13. Welscher, Y. M. T. *et al.* Natamycin Blocks Fungal Growth by Binding Specifically to Ergosterol without Permeabilizing the Membrane. *J. Biol. Chem.* **283**, 6393–6401 (2008).

14. Qiu, S. *et al.* Natamycin in the treatment of fungal keratitis: a systematic review and Meta-analysis. *Int. J. Ophthalmol.* **8**, 597–602 (2015).

15. Sienkiewicz, B. M., Łapiński, Ł. & Wiela-Hojeńska, A. Comparison of clinical pharmacology of voriconazole and posaconazole. *Contemp. Oncol. Poznan Pol.* **20**, 365–373 (2016).

16. Greer, N. D. Voriconazole: the newest triazole antifungal agent. *Proc. Bayl. Univ. Med. Cent.* **16**, 241–248 (2003).

17. Zotchev, S. & Caffrey, P. Chapter 11 Genetic Analysis of Nystatin and Amphotericin Biosynthesis. in *Methods in Enzymology* vol. 459 243–258 (Elsevier, 2009).

18. Dos Santos, A. G. *et al.* The molecular mechanism of Nystatin action is dependent on the membrane biophysical properties and lipid composition. *Phys. Chem. Chem. Phys. PCCP* **19**, 30078–30088 (2017).

19. Vareechon, C., Zmina, S. E., Karmakar, M., Pearlman, E. & Rietsch, A. Pseudomonas aeruginosa Effector ExoS Inhibits ROS Production in Human Neutrophils. *Cell Host Microbe* **21**, 611-618.e5 (2017).

CHAPTER 6: SUMMARY AND CONCLUSIONS

In summary, the pressing challenge of antibiotic resistance necessitates the exploration of novel antimicrobial strategies. The combination of pore-forming AMPs with histones presents a promising approach, particularly in combating Gram-negative bacteria. Through differential targeting of the bacterial membrane, histones significantly enhance the efficacy of AMP-derived antibiotics, such as polymyxin B, against *E. coli* and pathogenic *P. aeruginosa*. This alternative antimicrobial mechanism not only addresses the urgent need for novel antimicrobials, but also demonstrates potential applicability against pathogenic Gram-positive bacteria, including MRSA, and pathogenic fungi, *A. fumigatus* and *F. oxysporum*. Further exploration is required to understand how histones might physically interact with pore-forming antimicrobials to damage bacterial and fungal membranes as part of their microbial killing mechanisms. Assessing these antimicrobial combinations more thoroughly in *in vivo* models is additionally necessary for potential clinical application.

Taken together, the impressive synergy between histones and pore-forming AMPs, antibiotics, and antifungals underscores a significant advance in the context of dwindling antimicrobial options. Furthermore, this research provides valuable insights for enhancing the effectiveness of current antimicrobials and guiding the development of innovative antibiotic strategies across diverse microbial pathogens. Thus, increased understanding of this antimicrobial strategy and its optimization as an antimicrobial regimen will be particularly valuable in the ongoing battle against antimicrobial resistance.